Theory and application of explicitly correlated Gaussians

Jim Mitroy

ARC Center for Antimatter-Matter Studies, School of Engineering, Charles Darwin University, Darwin NT 0909, Australia

Sergiy Bubin

Department of Physics and Astronomy, Vanderbilt University, Nashville, Tennessee 37235, USA

Wataru Horiuchi

Department of Physics, Hokkaido University, Sapporo 060-0810, Japan

Yasuyuki Suzuki

Department of Physics, Niigata University, Niigata 950-2181, Japan, and RIKEN Nishina Center, Wako 351-0198, Japan

Ludwik Adamowicz

Department of Chemistry and Biochemistry and Department of Physics, University of Arizona, Tucson, Arizona 85721, USA

Wojciech Cencek and Krzysztof Szalewicz

Department of Physics and Astronomy, University of Delaware, Newark, Delaware 19716, USA

Jacek Komasa

Faculty of Chemistry, Adam Mickiewicz University, Grunwaldzka 6, Poznan 60-780, Poland

D. Blume

Department of Physics and Astronomy, Washington State University, Pullman, Washington 99164-2814, USA

Kálmán Varga*

Department of Physics and Astronomy, Vanderbilt University, Nashville, Tennessee 37235, USA

(published 6 May 2013)

The variational method complemented with the use of explicitly correlated Gaussian basis functions is one of the most powerful approaches currently used for calculating the properties of few-body systems. Despite its conceptual simplicity, the method offers great flexibility, high accuracy, and can be used to study diverse quantum systems, ranging from small atoms and molecules to light nuclei, hadrons, quantum dots, and Efimov systems. The basic theoretical foundations are discussed, recent advances in the applications of explicitly correlated Gaussians in physics and chemistry are reviewed, and the strengths and weaknesses of the explicitly correlated Gaussians approach are compared with other few-body techniques.

DOI: 10.1103/RevModPhys.85.693 PACS numbers: 31.15.ac, 21.60.De, 03.65.Nk

CONTENTS

*kalman.varga@vanderbilt.edu

I. INTRODUCTION

A. The quantum few-body problem

This review discusses the application of explicitly correlated Gaussians (ECGs) to the description of quantum few-body systems. The quantum few-body problem is as old as quantum mechanics. Immediately after the origin of quantum mechanics, one of the most significant problems to be solved was the correct prediction of the ionization energy of helium. This problem was put to E. Hylleraas by M. Born (Hylleraas, 1963). A series of increasingly sophisticated calculations using the Ritz (variational) method were then completed on states of the helium atom and two-electron ions (Hylleraas, 1928, 1929a, 1929b, 1930a). Agreement at the level of about 0.1 part per thousand was achieved (Hylleraas, 1929b). One of the key ingredients in these calculations was the use of a correlated basis explicitly involving the electron-electron distance $r_{12} = |\mathbf{r}_1 - \mathbf{r}_2|$.

Although many different approaches have been devised to solve few-body problems, this work focuses on those that exploit the Ritz variational principle, namely,

$$E_0 = \frac{\langle \Psi_0 | H | \Psi_0 \rangle}{\langle \Psi_0 | \Psi_0 \rangle} \geq E_{\text{exact}}. \tag{1}$$

The trial wave function Ψ_0 is constructed to minimize the energy E_0. The few-body problem is a subset of the N-body problem with the number of particles typically restricted to lie

between three and six. When solving the few-body problem, one seeks to develop from the outset techniques to precisely describe the interparticle correlations between all particles in the systems. In the N-body problem, mean-field approaches, such as the Hartree-Fock (HF) method, are often used as the starting point.

Few-body systems occur in many areas of physics and cover a wide range of energy and length scales. In particle physics, i.e., at the subnuclear level, the basic constituents are quarks. Assuming effective model interactions consistent with our understanding of the strong force, few-body techniques can help to determine the ordering of the energy levels of hadrons (baryons and mesons) and provide insights into the formation of clusters consisting of more than three quarks. At somewhat lower energy scales, around 1–20 MeV, the basic constituents are nucleons interacting through the strong and Coulombic forces. The ^{3}H, ^{3}He, and ^{4}He nuclei and other light nuclei including hypernuclei are important systems since a complete understanding of their structures and interactions is a necessary condition for better understanding of the nuclear interaction.

In atomic physics, the helium and lithium atoms are primary few-body examples. The basic constituents are the electrons, and their interactions are governed by the electromagnetic interactions. While the typical atomic energy scale is around 1–10 eV, interpretation of high precision measurements that are sensitive to relativistic corrections and possibly the shape of the nucleus require calculations that are accurate to an overall precision of 10^{-10} eV.

In molecular physics, one can identify H_2^+, H_2, He_2^+, LiH, and He_2 as "simple" few-body systems. Compared to atomic systems, the internuclear distance coordinate introduces new degrees of freedom, i.e., the vibrational and rotational degrees of freedom with typical energy scales of 10^{-1} and 10^{-3} eV, respectively. As in atomic physics, the charged particles interact via the electromagnetic interaction. The internuclear distance vector has traditionally been fixed using the Born-Oppenheimer approximation but recent developments have enabled calculations where this restriction is relaxed.

Examples of few-body systems that occur in soft condensed matter consist of two- and three-dimensional quantum dots which might contain only electrons and excitonic complexes which are made up of electrons and holes that interact electromagnetically and are confined externally. In these models, the electrons and holes interact immersed in a medium, and the effect of the medium is allowed for by effective masses.

Finally, recent developments in cold atom physics have greatly stimulated the investigation of Efimov physics and general studies of the stability of few-body systems. In these applications, the basic constituents are neutral atoms interacting through van der Waals potentials and the typical energy scales are of the order of 10^{-10} eV.

Much work in the field of few-body physics is related to low-energy collision processes. Description of the dynamics of collisions is particularly important for the investigation of nuclear and cold atom systems.

A variety of theoretical techniques have been developed to study few-body systems, for example, quantum Monte Carlo (QMC) methods, configuration-interaction (CI) methods, and the no-core shell model, methods that use hyperspherical coordinate systems, and variational methods using basis sets that represent further development of those originally developed by Hylleraas. This review focuses on ECGs, which have been successfully applied to the investigations of all the systems described above and other approaches are discussed only briefly in this review. In many cases, the results by the ECG approach are compared with those obtained by other methods. Some of the alternative approaches are listed in the List of Symbols and Abbreviations, which contains a list of the acronyms that are used in this review.

B. Explicitly correlated Gaussians

The fundamental results concerning ECGs were first put forward by Boys (1960) and Singer (1960). They proposed to describe the N-particle wave function with a basis of exponential functions with an argument involving the square of the distance between every pair of particles. Such a function can be written as

$$\psi = \exp\Big(-\sum_{i>j=1}^{N} \alpha_{ij}(\mathbf{r}_i - \mathbf{r}_j)^2\Big), \tag{2}$$

where α_{ij} are adjustable parameters. The advantage of this functional form is twofold. First, very high accuracy is achievable since the basis functions are correlated. This advantage is magnified for systems with strongly attractive interparticle interactions. Second, the quadratic form involving interparticle distances permits the reduction of the Hamiltonian matrix elements to very simple analytic expressions. The algebraic complexity of the matrix elements does not change at all for $N \geq 3$ and this has permitted calculations with correlated basis sets to be performed on systems which were previously inaccessible. They represent a major advantage over exponential functions with linear distance factors since these basis functions lead to matrix elements of increasing intractability as the number of particles increases (King, Quicker, and Langer, 2011).

Despite the computational advantages, the ECG basis was long regarded as inferior to the exponential $\exp(-\alpha r)$ form since the ECG basis functions do not have the correct functional form near the $r_{ij} \rightarrow 0$ coalescence point for Coulomb interactions. They also have the incorrect forms for the $r_{ij} \rightarrow \infty$ asymptote for short-range potentials. However, the ease with which matrix elements can be computed has allowed ECGs to be used to describe a number of diverse physical systems. Furthermore, it makes the extensive optimization of the Gaussian exponents computationally feasible (Kukulin and Krasnopol'skii, 1977; Alexander, Monkhorst, and Szalewicz, 1986; Cencek and Rychlewski, 1993; Varga and Suzuki, 1995), leading to very accurate energies and other properties.

While the fundamental results concerning ECGs have been known for a long time, it is mainly since the 1990s that it has been systematically used by a number of different research groups. Figure 1 shows the citations to the original Boys and Singer papers (Boys, 1960; Singer, 1960) by decade. The citation count increased markedly in the 1991–2000 and 2001–2010 decades. Prior to the 1991–2000 decade, the applications of ECG basis sets to the few-body problem are best described as intermittent. The lack of activity prior to the

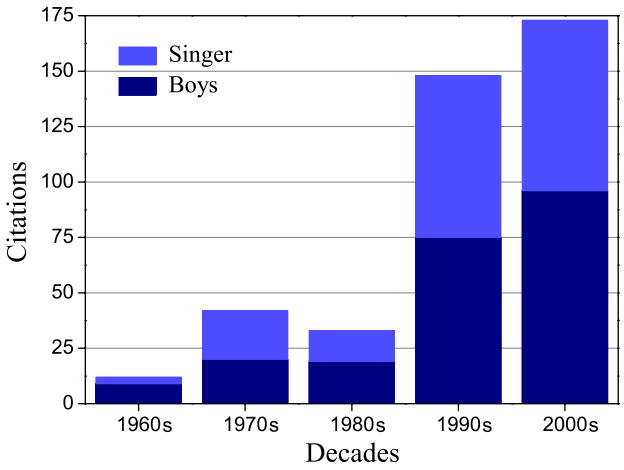

FIG. 1 (color online). Number of citations by decade to the original works (Boys, 1960; Singer, 1960). The data for both articles are taken from the ISI Web of Knowledge science citation database as of 1 October 2011. The last decade covers the years 2000–2011.

1991–2000 decade was probably due to a number of reasons. One contributing factor would have been that prior to the 1990s, much research in few-body physics was focused on three-body problems where the ECG basis does not have a competitive advantage over other methods.

To a certain extent, the development of the ECG basis set for few-body quantum physics mirrors the development of single-particle Gaussian basis sets (Boys, 1950; McWeeny, 1950) for the calculation of electronic structures for molecules. Initially there were concerns about the accuracy of the wave functions near the nuclear centers and in the $r \rightarrow \infty$ limit. However, the pragmatic consideration of simply being able to perform realistic calculations on molecules, regardless of whether they had two or more centers, overcame any considerations of the theoretical niceties and the field of quantum chemistry is now dominated by the use of Gaussian basis sets.

Another major advantage of ECGs is that the interparticle interactions can be treated with all pairs of particles being given equal prominence. This makes the ECG basis sets suitable for treating systems with attractive interactions that result in strong interparticle correlations. Examples of such systems include small nuclear systems with tendencies to form α-particle clusters (Varga, Suzuki, and Tanihata, 1995), exotic positron-atom systems with a tendency to form positronium clusters (Ryzhikh, Mitroy, and Varga, 1998b), and excitonic systems (Riva, Peeters, and Varga, 2000, 2001). The ECG basis has also been generalized to handle systems with strongly repulsive interactions (or "hard-core" potentials) (Kinghorn and Adamowicz, 1999b; Stanke *et al.*, 2006).

II. FORMALISM

A. Hamiltonian

Consider an N-particle system where the ith particle with mass m_i is described by the position vector $\mathbf{r}_i$. The Hamiltonian of the system reads

$$H = \sum_{i=1}^{N} \frac{\mathbf{p}_i^2}{2m_i} + \sum_{i=1}^{N} U_i(\mathbf{r}_i) + \sum_{j>i=1}^{N} V_{ij}(\mathbf{r}_i, \mathbf{r}_j), \tag{3}$$

where U_i is the one-body potential experienced by the ith particle in the presence of an external field and V_{ij} is the interaction potential between particles i and j. It is assumed that all particles interact via two-body forces. In the most general case, we can also introduce three- and many-body potentials, as well as consider the case of nonlocal interactions. Also, for some systems, the potentials may depend on additional degrees of freedom such as spin, isospin, flavor, etc. The specific interactions relevant to a particular system will be discussed as needed.

B. The variational principle

The fundamental result underpinning much work in bound-state few-body physics is the variational theorem, which states that the Hamiltonian expectation value of any approximate normalized wave function $|\Psi_0\rangle$ forms an upper bound to the exact energy (Kellner, 1927); see Eq. (1). This results in a widely used strategy to generate accurate wave functions and energies. The trial wave function $|\Psi_0\rangle$ is written as a linear combination of basis functions,

$$|\Psi_0\rangle = \sum_{i=1}^{\mathcal{N}} c_i |\psi_i(\{\alpha\}_i)\rangle. \tag{4}$$

The basis functions $\psi_i(\{\alpha_i\})$ will usually have some dependence on a set of parameters $\{\alpha\}_i$. The c_i coefficients and the parameters $\{\alpha\}_i$ are then adjusted to minimize the energy. Minimizing the energy leads to the generalized eigenvalue problem

$$H\mathbf{c} = ES\mathbf{c}, \tag{5}$$

where the H and S are $\mathcal{N} \times \mathcal{N}$ Hamiltonian and overlap matrices with the elements

$$H_{ij} = \langle \psi_i | H | \psi_j \rangle, \qquad S_{ij} = \langle \psi_i | \psi_j \rangle, \tag{6}$$

and $\mathbf{c}$ is an $\mathcal{N}$-component vector of linear coefficients c_i. Trying to minimize the energy with respect to the $\{\alpha\}$ parameters results in a nonlinear optimization problem. In general, Eq. (5) has $\mathcal{N}$ solutions. The Hylleraas-Undheim-McDonald theorem (Hylleraas, 1930b; MacDonald, 1933) states that the nth lowest eigenvalue of Eq. (5) gives an upper bound to the corresponding exact nth excited energy of the system in question.

C. Center-of-mass reduction

In the absence of external fields, it is natural to separate out the contribution from the center-of-mass motion and focus on the intrinsic motion of the system. The most convenient way of doing this is to introduce some set of relative coordinates. There are two common choices here: one is the Jacobi coordinate set, the other is the set of coordinates where the origin is placed on one of the particles (for example, at particle 1) (Suzuki and Varga, 1998). These choices are schematically illustrated in Fig. 2. The relation between the laboratory frame coordinates $(\mathbf{x}_1, \mathbf{x}_2, \ldots, \mathbf{x}_N)$ and the relative

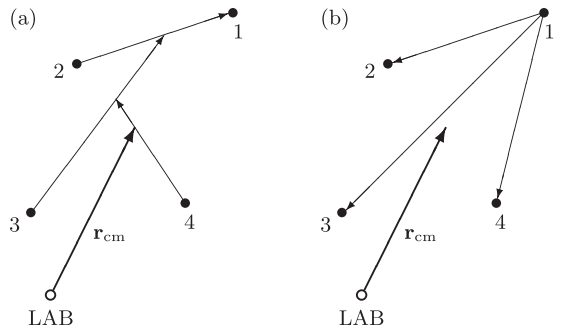

FIG. 2. Possible sets of relative coordinates: (a) the Jacobi coordinates, and (b) the coordinates where one of the particles (in this case the first one) serves as a reference particle.

(Jacobi) coordinates $(\mathbf{r}_1, \mathbf{r}_2, \ldots, \mathbf{r}_N)$ (here we assume that $\mathbf{r}_N$ is the position of the center of mass, $\mathbf{r}_{\rm c.m.}$) is linear and given by

$$\mathbf{r}_i = \sum_{j=1}^{N} \Omega_{ij}\mathbf{x}_j, \qquad \mathbf{x}_i = \sum_{j=1}^{N} (\Omega^{-1})_{ij}\mathbf{r}_j, \qquad i = 1, \ldots, N. \tag{7}$$

The explicit form of the transformation matrix Ω for the case of the Jacobi coordinates is the following:

$$\Omega_{\rm Jac} = \begin{pmatrix} 1 & -1 & 0 & \cdots & 0 \\ \frac{m_1}{M_2} & \frac{m_2}{M_2} & -1 & \cdots & 0 \\ \vdots & \vdots & \vdots & \ddots & \vdots \\ \frac{m_1}{M_{N-1}} & \frac{m_2}{M_{N-1}} & \frac{m_3}{M_{N-1}} & \cdots & -1 \\ \frac{m_1}{M_N} & \frac{m_2}{M_N} & \frac{m_3}{M_N} & \cdots & \frac{m_N}{M_N} \end{pmatrix}. \tag{8}$$

For the case of particle-1 relative coordinates, the transformation matrix is

$$\Omega_{\rm rel} = \begin{pmatrix} -1 & 1 & 0 & \cdots & 0 \\ -1 & 0 & 1 & \cdots & 0 \\ \vdots & \vdots & \vdots & \ddots & \vdots \\ -1 & 0 & 0 & \cdots & 1 \\ \frac{m_1}{M_N} & \frac{m_2}{M_N} & \frac{m_3}{M_N} & \cdots & \frac{m_N}{M_N} \end{pmatrix}, \tag{9}$$

where

$$M_k = \sum_{i=1}^{k} m_i. \tag{10}$$

The inverse transformation matrices can also be written explicitly (Suzuki and Varga, 1998). The choice of a coordinate system where the origin is placed at one of the particles may be natural in many practical situations, for example, when that particle is much heavier than the other ones (this situation occurs in an atom with its heavy nucleus and light electrons).

The new linear momenta $\mathbf{p}_i$ conjugated to Jacobi or particle-1 relative coordinates $\mathbf{r}_i$ can be obtained by applying the inverse transformation to the linear momentum conjugated to the laboratory frame coordinates:

$$\mathbf{p}_i = \sum_{j=1}^{N} (\Omega^{-1})_{ij}\mathbf{q}_j, \quad \mathbf{q}_i = \sum_{j=1}^{N} \Omega_{ij}\mathbf{p}_j, \quad i = 1, \ldots, N, \tag{11}$$

where $\mathbf{q}_i = m_i\dot{\mathbf{x}}_i$. After transforming the coordinates using Eq. (8) or (9), the kinetic energy operator T of the new Hamiltonian contains two terms: the kinetic energy of $n = N - 1$ (pseudo)particles moving in the new reference frame and the kinetic energy of the center of mass,

$$T = \frac{1}{2}\sum_{i,j=1}^{n} \Lambda_{ij}\mathbf{p}_i \cdot \mathbf{p}_j + T_{\rm c.m.}. \tag{12}$$

Here Λ is a $n \times n$ "mass" matrix with the elements

$$\Lambda_{ij} = \sum_{k=1}^{N} \frac{1}{m_k}\Omega_{ik}\Omega_{jk}. \tag{13}$$

The operator of the kinetic energy of the center of mass is given by

$$T_{\rm c.m.} = \frac{\mathbf{p}_{\rm c.m.}^2}{2M_N}, \tag{14}$$

where $\mathbf{p}_{\rm c.m.}$ is the total linear momentum. Since the potential in the absence of external fields depends only on the interparticle coordinates, the total Hamiltonian of the system in the new coordinates is independent of $\mathbf{r}_{\rm c.m.}$. Therefore, the total wave function can be represented as a product of the wave function describing the intrinsic motion of the system ψ and a plane wave corresponding to the motion of the system as a whole:

$$\psi_{\rm tot} = \exp(i\mathbf{k}_{\rm c.m.} \cdot \mathbf{r}_{\rm c.m.})\psi(\mathbf{r}_1, \ldots, \mathbf{r}_n), \tag{15}$$

where $\mathbf{k}_{\rm c.m.}$ is the wave vector belonging to $\mathbf{p}_{\rm c.m.}$. From now on, we concentrate on finding ways to approximate the intrinsic wave function.

D. Choice of basis functions

In this section, the ECG functions that are used to expand the system wave function are introduced. The ECGs, which depend on the relative coordinates, are defined as follows:

$$G_A(\mathbf{r}) = \exp(-\mathbf{r}'A\mathbf{r}), \tag{16}$$

where A is an $n \times n$ symmetric positive-definite matrix whose elements are variational parameters and the quadratic form in the exponent is defined as

$$\mathbf{r}'A\mathbf{r} = \sum_{i,j=1}^{n} A_{ij}\mathbf{r}_i \cdot \mathbf{r}_j. \tag{17}$$

Here and below the prime symbol is used to denote the vector or matrix transpose. The ECG function can be rewritten in a more intuitive form:

$$\exp(-\mathbf{r}'A\mathbf{r}) = \exp\Big(-\sum_{j>i=1}^{N} \alpha_{ij}(\mathbf{r}_i - \mathbf{r}_j)^2 - \sum_{i=1}^{N} \beta_i\mathbf{r}_i^2\Big). \tag{18}$$

The parameters α_{ij} and β_i can be expressed by the elements of matrix A and vice versa. The advantage of this notation is that it explicitly connects the nonlinear parameters α_{ij} to

the pair correlation between the particles i and j and thus explains the name "explicitly correlated Gaussians." The second part $\exp(-\sum_{i=1}^{N}\beta_i\mathbf{r}_i^2)$ is a product of independent single-particle Gaussians centered at the origin.

A variational trial wave function can be formed as a linear combination of ECGs:

$$\psi_{SM_S}(\mathbf{r},A)=\sum_{k=1}^{\mathcal{N}}c_k\mathcal{A}\{G_{A_k}(\mathbf{r})\chi_{SM_S}\}, \tag{19}$$

where the operator $\mathcal{A}$ is an antisymmetrizer (or symmetrizer in the case of bosons) and χ_{SM_S} is the spin function of the system with the total spin S and its projection M_S. The spin function is defined by coupling the single-particle spin functions $\xi(i)$ (i is the particle label) as

$$\chi_{SM_S}=[[[\xi(1)\xi(2)]_{S_{12}}\xi(3)]_{S_{123}}\cdots]_{SM_S} \tag{20}$$

using the common rules of the addition of angular momenta. In this scheme, $S_{12\cdots i}$ represents the intermediate total spin at each successive coupling. The accuracy of the trial function depends on the length of the expansion $\mathcal{N}$ and the nonlinear parameters A_k in Eq. (19).

1. Central potentials and states with small total orbital angular momentum

The ECGs of Eq. (16) are spherically symmetric (the quadratic form is invariant with respect to 3D rotations) and suitable for describing states with zero total orbital angular momentum. It should be noted that such functions can be used in calculations of systems where one of the particles is infinitely heavy (such as an atom with a clamped nuclei). In this case the origin of the laboratory coordinate system can be placed at the infinitely heavy particle and the positions of other particles in the laboratory frame will coincide with the relative coordinates with respect to that particle. For example, if the clamped particle is the Nth particle, then $\mathbf{r}_i=\mathbf{x}_i$, $i=1,\ldots,N-1$.

The formalism has to be extended to describe systems with nonzero angular momentum. It becomes necessary to construct basis functions that are eigenfunctions of the square of the total angular momentum operator with angular momentum L.

A common approach to building basis functions of proper rotational symmetry, i.e., those that correspond to a certain value of quantum numbers L and M, is to multiply $G_A(\mathbf{r})$ by a generalized solid spherical harmonic $\theta_{LM}(\mathbf{r})$,

$$\psi_k=\theta_{LM}(\mathbf{r})\exp(-\mathbf{r}'A_k\mathbf{r}). \tag{21}$$

$\theta_{LM}(\mathbf{r})$ can be formed by successively coupling solid spherical harmonics,

$$\theta_{LM}(\mathbf{r})=r_1^{l_1}\cdots r_n^{l_n}[[[Y_{l_1m_1}(\hat{\mathbf{r}}_1)Y_{l_2m_2}(\hat{\mathbf{r}}_2)]_{L_{12}M_{12}} Y_{l_3m_3}(\hat{\mathbf{r}}_3)]_{L_{123}M_{123}}\cdots Y_{l_nm_n}(\hat{\mathbf{r}}_n)]_{LM}. \tag{22}$$

According to the Wigner-Eckardt theorem, the energy of the system described by a spherically symmetric Hamiltonian is independent of M. In most calculations it is advantageous to choose $M=0$ in $\theta_{LM}(\mathbf{r})$ as such basis functions are real and the calculations do not require the use of complex arithmetic.

Using Eq. (22), it is possible to build basis functions for any value of the total orbital angular momentum and its z projection. Since the angular momenta of the relative motion [denoted $l_1,l_2,L_{12},l_3,L_{123},\ldots,L_{12\cdots(n-1)}$ in Eq. (22)] are not conserved quantities, it is sometimes necessary to include several sets of single-particle and intermediate angular momenta to have an accurate variational expansion. The inclusion of different sets of relative angular momenta is of particular importance in the case of nuclear few-body problems with noncentral interaction.

In the following, a few special cases are considered. For $L=1$, $M=0$ states with negative parity (the radial part is a single Cartesian coordinate), in which the dominant configuration corresponds to one particle with $l=1$ and all others with $l=0$, the ECGs have the following form:

$$\psi_k=z_{i_k}\exp(-\mathbf{r}'A_k\mathbf{r}), \tag{23}$$

where z_{i_k} is the z component of $\mathbf{r}_{i_k}$ and i_k is an integer variational parameter, which may take a value from 1 to n. In a variational expansion, each basis function (23) may have a different optimal value of i_k.

Similarly, for the positive parity $L=1$, $M=0$ states (the radial part is a product of two Cartesian coordinates), which arise when the dominant configuration is formed by two particles with $l=1$ and all others with $l=0$, the basis functions are

$$\psi_k=(x_{i_k}y_{j_k}-x_{j_k}y_{i_k})\exp(-\mathbf{r}'A_k\mathbf{r}),\qquad i_k\neq j_k. \tag{24}$$

Here both integers i_k and j_k are variational parameters.

Finally, the basis functions for the natural parity $L=2$, $M=0$ states (D states) read

$$\psi_k=(x_{i_k}x_{j_k}+y_{i_k}y_{j_k}-2z_{i_k}z_{j_k})\exp(-\mathbf{r}'A_k\mathbf{r}). \tag{25}$$

2. Global vector representation (GVR) for states with arbitrary L

Upon increasing the total L value in Eq. (22), the matrix elements of the corresponding $\theta_{LM}(\mathbf{r})$ function become progressively more complicated. Also, as mentioned previously, it may be necessary to include several different forms of $\theta_{LM}(\mathbf{r})$ simultaneously. As the number of such forms (which may or may not be relevant in a particular calculation) grows very rapidly, one faces a serious problem. The difficulty can be avoided by adopting a different form for the orbital part in Eq. (21) (Varga and Suzuki, 1995; Suzuki and Varga, 1998; Varga, Suzuki, and Usukura, 1998):

$$\theta_{LM}(\mathbf{r})=v^{2K+L}Y_{LM}(\hat{\mathbf{v}}), \tag{26}$$

where

$$\mathbf{v}=\sum_{i=1}^{n}u_i\mathbf{r}_i, \tag{27}$$

$v=|\mathbf{v}|$, and Y_{LM} is the usual spherical harmonic. Only the total orbital angular momentum value L and its projection appear in Eq. (26). These quantum numbers are good quantum numbers (assuming a central interaction). The vector $\mathbf{v}$, defined as a linear combination of all (pseudo)particle coordinates, is called the "global vector." The coefficients in the linear combination are treated as real-valued variational

parameters. In general, they are unique for each basis function, just like the Gaussian parameters. One may choose the optimal values of u_i based on the minimization of the energy functional. It is possible to take advantage of efficient optimization algorithms, which assume smoothness of the objective function (energy) with respect to small variations of variables. The integer variational parameter K, which can take any non-negative value, introduces an additional flexibility that can be used to improve the short-range behavior of the basis functions. A remarkable property of the orbital part in Eq. (26) is that all necessary matrix elements can be evaluated analytically in an algebraically compact form (Suzuki and Varga, 1998).

The scheme introduced in Eq. (26) (Varga and Suzuki, 1995) covers only states with natural parity [i.e., the parity $=(-1)^L$]. A generalization to handle unnatural parity states was recently proposed (Suzuki, Horiuchi *et al.*, 2008).

3. Explicitly correlated Gaussians with shifted centers

Molecular calculations in the Born-Oppenheimer (BO) approximation where the nuclear positions are fixed require the inclusion of coordinate shifts in the ECGs. The electrons are attracted to the nuclei and their densities are expected to peak around the nuclear positions. These shifts can be incorporated by writing

$$G_{A_k,\mathbf{s}_k}(\mathbf{r}) = \exp[-(\mathbf{r}-\mathbf{s}_k)'A_k(\mathbf{r}-\mathbf{s}_k)], \tag{28}$$

where the $3n$-component vectors $\mathbf{s}_k$ are variational parameters. In general, each ECG in the basis can have a unique shift $\mathbf{s}_k$. Such basis functions are sometimes called floating Gaussians. Shifted ECGs can also be used in molecular calculations where the BO approximation is relaxed. A more intuitive way to write these functions for a N-electron molecule in the BO approximation would be

$$\psi_k = \exp\Big(-\sum_{i=1}^{N}\alpha_{ki}(\mathbf{x}_i-\mathbf{a}_{ki})^2 - \sum_{i>j=1}^{N}\beta_{kij}(\mathbf{x}_i-\mathbf{x}_j)^2\Big). \tag{29}$$

The parameters α_{ki}, β_{kij}, and $\mathbf{a}_{ki}$ can be expressed in terms of the elements of matrix A_k and shifts $\mathbf{s}_k$ and vice versa. For diatomic molecules, the points $\mathbf{a}_{ki}$ are usually placed on the line connecting the two nuclei. A reasonable initial choice for the shifts in the fixed nuclei case is $\mathbf{s}=(\mathbf{R}_i,\mathbf{R}_j,\ldots)$, where $\mathbf{R}_i$ is the position vector of the ith nucleus. Depending on the choice of indices $i, j, \ldots$ in $(\mathbf{R}_i,\mathbf{R}_j,\ldots)$ the Gaussians may resemble an "ionic" or "covalent" product of atomic orbitals with additional electron-electron correlation factors. In the case of a homonuclear diatomic system, it is easy to build in the *gerade* or *ungerade* symmetries. For a gerade system, one simply creates a molecular wave function that is symmetric about the internuclear midpoint by adding to each ECG a term mapping $\mathbf{a}_{ki}\rightarrow-\mathbf{a}_{ki}$ (the coordinate origin is at the internuclear midpoint) and giving it the same linear coefficient.

The shifted ECGs of Eq. (28) are not eigenfunctions of the square of the total orbital angular momentum operator, unless the shift is zero. This is not a concern in the fixed nuclei case, where the total orbital angular momentum is not an integral of motion. In non-BO calculations, the shifted ECGs might not have the correct rotational symmetry. However, using a large basis set with sufficient variational flexibility results in a wave function that approaches the proper symmetry when the energy is optimized because the Hamiltonian and symmetry operators commute.

Alternatively, one can use an angular momentum projector and filter out the desired quantum state. The angular momentum projection operator is defined as (Peierls and Yoccoz, 1957; Blanco and Heller, 1983)

$$P^L_{MK} = \frac{2L+1}{8\pi^2}\int D^{L*}_{MK}(\Omega)R(\Omega)d\Omega, \tag{30}$$

where Ω denotes the Euler angles α, β, and θ, $R(\Omega)$ is a rotation operator

$$R(\Omega) = e^{i\alpha L_z}e^{i\beta L_y}e^{i\theta L_z}, \tag{31}$$

L_x, L_y, and L_z are angular momentum operators, and $D^{L*}_{MK}(\Omega)$ are the Wigner functions. Using P^L_{MK}, a matrix element with prescribed quantum numbers can be calculated as

$$\langle\psi_{LMi}|H|\psi_{LKj}\rangle = \langle\psi_i|HP^L_{MK}|\psi_j\rangle. \tag{32}$$

To calculate this matrix element, the rotation of the wave function can be evaluated by (Blanco and Heller, 1983)

$$R(\Omega)\psi_j(\mathbf{r}) = \psi_j(\mathbf{R}^{-1}(\Omega)\mathbf{r}), \tag{33}$$

where $\mathbf{R}(\Omega)$ represents the matrix of coordinate rotation by the Euler angles and the rotation acts on each coordinate $\mathbf{r}_i$ separately. The integrations over the Euler angles are usually carried out numerically.

4. Basis functions for systems in external fields

In some problems, e.g., in systems subjected to a magnetic field, it is advantageous to use basis functions with cylindrical symmetry. The magnetic field breaks the rotational symmetry and the Hamiltonian no longer commutes with the L^2 operator, while it still commutes with the L_z operator. To adapt the trial functions to this case, a deformed ECG (DECG) is used (Suzuki and Varga, 1998):

$$\exp\Big(-\sum_{i,j=1}^{n}A_{ij}(x_ix_j+y_iy_j) - \sum_{i,j=1}^{n}B_{ij}z_iz_j\Big), \tag{34}$$

where the nonlinear parameters are different (and independent) in the $\boldsymbol{\rho}$ direction and in the z direction [$\boldsymbol{\rho}_i=(x_i,y_i)$]. This extension brings a great deal of flexibility by allowing a separate description of the motion in the x-y plane and along the z axis. Such functions are eigenfunctions of the L_z operator. The above form of the DECG is restricted to $M=0$. To allow for $M\neq 0$ states, the basis functions are multiplied by

$$\prod_{i=1}^{n}\xi_{m_i}(\boldsymbol{\rho}_i), \tag{35}$$

where

$$\xi_m(\boldsymbol{\rho}) = \begin{cases}(x+iy)^m & m>0,\\ (x-iy)^{-m} & m<0.\end{cases} \tag{36}$$

Thus, the variational basis functions for systems in magnetic fields read

$$\psi^M(\mathbf{r}) = \mathcal{A}\Big[\Big(\prod_{i=1}^{n}\xi_{m_i}(\boldsymbol{\rho}_i)\Big)\exp\Big(-\sum_{i,j=1}^{n}A_{ij}\boldsymbol{\rho}_i\cdot\boldsymbol{\rho}_j - \sum_{i,j=1}^{n}B_{ij}z_iz_j\Big)\Big], \tag{37}$$

where $M = m_1 + m_2 + \cdots + m_n$.

5. Completeness of Gaussian basis sets

One important consideration relates to the completeness of Gaussian basis sets. For all practical purposes, the ECG functions form a complete basis set (King, 1967; Bukowski *et al.*, 1995; Jeziorski, Bukowski, and Szalewicz, 1997; Hill, 1998). Issues of linear dependence can arise during calculations since the Gaussian functions used are not mutually orthogonal. This is discussed later in Sec. III.F.

E. Matrix elements

The success of ECG-based methods ultimately relies on the simplicity of the matrix elements of the Hamiltonian and other operators. For example, the overlap of two spherically symmetric ECGs, Eq. (16), is

$$S(A_k, A_l) = \langle G(A_k)|G(A_l)\rangle = \left(\frac{\pi^n}{\det(A_{kl})}\right)^{3/2}, \tag{38}$$

where $A_{kl} = A_k + A_l$. The matrix element of the kinetic energy has the following form:

$$\langle G(A_k)|T|G(A_l)\rangle = 3\,\mathrm{tr}(A_kA_{kl}^{-1}A_l\Lambda)S(A_k, A_l). \tag{39}$$

In the above expressions, $\det(\cdots)$ and $\mathrm{tr}(\cdots)$ denote the determinant and trace of a matrix, respectively. The matrix elements of any one-body operator based on the spatial coordinate can be written as

$$\langle G(A_k)|V(\mathbf{r}_i)|G(A_l)\rangle = I(\beta_i)S(A_k, A_l). \tag{40}$$

In this equation, $I(\beta)$ is defined as

$$I(\beta) = \left(\frac{\beta}{\pi}\right)^{3/2}\int V(\mathbf{a})\exp(-\beta a^2)d\mathbf{a} \tag{41}$$

and

$$\frac{1}{\beta_i} = w_i'A_{kl}^{-1}w_i, \tag{42}$$

where w_i is a vector with elements $(w_i)_m = \delta_{im}$. The expression for matrix elements of a two-body interaction $V(\mathbf{r}_i - \mathbf{r}_j)$ is similar to that in Eq. (40),

$$\langle G(A_k)|V(\mathbf{r}_i - \mathbf{r}_j)|G(A_l)\rangle = I(\beta_{ij})S(A_k, A_l), \tag{43}$$

but now

$$\frac{1}{\beta_{ij}} = w_{ij}'A_{kl}^{-1}w_{ij}, \qquad (w_{ij})_m = \delta_{im} - \delta_{jm}. \tag{44}$$

There is almost no restriction on the functional form of the potential. In particular, for central interactions the integral of Eq. (41) is reduced to a one-dimensional integral, which can be easily evaluated either analytically or numerically. This is one of the fundamental reasons for the success of ECG basis sets. For example, for power law potentials, $V(r) = r^k$ $(k > -3)$, one finds

$$I(\beta) = \frac{2}{\sqrt{\pi}\beta^{k/2}}\Gamma\left(\frac{k+3}{2}\right), \tag{45}$$

where Γ is the Euler gamma function. Another remarkable property of the ECG basis is that the analytical complexity of the matrix elements does not change when the number of particles is increased. Assuming pairwise interactions, the computational effort associated with the evaluation of the matrix elements increases as $n^3 \times k!$, where k is the number of identical particles in the system (for an atom, $k = n$) and the $k!$ factor comes from the need to antisymmetrize the wave function. Another factor is that, given the same relative accuracy, the length $\mathcal{N}$ of the expansion has to increase when n increases. This increase, however, is slower than $k!$. The $k!$ dependence has so far limited the application of ECG methods to systems with no more than eight particles.

As a guide through the literature, a nonexhaustive list of papers that give technical details on the derivation of matrix elements for various types of ECGs is presented in Table I. Material on the related topic of evaluating multicenter integrals with Gaussian orbitals can be found in Obara and Saika (1986), Head-Gordon and Pople (1988), Brinkmann and Kleindienst (1991), Kuang and Lin (1997), and Petersson and Hellsing (2010), and references therein.

F. Relativistic and QED corrections

The relativistic and quantum electrodynamic (QED) effects in light atoms and molecules can be conveniently accounted for using the "nonrelativistic" QED expansion (Caswell and Lepage, 1986; Pachucki, 1997) of the bound-state energy in powers of the fine-structure constant α

$$E = \sum_k \alpha^k E^{(k)}. \tag{46}$$

Each term of this expansion can be given a clear physical interpretation. The nonrelativistic energy computed (after the center-of-mass motion separation) from the Schrödinger equation is $E^{(0)}$. The linear $\alpha E^{(1)}$ term is absent and the $\alpha^2E^{(2)}$ term represents the leading relativistic correction. The $\alpha^3E^{(3)}$ term, which contains also terms that depend logarithmically on α, describes the leading QED effects. The higher-order terms of the α expansion provide all the remaining relativistic and QED corrections proportional to α^k with $k \geq 4$.

The main advantage of this expansion is that its coefficients can be evaluated perturbatively using the nonrelativistic wave function ψ. The expressions for the leading coefficients are known from the literature for a long time now. $E^{(2)}$ can be evaluated from an expectation value of the Breit-Pauli Hamiltonian (Bethe and Salpeter, 1977), which in a simplified form (for nuclei at rest and for $^1\Sigma$ molecular electronic states) reads in atomic units

$$\alpha^{-2}H_{\mathrm{BP}} = -\frac{1}{8}\sum_i \mathbf{p}_i^4 + \frac{\pi}{2}\sum_{i,A}Z_A\delta(\mathbf{r}_{iA}) + \pi\sum_{i<j}\delta(\mathbf{r}_{ij}) - \frac{1}{2}\sum_{i<j}\left(\mathbf{p}_i\frac{1}{r_{ij}}\mathbf{p}_j + \mathbf{p}_i\cdot\mathbf{r}_{ij}\frac{1}{r_{ij}^3}\mathbf{r}_{ij}\cdot\mathbf{p}_j\right). \tag{47}$$

TABLE I. List of references describing the analytical calculation of ECG matrix elements. OPP denotes the orthogonalizing pseudoprojector method defined later.

Interaction or operators	ECG type	Form	Reference
Coulomb	Shifted ECGs	Direct	Boys (1960) and Singer (1960)
Coulomb	Shifted ECGs, one pair of electrons correlated	Direct	Cencek and Rychlewski (1993)
Coulomb	Shifted ECGs	Recursion	Saito and Suzuki (2001)
Coulomb	Spherical ECGs, $L = 0$, analytic energy gradient	Direct	Kinghorn (1996) and Kinghorn and Adamowicz (1999a)
Central	Complex ECGs, $L = 0, 1, 2$, analytic energy gradient	Direct	Bubin and Adamowicz (2006, 2008), and Sharkey, Bubin, and Adamowicz, 2011a)
J^2, J_z	Shifted ECGs with prefactors	Recursion	Kozlowski and Adamowicz (1995)
Coulomb	Shifted ECGs, analytical energy gradient	Direct	Kozlowski and Adamowicz (1992)
Coulomb	Shifted ECGs, analytic energy gradient	Direct	Cafiero and Adamowicz (2001)
Various interactions including noncentral	GVR ECGs, arbitrary L	Direct	Varga and Suzuki (1995) and Suzuki and Varga (1998)
Central and noncentral, relativistic kinetic energy	GVR ECGs, arbitrary L	Direct	Silvestre-Brac and Mathieu (2007, 2008)
Various interactions	GVR ECGs for unnatural parity states, arbitrary L	Direct	Suzuki, Horiuchi *et al.* (2008) and Aoyama *et al.* (2012)
Coulomb	Spherical ECGs with prefactors	Recursion	Harris and Monkhorst (2006)
Atomic core-exchange, OPP, three-body polarization	Spherical ECGs	Direct	Ryzhikh, Mitroy, and Varga (1998b)
General	Infinitesimally shifted ECGs for arbitrary L	Direct	Hiyama, Kino, and Kamimura (2003)

In the above formula, i and j stand for the electrons, A stands for the nuclei, Z_A is the charge of the Ath nucleus, $\mathbf{r}_{ij} = \mathbf{r}_i - \mathbf{r}_j$, $\mathbf{r}_{iA} = \mathbf{r}_i - \mathbf{R}_A$, and δ denotes the three-dimensional Dirac δ function. The subsequent terms are usually referred to as the mass velocity, the one- and two-electron Darwin, and the Breit contributions.

The leading QED correction can be expressed as

$$E^{(3)} = \sum_{i<j}\left\{\left[\frac{164}{15} + \frac{14}{3}\ln\alpha\right]\langle\delta(\mathbf{r}_{ij})\rangle + \langle H_{\mathrm{AS}}\rangle\right\} + \sum_{i,A}\left[\frac{19}{30} - 2\ln\alpha - \ln K\right]\frac{4Z_A}{3}\langle\delta(\mathbf{r}_{iA})\rangle. \tag{48}$$

In this expression, two terms require special consideration. The first one is the Araki-Sucher operator (Araki, 1957; Sucher, 1958),

$$H_{\mathrm{AS}} = -\frac{7}{6\pi}\mathcal{P}\left(\frac{1}{r_{ij}^3}\right), \tag{49}$$

defined (in atomic units) through the distribution $\mathcal{P}$, which takes care of the divergence at $r_{ij} = 0$,

$$\left\langle\mathcal{P}\left(\frac{1}{r_{ij}^3}\right)\right\rangle = \lim_{a\to 0}\langle r_{ij}^{-3}\Theta(r_{ij} - a) + 4\pi(\gamma + \ln a)\delta(\mathbf{r}_{ij})\rangle. \tag{50}$$

Here Θ is the Heaviside step function and γ is the Euler-Mascheroni constant. The other expression, that is difficult to compute in Eq. (48), is the Bethe logarithm

$$\ln K = \frac{\langle\mathbf{j}(H - E^{(0)})\ln[(H - E^{(0)})/\mathrm{Ry}]\mathbf{j}\rangle}{\langle\mathbf{j}(H - E^{(0)})\mathbf{j}\rangle}, \tag{51}$$

where $\mathbf{j}$ is the electric current operator, $\mathbf{j} = -(e/m_e)\sum_i\mathbf{p}_i$, and Ry is the Rydberg constant (1/2 Hartree in atomic units). For a long time, this quantity was accurately known only for one- or two-electron atoms and for the one-electron molecular hydrogen cation (Bukowski *et al.*, 1992). Only in recent years was progress made toward determination of the Bethe logarithm for larger atoms (Pachucki and Komasa, 2003, 2004b; Yan and Drake, 2003) as well as for molecules (Piszczatowski *et al.*, 2009).

Formulas for the $\alpha^4 E^{(4)}$ term are also known (Pachucki, 2005). Unfortunately, practical difficulties in evaluation of certain divergent terms prevent accurate calculations of this correction for systems with more than two electrons. From calculations for the hydrogen and helium atoms (Pachucki, 2006a, 2006b, 2007), however, it is known that the dominant contribution to the higher-order QED correction is the so-called one-loop term

$$E^{(4)}_{\text{one-loop}} = \pi\left(\frac{427}{96} - \ln 4\right)\sum_{i,A} Z_A^2\langle\delta(\mathbf{r}_{iA})\rangle, \tag{52}$$

which can be used as an estimate of $E^{(4)}$.

The relativistic and QED theory outlined above carries difficulties in evaluating certain quantities. This concerns not only the Bethe logarithm and Araki-Sucher operator but also the expectation values of the singular Dirac delta (δ) operators or the relativistic kinetic energy operator $\mathbf{p}^4$. The difficulties can be significantly diminished by special regularization techniques discussed in Sec. III.C.

G. Perturbative treatment of the finite mass effects

For molecules it is common to perform calculations within the framework of the BO approximation. The effects of the nuclear motion can be treated perturbatively with the adiabatic BO wave function taken as the unperturbed state. Here a

short theory is presented, which gives, in connection with the ECG wave functions, highly accurate results for light diatomic molecules.

1. Adiabatic approximation

In nonadiabatic perturbation theory (Pachucki and Komasa, 2008, 2009), the zeroth-order approximation to the wave function of a diatomic molecule is represented by the adiabatic ansatz

$$\phi_a(\mathbf{r}, \mathbf{R}) = \phi_{\rm el}(\mathbf{r}; \mathbf{R})\chi(\mathbf{R}), \tag{53}$$

where $\mathbf{r}$ stands for the coordinates of the electrons and $\mathbf{R}$ connects the positions of nuclei A and B. The Hamiltonian of the system is split into electronic and nuclear parts $H = H_{\rm el} + H_n$. The electronic Hamiltonian is

$$H_{\rm el} = \sum_i \frac{\mathbf{p}_i^2}{2m} + V, \tag{54}$$

where V is the Coulomb interaction between the electrons and the electrons and nuclei at fixed nuclear positions. The perturbation is defined by the nuclear part of the total Hamiltonian

$$H_n = -\frac{1}{2\mu_n}\nabla_R^2 - \frac{1}{8\mu_n}\left(\sum_i \boldsymbol{\nabla}_i\right)^2 + \left(\frac{1}{M_A} - \frac{1}{M_B}\right)\boldsymbol{\nabla}_R \cdot \sum_i \boldsymbol{\nabla}_i, \tag{55}$$

where $\mu_n = (1/M_A + 1/M_B)^{-1}$ is the nuclear reduced mass.

The adiabatic ansatz enables the separation of the nuclear and electronic variables. The electronic wave function $\phi_{\rm el}$ is a solution to the clamped-nuclei Schrödinger equation

$$[H_{\rm el} - \mathcal{E}_{\rm el}(R)]\phi_{\rm el} = 0 \tag{56}$$

and parametrically depends on the internuclear distance R. This equation is solved variationally.

The wave function of the nuclear motion is calculated from the nuclear Schrödinger equation. For a given nuclear angular momentum J, the nuclear equation becomes one dimensional

$$\left[-\frac{1}{R^2}\frac{\partial}{\partial R}\frac{R^2}{2\mu_n}\frac{\partial}{\partial R} + \frac{J(J+1)}{2\mu_n R^2} + \mathcal{E}_{\rm el}(R) + \mathcal{E}_a(R)\right]\chi_J(R) = E_a\chi_J(R), \tag{57}$$

with E_a the adiabatic approximation to the total energy. The adiabatic correction $\mathcal{E}_a(R)$ is given by the electronic matrix element

$$\mathcal{E}_a(R) = \langle H_n \rangle_{\rm el}. \tag{58}$$

From here and forth, the brackets $\langle \cdots \rangle_{\rm el}$ denote integration over the electronic coordinates only.

2. Nonadiabatic nuclear equation

Nonadiabatic perturbation theory yields a series of successive approximations to the total energy E expressed in progressive powers of the electron-nuclear mass ratio. Up to order μ_n^{-2}, they can also be found by solving the following nonadiabatic version of the nuclear equation:

$$\left[-\frac{1}{R^2}\frac{\partial}{\partial R}\frac{R^2}{2\mu_\parallel(R)}\frac{\partial}{\partial R} + \frac{J(J+1)}{2\mu_\perp(R)R^2} + \mathcal{Y}(R)\right]\tilde{\chi}_J(R) = E\tilde{\chi}_J(R). \tag{59}$$

The finite nuclear mass effects appear in this equation as R-dependent corrections to the nuclear reduced mass and to the interaction potential. The corrections to μ_n are given by the following two R-dependent functions:

$$\frac{1}{2\mu_\parallel(R)} = \frac{1}{2\mu_n} + \frac{1}{\mu_n^2}\sum_{i,j}\left\langle \frac{R^i}{R}\nabla_R^i \left| \frac{1}{(\mathcal{E}_{\rm el} - H_{\rm el})'} \right| \frac{R^j}{R}\nabla_R^j \right\rangle_{\rm el} \tag{60}$$

and

$$\frac{1}{2\mu_\perp(R)} = \frac{1}{2\mu_n} + \frac{1}{2\mu_n^2}\sum_{i,j}\left(\delta^{ij} - \frac{R^i R^j}{R^2}\right) \times \left\langle \nabla_R^i \left| \frac{1}{(\mathcal{E}_{\rm el} - H_{\rm el})'} \right| \nabla_R^j \right\rangle_{\rm el}, \tag{61}$$

where i and j are the Cartesian components and the prime symbol in the resolvent indicates the projection of the electronic reference state (Piela, 2007). The interaction potential is also corrected by an R-dependent nonadiabatic correction $\mathcal{Y}(R) = \mathcal{E}_{\rm el}(R) + \mathcal{E}_a(R) + \mathcal{E}_{na}(R)$. The internuclear potential can be further augmented by an R-dependent nonadiabatic correction and relativistic and QED potentials. In such a case, the eigenvalue of Eq. (59) accounts for all leading corrections resulting from the finite nuclear mass and the finite speed of light, and should be directly comparable to the experimental value.

III. COMPUTATIONAL METHODOLOGIES

A. Parameter optimization

Variational calculations employing ECGs can provide very accurate energies and wave functions and numerous examples will be presented later in this review. However, achieving high accuracy is possible only when the nonlinear parameters of the basis functions are carefully optimized. This sensitivity gets stronger for larger systems and excited states where the wave function in general has a more complicated structure. The most natural way to optimize the parameters of the basis functions is to minimize the total energy.

Finding the absolute minimum of the energy with respect to the nonlinear parameters for a large (dimension of 100–10 000) ECG expansion of the wave function is difficult due to the large number of parameters and the complicated energy hypersurface. However, it is only necessary to find a wave function that is sufficiently low lying in energy. This can be achieved by maintaining the right balance between the amount of effort spent on the optimization of nonlinear parameters and the additional amount of effort required when the dimension of the ECG basis is increased.

The importance of being able to systematically optimize the basis was outlined in the original paper that described the stochastic variational method (Kukulin and Krasnopol'skii, 1977). The paper also described how this optimization could

be carried out in a reasonably efficient manner. This work was not widely appreciated in atomic and molecular structure physics and the development of ECG-based methods here followed a course of parallel evolution leading to roughly the same outcome. In atomic physics, the importance of performing intensive optimization of the individual nonlinear parameters of the ECG basis became apparent during a series of calculations on the helium atom performed over a few decades (Longstaff and Singer, 1960, 1964; Poshusta, 1979; Regier and Thakkar, 1985; Rybak, Szalewicz, and Jeziorski, 1989; Alexander *et al.*, 1990; Komasa and Thakkar, 1995; Cencek and Kutzelnigg, 1996; Kinghorn and Adamowicz, 1997).

A similar pattern of events is apparent when one looks at the application of ECG functions to calculations of the H_2 molecule (Longstaff and Singer, 1960, 1964, 1965; Lester, Jr. and Krauss, 1964; Handy, 1973; Salmon and Poshusta, 1973; Jeziorski and Szalewicz, 1979; Alexander *et al.*, 1990). The potential utility of ECG-based approaches for describing molecular structure became more apparent by 1979, when the best ECG energy of H_2 had an error of 0.05 mhartree (Jeziorski and Szalewicz, 1979), which was unmatched by any other calculation except for those performed using a generalized James-Coolidge (GJC) basis that were accurate to 0.01 mhartree (Kołos and Wolniewicz, 1965). The full advantages of optimized ECG bases for molecular systems were realized when ECG-type wave function expansions gave the best variational energies for the H_2, LiH, and linear H_3 molecules (Cencek and Rychlewski, 1993; Rychlewski, Cencek, and Komasa, 1994; Cencek, Komasa, and Rychlewski, 1995).

ECGs have also been adopted to speed up the convergence of many-electron molecular structure calculations based on perturbation theory and coupled-cluster methods. The ECGs used in these calculations are usually restricted to two-electron functions which have been traditionally referred to as Gaussian-type geminals (GTGs). Optimization of the GTG parameters resulted in calculations that were able to exceed the best perturbative results for Be and LiH obtained by other methods (Alexander, Monkhorst, and Szalewicz, 1986, 1988).

There are two types of nonlinear optimization that are typically performed. The first occurs when the basis size is increased and new basis functions are included. Here stochastic optimization is normally used. The second type of optimization occurs when the basis size is kept fixed. Here one can use either a direct or stochastic optimization.

1. Stochastic optimization

Stochastic optimization methods are optimization methods that generate and use random variables. For stochastic problems, the random variables appear in the formulation of the optimization problem itself, which involves random objective functions or random constraints (Spall, 2003). The problem of optimizing the large number of nonlinear parameters of the ECG basis naturally lends itself to an application of a stochastic optimization procedure. The stochastic optimization of the ECG parameters, "the stochastic variational method" (SVM), was first proposed by Kukulin and Krasnopol'skii (1977).

In SVM, $\mathcal{K}$ different sets of nonlinear parameters A in Eq. (16) are generated randomly. The parameter set which gives the lowest variational energy is selected and the function corresponding to these parameters is retained in the set of ECGs.

The stochastic selection procedure differs slightly depending on whether the basis is being enlarged or the parameters of an existing basis are being refined.

(1) *Set up a new basis* (or enlarge an existing one): Assuming that the basis set has $\mathcal{N}-1$ elements, one generates $\mathcal{K}$ random basis states and calculates $(i=1,\ldots,\mathcal{K})$ new energies $E_{\mathcal{N}i}$ with the $\mathcal{N}$-dimensional bases. The new $\mathcal{N}$-dimensional bases contain the ith random element and the previously selected $\mathcal{N}-1$ basis elements. The random state giving the lowest energy is selected as a new basis state and added to the basis. The variational principle ensures that the eigenvalues of the $\mathcal{N}$-dimensional basis are always lower than the corresponding eigenvalues of the $(\mathcal{N}-1)$-dimensional basis. This procedure is guaranteed to give a better new upper bound to the ground state energy. The rate of convergence can be determined by examination of the $\epsilon_{\mathcal{N}}=E_{\mathcal{N}}-E_{\mathcal{N}-1}$ energy differences.

(2) *Refinement:* In the refinement process, the dimension of the basis is kept fixed while $\mathcal{K}$ new ECGs are generated randomly with the purpose of replacing the kth element of the basis. If the best energy obtained by substituting the kth basis state with a random candidate is lower than that of the original basis, then the kth basis state is discarded and the new random state is included in the basis. This procedure is repeated for $k=1,\ldots,\mathcal{N}$. As the dimension of the model space is fixed, this step does not necessarily give a lower energy, but in practice it usually does. In fact, if one cannot find better basis elements, it is an indication of a well-converged energy.

While the SVM described above is part of a fully variational calculation, the selection of the optimal parameters of the GTGs used in perturbative calculations is done in a process that has many features in common with the approaches described above (Alexander, Monkhorst, and Szalewicz, 1986, 1988; Bukowski, Jeziorski, and Szalewicz, 1994), as such calculations apply the Hylleraas variational principle.

2. Why extensive optimization is feasible

The process of optimization of the nonlinear parameters is performed at an individual level for each basis function. When this is done, the Hamiltonian matrix has a particularly simple structure. Since there exists an $(\mathcal{N}-1)\times(\mathcal{N}-1)$ block that is already diagonal, the full diagonalization of an $\mathcal{N}\times\mathcal{N}$ matrix is not needed. It is only necessary to calculate a new row of the Hamiltonian and overlap matrices. The simplicity of expressions for the ECG matrix elements ensures that this can be done quickly.

Furthermore, the determination of the energy eigenvalues is quick since the off-diagonal elements are confined to one row and one column of the Hamiltonian matrix. The diagonalization of this almost diagonal Hamiltonian can be completed by a

process similar to Schmidt orthogonalization (Varga and Suzuki, 1995) or by an iterative approach such as the one outlined by Bubin, Cafiero, and Adamowicz (2005).

3. Direct optimization

One of the advantages of the stochastic optimization is that it is easy and quick to implement. A disadvantage is that it does not utilize any information about the continuity, smoothness, and the gradient of the energy with respect to the nonlinear parameters. Knowledge of the energy gradient can greatly speed up any optimization process (Fletcher, 1987; Press *et al.*, 1992) and so a direct optimization strategy can improve the convergence of the energy for a given basis dimension.

Direct optimization methods require multiple evaluations of both the total energy of the system and the gradient of the energy. Once the number of nonlinear parameters $\mathcal{M}$ being optimized becomes large, the evaluation of the gradient based on the finite difference approximation becomes expensive because, at a single point, it requires at least $2\mathcal{M}$ energy evaluations. This problem can be avoided if the analytic gradient of the energy can be computed. The amount of computations needed to evaluate the gradient analytically is typically proportional to and a few times larger than the effort needed to form the Hamiltonian and overlap matrices and compute the energy.

The derivative of the total energy [see Eq. (1)] with respect to a nonlinear parameter α_i can be written as

$$\frac{\partial E}{\partial \alpha_i} = 2\,\mathrm{Re}\left[c_i^* \sum_{j=1}^{\mathcal{N}} c_j \left(\frac{\partial H_{ij}}{\partial \alpha_i} - E\frac{\partial S_{ij}}{\partial \alpha_i}\right)\right] - c_i c_i^* \left(\frac{\partial H_{ii}}{\partial \alpha_i} - E\frac{\partial S_{ii}}{\partial \alpha_i}\right), \tag{62}$$

where Re stands for the real part of an expression (in general, basis functions and their linear coefficients may be complex), the linear coefficients are frozen, and we assume that α_i appears in the ith basis function. By calculating such a derivative for each α_i, one can obtain the entire energy gradient. It is computationally advantageous to evaluate the derivatives of E with respect to the entire set of nonlinear parameters of a particular ECG since there are many operations for each individual parameter α_i that do not have to be repeated. The derivatives of H_{ij} and S_{ij} with respect to the nonlinear parameters can usually be evaluated in closed form when dealing with the ECG basis functions.

There are a variety of optimization algorithms that can be adopted when energy gradients are available, such as the Broyden-Fletcher-Goldfarb-Shanno (BFGS) algorithm (Fletcher, 1987) or the conjugate gradient algorithm (Powell, 1964).

B. Computational requirements

While calculations using optimized ECGs can be time consuming, they actually do not require much in the way of other computational resources. The basis dimension $\mathcal{N}$ of a large calculation would typically not exceed 10 000. Storage of the overlap and Hamiltonian matrix elements requires two dense $\mathcal{N} \times \mathcal{N}$ matrices. The amount of available random access memory is almost never an issue in ECG calculations. The only conceivable circumstance when memory may become a bottleneck would be if one decided to optimize the nonlinear parameters of all basis functions simultaneously, something that is rarely done in practice for large basis dimensions. Even here, the memory requirements of the optimization algorithm such as limited memory BFGS or conjugated gradient grow sufficiently slowly [the memory requirements for conjugate gradient scale as $\mathcal{O}(n_p\mathcal{N})$, where n_p is the number of nonlinear parameters per basis function] to become a problem. Many of the calculations described have literally been done using single processors on personal computers.

The amount of CPU time required is dictated primarily by such factors as the number of particles in the system, functional form of the interaction, complexity of the wave function for a particular state, maximum number of basis functions, and thoroughness of the optimization. Some of the calculations reported here involved more than one year of optimization. Others can be done in a matter of minutes on a desktop computer. Human intervention can normally be kept to a minimum. Typically, an initial analysis based on wave functions obtained in a (relatively) small basis-set calculation would be made. Once that is done, a favorable strategy of growing the basis and optimizing nonlinear parameters of basis function can be deduced.

To speed up calculations and/or make it possible to consider systems with a larger number of particles, one can parallelize the computer code. The two major tasks that consume most of the computational time are the evaluation of the Hamiltonian and overlap matrix elements and the solution of the generalized eigenvalue problem, Eq. (5). The first task can be effectively parallelized in a straightforward manner with nearly perfect scalability. The second one also allows for a certain degree of parallelization (although the scalability may be somewhat worse).

C. Improving the convergence of the expectation values of singular operators

As mentioned in the Introduction, ECGs have incorrect asymptotics with respect to what is expected on the basis of some theoretical considerations, e.g., the Kato cusp conditions at the interparticle coalescence points (Kato, 1957). This deficiency slows the convergence of the energy and other properties, but has a particularly severe effect on the expectation values of operators that are singular at coalescence points. This problem also occurs for variational calculations that employ other basis sets (Puchalski, Kedziera, and Pachucki, 2011). Calculations of relativistic and QED effects required the development of methods to accelerate the convergence of the expectation values of singular operators. These methods are described next.

1. Expectation value identities

One acceleration technique replaces the expectation value of the singular Dirac delta function $\langle\delta(\mathbf{r}_{ij})\rangle$ by the expectation value of a global operator which yields the same result if the wave function is exact (Hiller, Sucher, and Feinberg, 1978;

Drachman, 1981; Challacombe and Cioslowski, 1994; Sundholm, 1995; Rassolov and Chipman, 1996; Cioslowski and Lopez-Boada, 1998). It can be shown that

$$4\pi\langle\delta(\mathbf{r}_{jk})\rangle = 2\left\langle\frac{1}{r_{jk}}(E-V)\right\rangle - \sum_i\left\langle\nabla_i\left|\frac{1}{r_{jk}}\right|\nabla_i\right\rangle, \quad (63)$$

where V is the potential energy operator. Atomic units ($\hbar = e = m_e = 1$) are assumed in all expressions. For an approximate function, the right-hand side converges faster toward the exact value than the original expression. A similar regularization method can be applied to the mass-velocity term of the relativistic correction, e.g.,

$$\left\langle\sum_i\nabla_i^4\right\rangle = 4\langle(E-V)^2\rangle - 2\sum_{i>j}\langle\nabla_i^2|\nabla_j^2\rangle. \quad (64)$$

An analogous identity has been found for the singular Araki-Sucher term present in the QED correction (Pachucki, Cencek, and Komasa, 2005).

The identities listed above hold independently of the basis functions employed to expand the wave function. The penalty associated with the faster convergence is that the matrix elements become more complicated. Fortunately, in the atomic case, all integrals can be evaluated analytically. This is generally not true for the molecular case.

Table II illustrates the convergence of some operators involved in the relativistic and QED calculations for the ground state of the beryllium atom, using increasingly large ECG bases. In all cases, the results from expectation value identities (EVI) with 200 ECGs are superior to those evaluated directly with 1600 ECGs. This is particularly visible in the case of the Araki-Sucher distribution $\mathcal{P}(1/r_{ij}^3)$ for which the direct evaluation of the integral gives only the leading digit correctly.

2. Integral transform technique

Another regularization technique utilizes integral representations of the singular operators. The great advantage of the integral transform (IT) methodology (Pachucki, Cencek, and Komasa, 2005), in contrast to EVI, is its similar difficulty in applications to both atoms and molecules.

TABLE II. Convergence of the expectation values computed directly and using the technique of the expectation value identities (EVI). Results are shown for the ground state of the beryllium atom (Pachucki, Cencek, and Komasa, 2005). $\mathcal{N}$ is the dimension of the ECG basis. All values are in atomic units.

$\mathcal{N}$	Direct	EVI	Direct	EVI
	$\langle\delta(\mathbf{r}_i)\rangle$		$\langle\delta(\mathbf{r}_{ij})\rangle$	
100	33.379 145	35.174 770	1.627 741	1.604 558
200	34.897 648	35.339 657	1.618 229	1.605 055
400	35.029 311	35.340 791	1.610 911	1.605 253
800	35.297 307	35.368 099	1.608 106	1.605 293
1600	35.317 352	35.368 900	1.606 742	1.605 303
	$\langle p_i^4\rangle$		$\langle\mathcal{P}(1/r_{ij}^3)\rangle$	
100	2137.407	2164.851	−8.552 39	−7.304 29
200	2153.618	2165.594	−8.123 10	−7.318 37
400	2155.764	2165.567	−7.730 23	−7.324 54
800	2161.966	2165.644	−7.552 88	−7.326 22
1600	2162.989	2165.637	−7.455 34	−7.326 63

For instance, the expectation value of the Dirac delta can be represented as

$$\langle\delta(\mathbf{r})\rangle = \frac{1}{2\pi^{3/2}}\int_0^\infty\langle 2t^2(3-2t^2r^2)e^{-t^2r^2}\rangle dt. \quad (65)$$

The expectation value within the integral can be evaluated with high accuracy by an ECG basis provided that the value of t is not excessively large. For large values of t, this integrand can be replaced by its asymptotic form with the prefactor known from the Kato's cusp condition (Kato, 1957)

$$\frac{4Z}{\sqrt{\pi}t^2}\langle\delta(\mathbf{r})\rangle\left(1+\sum_i\frac{A_i}{t^i}\right). \quad (66)$$

The first few leading coefficients A_i are then determined by fitting to the integrand evaluated on a large-t grid. Because of the presence of $\langle\delta(\mathbf{r})\rangle$ in Eq. (66), the whole procedure has to be performed iteratively.

An analogous expansion has been found for the expectation value of the Araki-Sucher distribution

$$\left\langle\mathcal{P}\left(\frac{1}{r_{ij}^3}\right)\right\rangle = \int_0^\infty(2\ln t-\gamma)f(t)dt, \quad (67)$$

where

$$f(t) = \left\langle 2t\left(t^2r_{ij}-\frac{1}{r_{ij}}\right)e^{-t^2r_{ij}^2}\right\rangle, \quad (68)$$

having the following asymptotic form:

$$f(t) = \frac{\pi^{3/2}}{t^2}\langle\delta(\mathbf{r}_{ij})\rangle\left(1+\sum_i\frac{A_i}{t^i}\right). \quad (69)$$

The IT regularization of the mass-velocity operator is more involved. Its expectation value is first expressed by an integral over the radial momentum density $I(p)$, which can be easily evaluated for not too large arguments. For large electron momentum p, it is expressed by its asymptotic form

$$I(p) = \frac{s_6}{p^6} + \frac{s_7\sin(pR)}{p^7} + \mathcal{O}(p^{-8}). \quad (70)$$

The leading coefficients s_6 and s_7 are given by

$$s_6 = 32\sum_{i=1}^N\left(Z^2\langle\delta(\mathbf{r}_i)\rangle + \frac{1}{2}\sum_{j>i}^N\langle\delta(\mathbf{r}_{ij})\rangle\right) \quad (71)$$

and

$$s_7 = 0 \quad (72)$$

for atoms. For diatomic molecules with internuclear separation R, one can write

$$s_6 = 32\sum_{i=1}^N\left(Z_A^2\langle\delta(\mathbf{r}_i-\mathbf{r}_A)\rangle + Z_B^2\langle\delta(\mathbf{r}_i-\mathbf{r}_B)\rangle + \frac{1}{2}\sum_{i>j}^N\langle\delta(\mathbf{r}_{ij})\rangle\right) \quad (73)$$

and

$$s_7 = 64NZ_AZ_BR^{-1}\rho(R). \quad (74)$$

The quantity ρ, appearing in the last equation, is the one-electron density matrix evaluated at the positions $\mathbf{R}_A$ and $\mathbf{R}_B$

TABLE III. Convergence of the relativistic correction expectation values for the helium dimer at the equilibrium separation, computed directly and using the integral transform technique (IT) (Pachucki, Cencek, and Komasa, 2005). All values are in atomic units.

$\mathcal{N}$	Direct	IT	Direct	IT
	$\langle\delta(\mathbf{r}_{iA})\rangle$		$\langle\delta(\mathbf{r}_{ij})\rangle$	
600	7.229 13	7.241 464	0.213 116	0.212 737 8
1200	7.235 67	7.241 585	0.212 907	0.212 698 7
2400	7.236 50	7.241 603	0.212 824	0.212 689 3
4800	7.237 58	7.241 606	0.212 783	0.212 687 7
	$\langle p_i^4\rangle$		$\langle\mathcal{P}(1/r_{12}^3)\rangle$	
600	216.029	216.348 90	0.324 16	0.333 518
1200	216.196	216.348 93	0.326 58	0.333 797
2400	216.218	216.348 81	0.327 63	0.333 882
4800	216.246	216.348 74	0.328 20	0.333 898

of the two nuclei. For atoms, the convergence speedup is similar to that observed for the EVI method. Tests on molecules, in particular, the helium dimer (see Table III), show that the IT regularization gives expectation values that are 1 to 3 orders of magnitude more accurate than the direct evaluation for a given basis.

3. ECG basis functions with linear prefactors

Still another approach modifies the ECG functional forms by multiplying them by linear prefactors in the interparticle distance (Pachucki and Komasa, 2004a). This enhances the convergence of the singular relativistic correction operators. Furthermore, such a modification makes it possible to satisfy the Kato cusp conditions (Kato, 1957) involving the ratio of expectation values at the coalescence points, e.g., $\mathrm{cusp}(\mathbf{r}) = \langle\delta(\mathbf{r})\partial/\partial r\rangle/\langle\delta(\mathbf{r})\rangle$. The Kato cusp conditions can never be exactly fulfilled with the original ECG basis.

While explicit expressions for the matrix elements for systems involving three electrons exist (Pachucki and Komasa, 2004c), the method has been applied only to the helium atom (Pachucki and Komasa, 2004a). The use of a linearized ECG basis resulted in helium-atom cusp conditions that were accurate to better than 0.05% for a basis dimension of 600. The convergence for δ-function operators was significantly improved.

To some extent the use of ECGs with linear prefactors runs counter to the philosophy underpinning the success of ECGs. One reason behind the extraordinary success of ECGs has been the ease with which most matrix elements can be evaluated. The additional complications resulting from adding linear multiplying factors to ECGs have prevented their widespread application and there have been almost no applications of these modified ECGs since their initial usage. Note that prefactors in the form of integer powers of electronic coordinates (rather than in the form of interparticle distances) do not lead to significant complications and have often been used.

D. Strongly repulsive interactions

Strongly repulsive interactions pose a particular problem in variational calculations. Consider the Schrödinger equation for two particles interacting through the central potential $V(r)$. When the product $r^2 2\mu V(r)/\hbar^2$ is as large as $r \to 0$, the wave function has to have an extremely rapid decay for $r \to 0$. It is difficult to describe such systems using global basis functions such as $\exp(-\lambda r)$ or $\exp(-\lambda r^2)$. The finite size of any ECG close to the origin leads to large positive matrix elements. Attempting to construct a linear superposition of basis functions for $\Psi(\mathbf{r})$ by optimizing nonlinear parameters results in a set of basis functions with similar exponents and linear coefficients that have alternate signs. This leads to a loss of numerical significance even before linear dependence effects cause the calculation to fail.

The nucleon-nucleon interaction is well known to possess a strongly repulsive short-range core (Epelbaum, Hammer, and Meißner, 2009). Similarly, the interaction between two atoms, e.g., the two hydrogen atoms in the H_2 molecule, also has a strongly repulsive core. To some extent, the strongly repulsive core problem is a computational problem as opposed to a physics problem. For example, it is difficult to calculate the vibrational states using a Gaussian basis directly, but one can easily find the vibrational states by numerical integration of the Schrödinger equation with a H-H interatomic potential.

One solution to the hard-core problem is to simply modify the potential to effectively soften the repulsive hard core. Effective-field theory provides one framework by which this can be done (Lepage, 1997; Epelbaum, Hammer, and Meißner, 2009). When the two-body interaction is modified, it is sometimes necessary to add a compensating three-body interaction. In effect, one modifies the interaction to solve a computational problem.

An alternative approach is to modify the basis functions so that they are able to better represent the very small amplitude for the interparticle wave functions. One solution is to add basis functions that are obtained by multiplying the exponential parts of the ECG by prefactors r_{ij}^{2m} with some large m integers. This naturally leads to a decreased probability amplitude for the wave function when the two particles are close together. Using even powers as the prefactor leads to simpler matrix elements. In the case of a diatomic molecule, where the two nuclei are treated on the same footing as the electrons, the ECGs of Eq. (16) become (Kinghorn and Adamowicz, 1999a)

$$\psi_k = r_1^{2m_k} \exp(-\mathbf{r}' A_k \mathbf{r}), \tag{75}$$

where r_1 is the distance between the two nuclei. The values m_k can be treated as variational parameters. Typically, they are chosen in the range 0–100. Prefactors have also been used in calculations of the H_2^+ molecular ion using the Hylleraas basis (Yan, Zhang, and Li, 2003).

The matrix elements with ECGs containing r_{ij}^{2m} prefactors can be derived by parametric differentiation of the exponents in the standard formulas. They become quite involved for the case when more than one prefactor with a large power is used.

E. Highly excited states

Highly excited states with a number of oscillations and nodes are difficult to reproduce with a Gaussian basis set. The problems can be alleviated by choosing ECGs with complex

exponential parameters (Hiyama, Kino, and Kamimura, 2003; Bubin *et al.*, 2007):

$$\psi_k = \exp(-\mathbf{r}'[A_k + iB_k]\mathbf{r}). \tag{76}$$

Such basis functions have a sinususoidal component, e.g., $\sin(kr^2)$, as well as an exponentially decaying component. Numerical tests have shown that ECGs with a complex component give orders of magnitude better estimates of the highly excited states of the harmonic oscillator than do real ECGs (Hiyama, Kino, and Kamimura, 2003).

A practical disadvantage of complex ECGs is that the optimization of nonlinear parameters, A_k and B_k of Eq. (76), is much more time consuming. However, the analytic complexity of the matrix elements is comparable to that for the normal ECGs with real exponents.

ECGs with complex exponents can also be used to treat systems with strongly repulsive interactions, although generally they exhibit significantly worse performance than functions with prefactors given by Eq. (75).

F. Linear dependence issues

Since the ECGs are not mutually orthogonal, it is possible that the ECG basis could become nearly linearly dependent as the basis is increased in size during the optimization. Linear dependences sometimes occur when the ECGs are not well adapted to describe aspects of the wave function of the system or state under investigation.

One common problem arises when trying to approximate a wave function that vanishes abnormally quickly, e.g., as in the case of the relative wave function for two particles interacting via a strongly repulsive potential. The relative wave function can be described using Gaussians with roughly equal exponents and equal in magnitude and opposite in sign linear coefficients. For example, at small x and δ the wave function $\phi(x) = \exp(-ax^2) - \exp[-(a+\delta)x^2]$ will reduce to $\phi(x) \propto x^2 \exp(-ax^2)$. The relative wave function is now small, but the basis functions have a higher degree of linear dependence.

Linear dependences between basis functions have the potential to cause numerical instabilities in the calculation of the energy eigenvalue. Some linear dependences may cause no harm at all, provided a proper algorithm is chosen for solving the generalized eigenvalue problem. However, when two (or more) basis functions with near unity overlaps acquire large linear coefficients that add up to nearly zero total magnitude, this almost always leads to a problem.

Consider two basis functions ψ_i and ψ_j that have $S_{ij} \approx 1$. Each eigenvalue of Eq. (5), as well as the expectation value of any operator, can be represented as a simple Rayleigh quotient. The contribution of these terms to the expectation value of any operator O,

$$\langle\psi_i|O|\psi_i\rangle + \langle\psi_j|O|\psi_j\rangle - \langle\psi_i|O|\psi_j\rangle - \langle\psi_j|O|\psi_i\rangle \tag{77}$$

(assuming equal magnitudes of linear coefficients), will lead to loss of numerical significance due to cancellation of leading digits arising from the subtraction. The contribution to the final result from the near linearly dependent basis functions will be of reduced precision and this can impact the overall accuracy. A loss of precision in the energy will degrade the optimization of nonlinear parameters of the basis. In the worst case scenario, the energy eigenvalue may become completely unphysical.

There are a variety of ways to keep the linear dependence problem under control. One straightforward approach is to eliminate linearly dependent basis functions as they appear. For example, the value of the overlap integral between the new function and all accepted functions can be monitored and ECGs functions with an overlap close to unity are rejected. Typical values of the critical overlap range from 0.95 to 0.99.

The situation becomes somewhat more complicated when optimizing the nonlinear parameters of an existing ECG basis that has become linearly dependent. Discarding one (or several) of the ECGs which contribute to the linear dependence may significantly worsen the total energy. A possible solution is to introduce a penalty function to the total energy during optimization. This function increases the energy whenever S_{ij} is larger than a given threshold. The penalty function $\mathcal{P}$ should be constructed to be smooth so as not to interfere with the optimization algorithm. One such function is

$$\mathcal{P} = \sum_{ij} \mathcal{P}_{ij}, \tag{78}$$

where the sum is over all pairs of basis functions, and

$$\mathcal{P}_{ij} = \begin{cases} \beta \frac{|S_{ij}|^2 - t^2}{1 - t^2}, & |S_{ij}| > t, \\ 0, & |S_{ij}| \le t. \end{cases} \tag{79}$$

In the above expression, t is the value of the overlap threshold, and β controls the weight of the penalty term for each overlap. The choice of parameters t and β is based on experience. Typical values might be $t = 0.99$ and β is chosen so the energy would be affected at the 0.001%–0.00001% level. The value of β can be decreased as the energy gets closer to convergence.

G. Fixed core methods

The range of fermionic systems for which ECG methods can be usefully applied can be extended by the use of frozen core approximations. The tendency for fermionic systems to form closed shells naturally leads to approximations with the particles separated into inert particles in the core and active valence particles.

Two modifications to the Hamiltonian need to be made for fixed core calculations. An effective interaction between the core and the active particles needs to be constructed. The effective interaction can be based on a microscopic model of the core wave function, or a more empirical model potential approach can be adopted. An example of the microscopic approach is the series of calculations demonstrating positron binding to a variety of atoms (Ryzhikh, Mitroy, and Varga, 1998b). The core wave function was represented by a HF wave function. The direct interaction with the core was straightforward to compute since this was effectively a single-particle potential. The exchange interaction with the core could also be computed provided the core single electron orbitals were expanded as a linear combination of Gaussians (Ryzhikh, Mitroy, and Varga, 1998b). Model potentials used

to describe interactions with closed-shell systems tend to be more phenomenological in nature.

When fixed core potentials are used, the Pauli principle requires that the valence particles be prevented from occupying the already occupied core states. The orthogonalizing pseudoprojector (OPP) (Krasnopol'skii and Kukulin, 1974; Kukulin and Pomerantsev, 1978) and the orthogonality condition model of Saito (1969) can be used to enforce the requirements of the Pauli principle. In the area of quantum chemistry, Bonifacic and co-workers developed a model potential method (Bonifacic and Huzinga, 1974) that is related to OPP. The full projection operator of the $\hat{Q}\hat{H}\hat{Q}$ form (where $Q = 1 - P$, and P is the projector on the occupied states) is not used due to the computational expense of evaluating its matrix elements.

The basic philosophy of the OPP as put forward by Krasnopol'skii and Kukulin is to add a penalty function $\lambda\hat{P}$ to the Hamiltonian to enforce orthogonality with those orbitals to be excluded from the active space. The penalty function is an operator of the type

$$\lambda\hat{P} = \sum_i \lambda |\varphi_i\rangle\langle\varphi_i|, \tag{80}$$

where $\lambda\hat{P}$ is constructed by summing over the single-particle orbitals to be excluded from the calculation (typically the orbitals occupied by the core electrons). Provided λ is positive, the expectation value of this operator is always positive. When λ is chosen to be a sufficiently large number, any component of the wave function which is not orthogonal to the core will tend to increase the energy. The orbitals $|\varphi_i\rangle$ in Eq. (80) have a Gaussian form. Therefore, any variational method which seeks to minimize the energy will attempt to construct a wave function with a minimum overlap with the core orbitals. This can be seen in Fig. 3, which depicts the expectation value $\langle\hat{P}\rangle$ as a function of λ. Application of the pseudoprojection operator causes an abrupt change in the structure of the valence wave function once λ becomes large enough (Mitroy and Ryzhikh, 1999c).

The OPP method is most effective when the number of excluded states is relatively small. When the core complexity increases, the complexity of the nodal surfaces increases, requiring a larger ECG expansion for the valence particles. In addition, the projector results in some of the basis functions having large positive energy expectation values. The overall numerical precision of the calculation is degraded by the cancellation of the large positive matrix elements inherent to the eigenvalue calculation. The evaluation of the $\lambda\hat{P}$ matrix elements and any exchange matrix elements involving the core also becomes more time consuming as the complexity of the core increases.

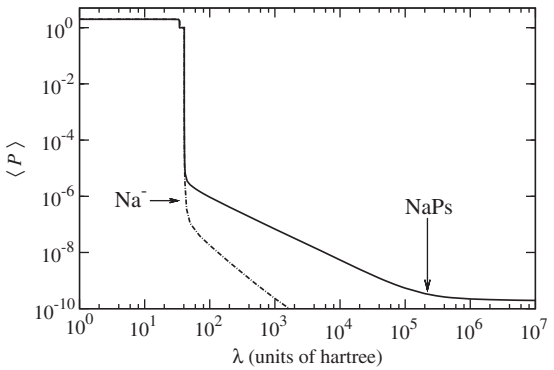

FIG. 3. The expectation value of the projection operator $\langle\hat{P}\rangle$ for the Na^- ion and the sodium plus positronium (NaPs) ground state as a function of λ (Na^+ core has been assumed). Adapted from Mitroy and Ryzhikh, 1999c.

H. The Gaussian expansion method

The Gaussian expansion method (GEM), also known as the coupled-rearrangement-channel Gaussian basis, was first developed in the late 1980s (Kamimura, 1988; Kameyama, Kamimura, and Fukushima, 1989; Hiyama, Kino, and Kamimura, 2003) to determine the structure of muonic molecules, specifically the $dt\mu$ three-body system. The wave function was written as

$$\Psi = \psi_{t\mu}(\mathbf{r}_1)\psi_d(\mathbf{R}_1) + \psi_{d\mu}(\mathbf{r}_2)\psi_t(\mathbf{R}_2) + \psi_{dt}(\mathbf{r}_3)\psi_\mu(\mathbf{R}_3). \tag{81}$$

The channel wave function $\psi_{t\mu}(\mathbf{r}_1)$ describes the structure of the $t\mu$ cluster while $\psi_d(\mathbf{R}_1)$ describes the motion of d about the $t\mu$ cluster. All channel functions are written as linear combinations of Gaussians, which allows for an easy evaluation of the matrix elements. Figure 4 shows the different sets of Jacobi coordinates that would be used in the construction of the three-body wave function. The GEM method is essentially an ECG-based approach, but based on a physically motivated coupled-channels expansion of the total wave function.

The Gaussian basis functions used to represent the radial dependence for a particular channel in GEM often have their exponents chosen to be a geometric progression

$$\alpha_n = \alpha_1/A^{n-1}. \tag{82}$$

This basis is sometimes called an even-tempered basis. The value of A depends on the shape and range of the interaction. It is typically between 1.15 and 1.5. The overlap between adjacent basis functions is constant in this basis. Such a basis is characterized by three parameters, α_1, A, and $\mathcal{N}$, the number of Gaussians. It is relatively simple to optimize such a basis. To some extent, the GEM substitutes the time-consuming optimizations of the SVM by using a larger basis that does not need an intensive optimization of the nonlinear parameters. The extension of the GEM to four- and five-body systems results in a significant increase in the basis-set dimension as the number of different sets of Jacobi

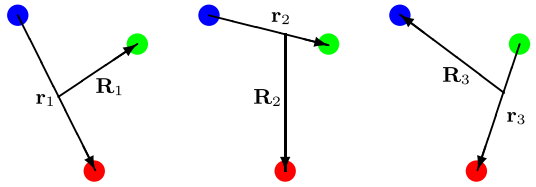

FIG. 4 (color online). Schematic diagram showing the three different sets of Jacobi coordinates that are used in the GEM representation of a three-body system.

recouplings increases rapidly (Hiyama, Kino, and Kamimura, 2003; Hiyama *et al.*, 2005).

I. Other types of basis functions

1. Hylleraas and related functions

Hylleraas and related basis functions have been used to get very accurate energies for small atoms with no more than three electrons. In particular, extremely high accuracy (more than 40 digits for the energy) has been achieved for helium (Schwartz, 2006a, 2006b; Nakashima and Nakatsuji, 2007). Not all approaches to the determination of the helium ground state wave function are equally useful. Comparison with experiment requires calculations of relativistic corrections to the energy through the use of perturbation theory. This becomes difficult if the mathematical structure of the basis functions is excessively complex. For example, the calculations of Schwartz include logarithmic factors in the basis functions. Hylleraas basis functions satisfy the dual criteria of being able to generate very accurate energies as well as permit the evaluation of relativistic corrections (Drake, 1987). Recently, a novel method of solving the Schrödinger equation, the iterative-complement-interaction (ICI) method, was developed and has been used with correlated basis functions to generate very accurate energies for the He and H_2 ground states (Nakashima and Nakatsuji, 2007; Nakatsuji *et al.*, 2007).

The Hylleraas basis functions for a three-electron system are written as

$$r_1^{j_1} r_2^{j_2} r_3^{j_3} r_{12}^{j_{12}} r_{23}^{j_{23}} r_{31}^{j_{31}} e^{-\alpha_t r_1 - \beta_t r_2 - \gamma_t r_3} \mathcal{Y}^{LM}_{(\ell_1\ell_2)\ell_{12},\ell_3}(\hat{\mathbf{r}}_1, \hat{\mathbf{r}}_2, \hat{\mathbf{r}}_3), \tag{83}$$

where $\mathcal{Y}^{LM}_{(\ell_1\ell_2)\ell_{12},\ell_3}$ is a vector coupled product of one-electron spherical harmonics. The index t labels different sets of nonlinear parameters. Except for some truncations to avoid linear dependence, all terms are included such that

$$j_1 + j_2 + j_3 + j_{12} + j_{23} + j_{31} \le \Omega, \tag{84}$$

where Ω is some integer. Calculations using these basis sets are typically performed using multiple precision arithmetic and often use double or multiple sets of exponential parameters (Yan *et al.*, 1996; Puchalski and Pachucki, 2006, 2008; L. M. Wang *et al.*, 2011).

A variation on the Hylleraas basis is the correlated Slater basis (Thakkar and Smith, Jr., 1977; Frolov and Smith, Jr., 1995; Korobov, 2000; Puchalski, Kędziera, and Pachucki, 2009). The radial part of such a function is written as

$$\psi = \exp(-\alpha_1 r_1 - \alpha_2 r_2 - \alpha_3 r_3 - \alpha_{12} r_{12} - \alpha_{13} r_{13} - \alpha_{23} r_{23}). \tag{85}$$

No distinction is made between the correlated Slater basis and the Hylleraas basis in this review. The most accurate energies (including relativistic corrections) for Li and Li-like ions have been computed with Hylleraas basis functions (L. M. Wang *et al.*, 2011).

2. James-Coolidge–type functions for H_2

Generalizations of the James and Coolidge (GJC) functions (James and Coolidge, 1933) have been used for calculations of the hydrogen molecule. The GJC functions have the form

$$\begin{aligned}\phi(1,2) = {} & \exp(-\alpha_1\xi_1 - \alpha_2\xi_2)\xi_1^{n_a}\eta_1^{n_b}\xi_2^{n_c}\eta_2^{n_d}(r_{12}/R)^{n_e} \\ & \times \exp(\beta_1\xi_1 + \beta_2\xi_2)[\exp(\beta_1\eta_1 + \beta_2\eta_2) \\ & + (-1)^P \exp(-\beta_1\eta_1 - \beta_2\eta_2)],\end{aligned} \tag{86}$$

where $\xi_i = (r_{iA} + r_{iB})/R$, $\eta_i = (r_{iA} - r_{iB})/R$, and P equals 0 and 1 for gerade and ungerade symmetries, respectively (Kołos and Wolniewicz, 1965; Kolos and Rychlewski, 1993). The GJC functions cannot only be used to treat the H_2 in the BO (fixed nuclear positions) approximation. Adiabatic and nonadiabatic corrections can be computed as well (Wolniewicz, 1995). Also relativistic corrections to the energy can be evaluated (Kołos and Wolniewicz, 1964a, 1964b, 1965).

3. Expansions in products of orbitals

Most atomic structure calculations use the orbital-based methods. The basic building block is the state function constructed from antisymmetric products of orbitals (Hibbert, 1975). The limitations of this approach for high precision work are exposed by considering the helium atom.

The general properties of the CI expansion have been known since the work of Schwartz (1962), which provided the underlying foundation for later investigations (Carroll, Silverstone, and Metzger, 1979; Hill, 1985; Ottschofski and Kutzelnigg, 1997; Bromley and Mitroy, 2007a). The orbital CI expansion is slowly convergent with respect to $L_{\max}$, the maximum angular momentum of any orbital included. In particular, the leading term to the energy increment is expected to behave at high L as

$$\Delta E_L = \langle E\rangle_L - \langle E\rangle_{L-1} \approx \frac{A}{(L+\frac{1}{2})^4}. \tag{87}$$

The most recent numerical investigation of this issue was carried out by Bromley and Mitroy (2007a). A large CI calculation, consisting of 465 single particle states, including orbitals up to $L_{\max} = 12$, gave an energy of $-2.903\,712\,786$ hartree for the helium atom to be compared with $-2.903\,724\,377$ hartree (Drake, 1996). The expectation value for the coalescence matrix element $\langle\delta(\mathbf{r}_1 - \mathbf{r}_2)\rangle$ was 0.1097 a.u. which is 3% larger than the exact value of 0.1063 (Drake, 1996).

Extrapolation techniques need to be applied for CI calculations to produce results even remotely close to the precision achievable by correlated basis sets. Extrapolations need to be applied to both the radial and angular basis sets. When this is done, the energy is $-2.903\,724\,38$ hartree (Bromley and Mitroy, 2007a).

The helium atom to some extent represents the best case scenario for the convergence of an orbital CI expansion. The convergence is much slower if the system exhibits any degree of clustering. Extreme examples of the slow convergence of the CI method occur for exotic positron binding atoms. The maximum L in a (fixed core) CI calculation of the e^+Li

ground state was $L_{\max} = 30$ and even then the binding energy after extrapolation was grossly underestimated (Bromley and Mitroy, 2002b).

The analog of the CI method in nuclear structure physics is the no-core shell model (Navrátil *et al.*, 2009). These calculations are based on realistic two-nucleon or two- plus three-nucleon interactions. The strongly repulsive nature of the interaction can slow down the convergence unless various techniques such as modifying the interaction are used to circumvent the problem.

Besides the CI approach, there is another popular method based on single-particle orbitals. This is the nonvariational coupled-cluster (CC) method, which is widely used in quantum chemistry (Cizek, 1966; Bartlett and Musiał, 2007). The coupled-cluster method with single, double, and noniterative triple [CCSD(T)] excitations is particularly popular.

One way to improve convergence of CI calculations is to include Slater determinants multiplied by r_{ij} correlation factors (Sims and Hagstrom, 1971; Kutzelnigg, 1985; Sims and Hagstrom, 2011). Such calculations are sometimes referred to as R12-CI calculations.

J. Many-body perturbation theories and coupled-cluster methods

The slow $O(L^{-4})$ convergence of the energy for orbital CI-type calculations involving the Coulomb interaction also manifests itself in calculations based on many-body perturbation theory (MBPT) or CC methods. Generating precise estimates of perturbation theory energies using orbital basis sets requires a large number of partial waves typically followed by an extrapolation to the $L \rightarrow \infty$ limit.

In atomic and molecular physics, MBPT is most often associated with the Møller-Plesset partition of the Hamiltonian (Møller and Plesset, 1934), i.e., the zeroth-order Hamiltonian is the Fock operator. The nth-order energy correction in this approach is usually denoted as MPn.

The convergence of MP2 theory can be accelerated by writing the two-electron virtual excitations as ECG-type functions as opposed to the product of two single electron states (Szalewicz and Jeziorski, 2010). Such two-electron functions have in the context of MP2 calculations been typically referred to as GTGs (note that it is also common in quantum chemistry calculations on two-electron systems to refer to GTGs as opposed to ECGs). To use the GTGs in MBPT or CC, one has to develop the first-quantized version of such approaches.

In the first-quantized formulation of the CCSD theory, the correlation energy of a closed-shell N-electron system can be expressed as

$$E_{\rm corr} = \langle \Phi | H T_2 \Phi \rangle + \tfrac{1}{2} \langle \Phi | H T_1^2 \Phi \rangle, \tag{88}$$

where H is the Hamiltonian, $\Phi(1, 2, \ldots, N)$ is the HF function, and T_1 and T_2 are the one- and two-electron cluster operators

$$T_1 = \sum_{i=1}^{N} \hat{t}_1(i), \qquad \hat{t}_1 = \sum_{\alpha=1}^{N/2} |\tau_\alpha\rangle\langle\phi_\alpha|, \tag{89}$$

$$T_2 = \sum_{j>i=1}^{N} \hat{t}_2(i, j),$$
$$\hat{t}_2 = \sum_{\alpha,\beta=1}^{N/2} |\tau^1_{\alpha\beta}\rangle\langle\phi^1_{\alpha\beta}| + |\tau^3_{\alpha\beta}\rangle\langle\phi^3_{\alpha\beta}|. \tag{90}$$

In the equations above, ϕ_α are the canonical HF orbitals, $\phi^s_{\alpha\beta}$ are their (anti)symmetrized products

$$\phi^s_{\alpha\beta} = [1 + (2 - s)P_{12}]\phi_\alpha(1)\phi_\beta(2), \tag{91}$$

where P_{12} permutes the electrons, τ_α are one-electron cluster functions, and $\tau^s_{\alpha\beta}$ are (anti)symmetrized two-electron cluster functions, fulfilling the orthogonality and strong orthogonality (SO) conditions, respectively, relative to the occupied space. The cluster functions are solutions of the equations

$$[\hat{f} - \varepsilon_\alpha]\tau_\alpha = S_\alpha, \tag{92}$$

$$[\hat{f}(1) + \hat{f}(2) - \varepsilon_\alpha - \varepsilon_\beta]\tau^s_{\alpha\beta} = R^s_{\alpha\beta}, \tag{93}$$

where $\hat{f}$ and ε_α are the one-electron Fock operators and orbital energies, respectively, and the right-hand sides are defined by Bukowski, Jeziorski, and Szalewicz (1999, 2003).

Each of the terms S_α ($R^s_{\alpha\beta}$) depends, in general, on all functions $\tau_{\alpha'}$ ($\tau_{\alpha'}, \tau^s_{\alpha'\beta'}$). Therefore, except for the MP2 approach, Eqs. (92) and (93) define coupled sets of equations that must be solved iteratively. Equation (93) is solved by a minimization of the Hylleraas functional

$$\mathcal{J}^s_{\alpha\beta}[\tilde{\tau}] = \langle\tilde{\tau}|\hat{f}(1) + \hat{f}(2) - \varepsilon_\alpha - \varepsilon_\beta|\hat{q}_2\tilde{\tau}\rangle - 2\,\mathrm{Re}\langle\tilde{\tau}|R^s_{\alpha\beta}\rangle, \tag{94}$$

where the trial functions $\tilde{\tau}$ approximating $\tau^s_{\alpha\beta}$ are expanded in a GTG basis and $\hat{q}_2$ is the SO projector. Since in the coupled-cluster method the term involving $R^s_{\alpha\beta}$ is difficult to calculate, the functional is usually minimized only with respect to the linear parameters of the GTG expansion. This involves solving a linear system of equations. The nonlinear GTG parameters can be optimized in advance at the MP2 level. In most cases, the MP2-optimized bases lead to satisfactory convergence of the coupled-cluster energies. Recently, a new, infinite-order functional was presented (Przybytek, Jeziorski, and Szalewicz, 2009), which can be used in cases where post-MP2 contributions to the CCD or CCSD energies are large.

Even at the MP2 level, the straightforward variational solution of Eq. (94) (Pan and King, 1970, 1972; Adamowicz and Sadlej, 1978) leads to serious complications, because the presence of both the SO projector $\hat{q}_2$ and the Fock operators $\hat{f}(i)$ results in a large number of three- and four-electron integrals. This problem has been remedied by adding a penalty term which vanishes for orthogonal pair functions. This approach is called the weak-orthogonality method (Szalewicz *et al.*, 1982; Wenzel *et al.*, 1986) and is somewhat similar to the OPP projection discussed in Sec. III.G.

Additional approximations are necessary in coupled-cluster calculations since the $\hat{q}_2$ projector contained in the $R^s_{\alpha\beta}$ term still renders the calculations very time consuming. The most efficient approach currently used in practical calculations is called "superweak orthogonality plus projection" (Szalewicz *et al.*, 1984). In this method, $\hat{q}_2$ is replaced by the much simpler operator $1-\hat{p}(1)\hat{p}(2)$, where $\hat{p}(i)$ ensures orthogonality to the occupied orbital space. The cluster functions obtained as solutions of Eq. (93) contain then some SO violating components, which can be, however, projected out before using these functions in the next iteration. In this projection, instead of the original SO operator $\hat{q}_2$, one uses an approximate SO operator defined as $\hat{q}_B = \hat{P}_B\hat{q}_2$, where $\hat{P}_B$ is the orthogonal projector on the geminal basis set used. Since the superweak plus projection approach becomes equivalent to the exact SO projection in the limit of the complete GTG basis, all practical calculations converge to the correct result as the basis goes to completeness. The superweak plus projection method leads to a dramatic reduction of the computational cost. In particular, no integrals more complicated than three-electron ones appear at the factorizable CCD level. This is of considerable practical importance, because the contributions beyond factorizable coupled cluster are less sensitive to electron correlations and are relatively easy to saturate with orbital methods (Cencek *et al.*, 2004; Patkowski *et al.*, 2007).

Another group of methods using explicitly correlated functions in MBPT and CC calculations are the so-called R12 and F12 approaches. The convergence of a CI expansion can be dramatically improved by multiplying only the leading configuration by the factor r_{12} (Kutzelnigg, 1985). The resulting many-electron integrals can be reduced to two-electron ones by inserting an approximate resolution of the identity and this has been done at various levels of MBPT and CC theory (Kutzelnigg and Klopper, 1991; Klopper and Noga, 2003; Helgaker, Klopper, and Tew, 2008). One consequence of this is that the R12-MP2 energies are no longer upper bounds to the exact MP2 values (May *et al.*, 2005).

A weakness of the linear-r_{12} factor is that at large interelectronic separations it is difficult to damp it by exponential terms. This observation led to a family of the so-called F12 methods where r_{12} is replaced by a function $f(r_{12})$ which behaves similarly to r_{12} at small separations but does not diverge at large ones. This function can be written as a linear combination of GTGs (Bukowski, Jeziorski, and Szalewicz, 1994; Persson and Taylor, 1996; Dahle *et al.*, 2007). After the inclusion of the resolution of identity technique (May and Manby, 2004), the F12 method was implemented in standard quantum chemistry packages (Adler, Knizia, and Werner, 2007; Shiozaki *et al.*, 2009). A way of including such factors in the triple-excitation functions at the CCSD(T) level was recently proposed by Kohn (2009).

Whereas the most effective implementations of F12-MBPT and F12-CC methods use only modestly larger computer resources than calculations in the same orbital-only basis and at the same level of theory, this effectiveness has been achieved by applying a series of approximations. As a result F12-MBPT and F12-CC approaches may not be competitive with orbital calculations in very large basis sets followed by extrapolations to the complete basis-set limit if one aims at benchmark accuracies (Patkowski and Szalewicz, 2010; Patkowski, 2012).

K. Hyperspherical methods

The hyperspherical and hyperspherical-harmonic methods constitute general approaches to the solution of the three- and N-body systems (Fabre de La Ripelle, 1983; Lin, 1995; Viviani, Kievsky, and Rosati, 1995; Krivec, 1998; Rittenhouse *et al.*, 2011). One typically refers to hyperspherical calculations for the three-body calculation and hyperspherical harmonics (HH) for systems with $N>3$. The HH wave function expands the relative wave function Ψ in terms of a complete set of channel functions $\Phi_\nu(\mathbf{\Omega};R)$, which depend parametrically on the hyperradius R, and weight functions $F_{\nu q}(R)$:

$$\Psi = \sum_{\nu q} R^{-(3N-4)/2} F_{\nu q}(R)\Phi_\nu(\mathbf{\Omega};R). \tag{95}$$

Here $\mathbf{\Omega}$ collectively denotes the $3N-4$ hyperangular coordinates and R is the hyperradius, $\mu R^2 = \sum_{j=1}^{N} m_j \mathbf{r}_j^2$; μ denotes the hyperradial mass, which can be viewed as a conveniently chosen scaling parameter (Rittenhouse *et al.*, 2011). The hyperradius R can be interpreted as a measure of the overall size of the system and plays a role analogous to the radial distance coordinate in the reduced mass two-body problem. By construction, in the adiabatic hyperspherical representation the channel functions Φ_ν are solutions to the hyperangular Schrödinger equation

$$H_{\rm ad}\Phi_\nu(\mathbf{\Omega};R) = U_\nu(R)\Phi_\nu(\mathbf{\Omega};R), \tag{96}$$

where

$$H_{\rm ad} = \frac{\hbar^2\Lambda^2}{2\mu R^2} + \frac{\hbar^2(3N-4)(3N-6)}{8\mu R^2} + V_{\rm int}. \tag{97}$$

The grand angular momentum operator Λ contains derivatives with respect to the $3N-4$ hyperangles and can be formally viewed as a generalized angular momentum operator. Plugging Eq. (95) into the relative Schrödinger equation $(T_{\rm rel}+V_{\rm int})\Psi = E_{\rm rel}\Psi$, where $T_{\rm rel}$ denotes the kinetic energy operator associated with the relative degrees of freedom, results in an infinite set of coupled ordinary differential equations that depend on the hyperangular eigenvalues $U_{\nu'}(R)$ and the hyperangular coupling matrix elements $P_{\nu'\nu}(R)$ and $Q_{\nu'\nu}(R)$, which involve the first and second derivatives of the channel functions Φ_ν with respect to R (Rittenhouse *et al.*, 2011).

L. Monte Carlo techniques

Monte Carlo approaches (Ceperley and Alder, 1986; Hammond, Lester, Jr., and Reynolds, 1994) exhibit a more favorable scaling with respect to the computational effort associated with an increasing number of degrees of freedom than the ECG approach. A key advantage of Monte Carlo methods is that they can be applied to few-body systems as well as large systems with as many as a few thousand particles (Lester, Jr., Rothstein, and Tanaka, 2002).

Commonly employed Monte Carlo approaches are the variational Monte Carlo (VMC) and the diffusion Monte Carlo (DMC) or Green's function Monte Carlo (GFMC) approaches (Reynolds *et al.*, 1982; Hammond, Lester, Jr., and Reynolds, 1994; Kosztin, Faber, and Schulten, 1996), the path integral Monte Carlo (Ceperley, 1995; Boninsegni, Prokof'ev, and Svistunov, 2006) approach, and the auxiliary field Monte Carlo approach (Blankenbecler, Scalapino, and Sugar, 1981; Zhang and Krakauer, 2003). For this review, the VMC and DMC techniques are the most relevant.

The VMC approach is built on the Ritz variational principle. As in the ECG approach, the wave function of the state of interest is parametrized in terms of a set of variational parameters. However, in contrast to the ECG approach, the Hamiltonian matrix elements are generally not known analytically but instead evaluated stochastically. The stochastic nature of the algorithm introduces a statistical uncertainty of the energy expectation value, which can be decreased systematically by increasing the sampling. The variational parameters are typically optimized by minimizing some combination of the energy expectation value and its variance, and the treatment of excited states is possible through application of the Gram-Schmidt orthogonalization scheme. Expectation values such as structural properties can be calculated fairly straightforwardly. The accuracy of the VMC results crucially depends on the quality of the variational wave function employed. In certain cases, the resulting variational description is sufficient for the task at hand. More often, though, the variational wave function serves as an input for the DMC approach.

In the DMC approach, the ground state energy and structural ground state properties are obtained by starting with an initial "walker distribution," which can be thought of as a stochastic representation of the many-body wave function, and by then projecting out the lowest stationary eigenstate using a time propagation. The time propagation in the DMC algorithm is similar to that of the "standard" propagation scheme in imaginary time (Press *et al.*, 1992). However, to allow for efficient treatment of systems with many degrees of freedom, a stochastic realization of the short-time Green's function propagator is used. In most applications, importance sampling is employed so that the walker distribution represents the product of the true wave function and the so-called guiding function (which is, in most cases, obtained by the VMC approach). If the eigenstate of interest and the guiding function employed are nodeless, as is the case for the ground state of bosonic systems, the DMC method results in the exact ground state eigenenergy, within statistical uncertainties.

The fermionic wave functions exhibit nodal surfaces which cannot be crossed by the walkers. Therefore, for fermionic systems, the fixed-node DMC method is used (Reynolds *et al.*, 1982). In the fixed-node DMC method, the nodal surface of the many-body wave function coincides with that of the guiding function and is, in general, only known approximately. The fixed-node DMC method results in an upper bound to the ground state of fermionic systems (Reynolds *et al.*, 1982). In the DMC and fixed-node DMC approaches, the determination of expectation values that do not commute with the Hamiltonian can be done using the so-called mixed or pure estimators. The former results in expectation values that are calculated with respect to the mixed density, i.e., the product of the exact eigenstate and the guiding function, while the latter is exact within statistical uncertainties.

IV. ATOMIC STRUCTURE APPLICATIONS

A. Motivation

One of the most important and popular applications of the few-body methods is the solution of the Schrödinger equation for light few-electron atomic systems. Such systems can be "ordinary" atomic systems, but also exotic systems exist where the Coulombic particles, positrons, muons, and antiprotons are bound to the atom. As illustrated in this section, the ECG methodology proved to be very successful in solving atomic few-body problems.

One area of activity is determination of the energies and wave functions of ordinary atoms with less than six electrons to increasingly higher precision. These calculations serve to benchmark the theoretical methods used to calculate atomic properties for larger atoms. In addition, highly precise calculations coupled with highly precise experiments provide a stringent test bed for the fundamental principles of quantum mechanics and QED that underlie modern physics. Another area of activity is the investigation of exotic atoms which can be difficult to describe with the more generic methods usually applied in atomic structure calculations.

Accurate ECG calculations can provide benchmark tests for other approaches. They also allow for the extraction of correlation functions that can be used in model calculations or to depict structural information. The ECG approach can also be used to calculate the properties of atomic systems in external potentials (e.g., atoms in magnetic fields or atoms confined in cavities or optical traps).

B. Benchmark nonrelativistic calculations for atoms

The most accurate energies for two- and three-electron atoms have been obtained with Hylleraas-type wave functions. For four- and five-electron atomic systems, the most accurate energies and wave functions have been obtained using the ECGs. In this section, we first report on the nonrelativistic calculations assuming infinite nuclear mass. Table IV gives energies for atoms and ions with two to five electrons. All energies in this section are given in hartree (1.0 hartree = 27.211 385 05 eV). Sometimes high precision *ab initio* calculations include extrapolations to the estimated nonrelativistic limit. No such estimated variational limits are included in Table IV. Corrections due to finite nuclear mass, relativistic, and QED effects are discussed later.

1. The hydrogen atom

The energy (-0.50 hartree) of the hydrogen atom is known exactly. Gaussian basis sets do a reasonable job of reproducing the hydrogen energy. An optimized basis of dimension 20 is accurate to 10^{-10} hartree while a basis of dimension 40 is accurate to 10^{-15} hartree (Cencek and Kutzelnigg, 1996).

TABLE IV. Total nonrelativistic energies (assuming infinite nuclear mass) for the ground and excited states of some few-electron atoms and ions. All values are given in hartrees. The values in parentheses for DMC calculations give the statistical uncertainty, while those for other calculations give an estimate of the energy uncertainty arising from the finite basis set.

System	Method	Basis size	Energy
He($1s^2$)	CI (Bromley and Mitroy, 2007a)	8 586	−2.903 712 786
	ECG (Rybak, Szalewicz, and Jeziorski, 1989)	100	−2.903 723 818 0
	ECG (Cencek and Kutzelnigg, 1996)	1 200	−2.903 724 377 030 1
	ECG (Komasa, 2001)	600	−2.903 724 377 022
	HYL (Drake, Cassar, and Nistor, 2002)	2 358	−2.903 724 377 034 119 598 305
	HYL (Korobov, 2002)	5 200	−2.903 724 377 034 119 598 311 1587
	ICI (Nakashima and Nakatsuji, 2007)		−2.903 724 377 034 119 598 311 159 245 194 404 446 696 905 37
	HYL-LOG (Schwartz, 2006a, 2006b)	24 099	−2.903 724 377 034 119 598 311 159 245 194 404 446 696 925 309 838
Li($1s^2 2s$)	CI (Jitrik and Bunge, 1997)		−7.478 025 4
	ECG (Komasa, 2001)	1 536	−7.478 060 314 3
	ECG (Stanke *et al.*, 2008b)	10 000	−7.478 060 323 81
	HYL (L. M. Wang *et al.*, 2011)	26 520	−7.478 060 323 910 134 843
Li($1s^2 2p$)	ECG (Komasa, 2001)	3 700	−7.410 156 22
	HYL (L. M. Wang *et al.*, 2011)	30 224	−7.410 156 532 650 66
Li($1s^2 3d$)	ECG (Sharkey, Bubin, and Adamowicz, 2011c)	4 000	−7.335 523 542 97(60)
	HYL (Wang *et al.*, 2012)	32 760	−7.335 523 543 524 685
Be^+($1s^2 2s$)	ECG (Stanke *et al.*, 2008a)	8 000	−14.324 763 176 4
	HYL (Puchalski, Kędziera, and Pachucki, 2009)	13 944	−14.324 763 176 790 150
Li^-($1s^2 2s^2$)	ECG (Bubin, Komasa *et al.*, 2009)	10 000	−7.500 776 613 4(200)
Be($1s^2 2s^2$)	CI (Bunge, 2010)	2 614 689	−14.667 347 30
	ECG (Komasa, Cencek, and Rychlewski, 1995)	1 200	−14.667 355 0
	ECG SVM (Mitroy, 2011)	1 800	−14.667 354 0
	ECG (Komasa, Rychlewski, and Jankowski, 2002)	1 600	−14.667 355 5
	ECG (Stanke, Komasa *et al.*, 2009)	10 000	−14.667 356 486(15)
	CI-R12 (Sims and Hagstrom, 2011)	41 871	−14.667 356 411
Be($1s^2 2s 2p$)	ECG (Bubin and Adamowicz, 2009)	5 000	−14.473 451 311(70)
Be($1s^2 2s 3s$)	ECG (Stanke, Komasa *et al.*, 2009)	10 000	−14.418 240 328(30)
B^+($1s^2 2s^2$)	CI (Almora-Diaz and Bunge, 2010)	530 335	−24.348 861 07
	ECG (Komasa, Rychlewski, and Jankowski, 2002)	1 600	−24.348 883 2
	ECG (Bubin *et al.*, 2010b)	10 000	−24.348 884 446(35)
C^{2+}($1s^2 2s^2$)	ECG (Komasa, Rychlewski, and Jankowski, 2002)	1 600	−36.534 849 7
	ECG (Bubin *et al.*, 2010a)	10 000	−36.534 852 338(35)
B($1s^2 2s^2 2p$)	CI (Almora-Diaz and Bunge, 2010)	16 352 813	−24.653 837 33
	ECG (Bubin and Adamowicz, 2011b)	5 100	−24.653 866 08(250)
	DMC (Seth, Ríos, and Needs, 2011)		−24.653 79(3)
B($1s^2 2s^2 3s$)	ECG (Bubin and Adamowicz, 2011b)	5 100	−24.471 393 06(50)
C^+($1s^2 2s^2 2p$)	ECG (Bubin and Adamowicz, 2011a)	5 100	−37.430 880 49(250)
	DMC (Seth, Ríos, and Needs, 2011)		−37.430 73(4)

2. Two-electron atoms

Table IV shows a sampling of energies for a variety of calculations based on ECGs and compares the results with other methods. The slow convergence of the CI energy is very apparent. The best ECG-based wave function, namely, the 1200 term function (Cencek and Kutzelnigg, 1996) is accurate to 4×10^{-12} hartree. This is still much less accurate than calculations based on Hylleraas-type wave functions with logarithmic factors which are converged to more than 40 significant digits (Schwartz, 2006a, 2006b; Nakashima and Nakatsuji, 2007).

Helium-atom calculations using ECGs have to a certain extent been motivated by a desire to test ECG methods as opposed to a desire to obtain the most accurate energies. The results of some of the earlier calculations which did not extensively optimize the nonlinear parameters of the ECG basis are also listed in Table IV.

3. Three-electron atoms

The best three-electron atom energies are obtained with Hylleraas-type wave functions. Although the accuracy reached with such functions for lithium is far from that

achievable for helium, it is sufficient to extract very subtle QED effects by comparison of the theoretical results with the most sophisticated contemporary experiments (Puchalski and Pachucki, 2008; Yan, Nörtershäuser, and Drake, 2008). The first ECG calculations for Li were reported in 1993 (Kinghorn and Poshusta, 1993). Since then much progress has been made in obtaining accurate ground and excited state wave functions (Komasa, 2001; Rychlewski and Komasa, 2003; Stanke *et al.*, 2008b; Sharkey, Bubin, and Adamowicz, 2011c), as seen by the energies in Table IV. The best ECG energies are accurate to about 10^{-10} hartree. The ECG results for the ground state lithium atom are compared with the state-of-the-art result from Hylleraas-type (L. M. Wang *et al.*, 2011) wave functions.

There have been applications of ECG functions to the three-electron Be^+ ion (Pachucki and Komasa, 2004b; Stanke *et al.*, 2008a). The ground state energy obtained with an 8000-term ECG basis (Stanke *et al.*, 2008a) is only 0.4 nanohartree different from the best Hylleraas energy (Puchalski, Kędziera, and Pachucki, 2009).

4. Four-electron atoms

The first and rather preliminary ECG calculations for the total energy of the beryllium atom achieved near millihartree accuracy (Schwegler, Kozlowski, and Adamowicz, 1993). Since then, there have been numerous treatments reporting precisions of close to or better than 10^{-6} hartree (Komasa, Cencek, and Rychlewski, 1995; Komasa, 2001; Komasa, Rychlewski, and Jankowski, 2002; Pachucki and Komasa, 2006b; Stanke *et al.*, 2007a; Stanke, Komasa *et al.*, 2009) with the best ECG wave functions having energies precise to 10 nanohartree (Stanke *et al.*, 2007a; Stanke, Komasa *et al.*, 2009). All these calculations achieved a lower energy than the most recent CI calculation employing 2 614 489 configurations (Bunge, 2010). Recently a CI-R12 calculation achieved a comparable accuracy (Sims and Hagstrom, 2011) but its upper bound is still inferior to the most recent ECG energy (Stanke, Komasa *et al.*, 2009).

Calculations have been extended to treat members of the Be isoelectronic series (Komasa, Rychlewski, and Jankowski, 2002). They include the low-lying excited states and encompass states with nonzero angular momentum (Komasa and Rychlewski, 2001; Stanke *et al.*, 2007b; Stanke, Komasa *et al.*, 2009; Sharkey, Bubin, and Adamowicz, 2011b).

The advantages of applying a direct versus a stochastic optimization can be seen in Table IV. The best SVM energy for Be equals to −14.667 354 hartree with 1800 ECGs is 10^{-6} hartree higher than the energy of Komasa, Cencek, and Rychlewski (1995) obtained with only 1200 ECGs.

The B^+ ECG binding energy is 4×10^{-5} hartree smaller in magnitude than the best semiempirical estimate of the exact nonrelativistic energy, namely, −24.348 92 hartree (Chakravorty *et al.*, 1993). The semiempirical estimates were derived by performing the relativistic CI calculations to estimate the relativistic contribution to experimental ionization energies. A similar disagreement occurs for C^{2+}, where the semiempirical binding energy, namely, −36.534 99 hartree (Chakravorty *et al.*, 1993) is more than 10^{-4} hartree larger than the best ECG energy. Since there have been independent calculations for four-electron atoms using ECGs that give energies in mutual agreement at the level of 10^{-6} hartree, the conclusion to be drawn is that such calculations give better estimates of the exact nonrelativistic energies than those derived from experiment. This is of broader significance since the semiempirical energies (Chakravorty *et al.*, 1993) are often used as fundamental reference data to test atomic structure calculations for atoms and ions up to the nuclear charge of 28. An update of the recommended table of nonrelativistic energies is probably desirable with the ECG energies being adopted to give the reference for four-electron ions.

5. Five-electron atoms

Recently, ECG-based methods were applied to determine the wave functions of five-electron atoms. Table IV gives the energies of the ground $^2P^o$ state and the excited $^2S^e$ state of the B atom. The latest ECG energies are estimated to have better than 10^{-5} hartree accuracy (Bubin and Adamowicz, 2011b). The ECG-based wave functions give lower energies than the CI calculations (Almora-Diaz and Bunge, 2010) and a DMC calculation (Seth, Ríos, and Needs, 2011). The level of accuracy achieved for five-electron atoms is about 2 orders of magnitude worse than that achieved for four-electron atoms due to additional wave function complexity resulting from an extra electron.

The B $^2P^o$ ECG binding energy is 4×10^{-5} hartree smaller in magnitude than the best semiempirical estimate of the exact nonrelativistic energy, namely, −24.653 91 hartree (Chakravorty *et al.*, 1993). The difference between the ECG and semiempirical energies is about the same size as the difference for B^+. The ECG energy is likely to be more reliable.

6. Inclusion of relativistic effects

Comparison of high precision calculations with experiment requires inclusion of relativistic effects using Eq. (46). This has been accomplished for several lithiumlike and berylliumlike ions (Pachucki and Komasa, 2004b, 2006a, 2006b; Bubin and Adamowicz, 2008; Stanke *et al.*, 2008a, 2008b; Bubin, Komasa *et al.*, 2009; Stanke, Komasa *et al.*, 2009; Bubin *et al.*, 2010a). Table V shows the importance of relativistic effects in the determination of the energy of the $\Delta E(2^1S \rightarrow 3^1S)$ transition of beryllium. The relativistically corrected energy agrees with the experimental value to 0.1 cm^{-1} which is equal to the experimental uncertainty.

TABLE V. Contributions from subsequent terms of the expansion (46) to the Be($2^1S \rightarrow 3^1S$) excitation energy (Stanke, Komasa *et al.*, 2009).

Contribution	ΔE (cm^{-1})
$^{\infty}$Be $E^{(0)}$	54 674.677(2)
^{9}Be $E^{(0)}$	54 671.219(2)
$\alpha^2 E^{(2)}$	6.688(18)
$\alpha^3 E^{(3)}$	−0.506(4)
$\alpha^4 E^{(4)}$	−0.023(6)
E	54 677.378(30)
E_{exp} (Kramida and Martin, 1997)	54 677.26(10)
Difference	0.12(13)

The ability to achieve this level of accuracy rests on two factors. First, the accuracy of the underlying nonrelativistic calculations is about 10^{-8} hartree. Second, the techniques described in Sec. III.C to evaluate the expectation values of the Breit-Pauli Hamiltonian and of the Araki-Sucher operator greatly improve the accuracy of the relativistic and QED corrections.

C. Atoms in magnetic fields

The theoretical interest in the studies of atomic and molecular systems in magnetic field is motivated by the discovery of the strong magnetic field on white dwarfs (Kemp *et al.*, 1970; Angel, Borra, and Landstreet, 1981) ($\approx 10^7$ G) and on the surface of neutron stars (Truemper *et al.*, 1978) ($\approx 10^{12}$ G). The strongest magnetic fields available in the laboratory are about 10^6 G.

In a magnetic field the spherical symmetry of the Coulomb interaction is broken. The geometry of the highly anisotropic charge distribution is challenging for conventional theoretical approaches and high accuracy solutions are only available for the H and He atoms. Precise calculation of the spectra of light elements in the magnetic field assists in the interpretation of the optical absorption spectra and therefore the understanding of the composition of stars' atmosphere.

Various approaches have been used to calculate the energies of atoms in magnetic fields including variational (Vincke and Baye, 1989; Nakashima and Nakatsuji, 2010), HF (Proschel *et al.*, 1982; Jones, Ortiz, and Ceperley, 1996), QMC (Jones, Ortiz, and Ceperley, 1997), and CI (Al-Hujaj and Schmelcher, 2003) calculations.

The Hamiltonian of the few-body system in magnetic field is given by

$$H = \sum_{i=1}^{n} \frac{1}{2m_i}\left(\mathbf{p}_i + \frac{e_i}{c}\mathbf{A}_i\right)^2 + \sum_{i<j}\frac{e_i e_j}{\kappa r_{ij}}, \tag{98}$$

where $\mathbf{A}_i = \frac{1}{2}\mathbf{r}_i \times \mathbf{B}$, $\mathbf{B}$ is the magnetic field, m_i and e_i are the masses and charges, and $\kappa = 4\pi\epsilon$ (ϵ is the dielectric constant of the medium).

The energies of the He and Li atoms (see Tables VI and VII) have been computed with SVM using modified ECGs defined in Eq. (37) (Varga, 2011). The magnetic field is characterized by the parameter $\beta = B/2B_0$, with $B_0 = 2.35 \times 10^{15}$ T. The calculated results are in good agreement with other calculations, in most cases improving the accuracy compared to previous results.

D. Atomic polarizability calculations

While the best nonrelativistic calculations of the $^{\infty}$He dipole polarizability have been performed using Hylleraas basis functions and gave the value of 1.383 192 174 455 (1) a.u. (Pachucki and Sapirstein, 2000), this result cannot be compared with experiment since finite mass, relativistic, and QED effects need to be taken into account. The relativistic corrections up to order α^2 were computed with the ECG basis (Cencek, Szalewicz, and Jeziorski, 2001) and agree with Hylleraas basis calculations (Pachucki and Sapirstein, 2000) and exponentially correlated Slater basis calculations (Łach, Jeziorski, and Szalewicz, 2004) to within 0.02×10^{-6} a.u. The set of α^3 QED corrections, including the electric field correction to the Bethe logarithm, were computed with the exponentially correlated Slater basis (Łach, Jeziorski, and Szalewicz, 2004). The final value of 1.383 760 79(23) a.u. is accurate to about 0.2 ppm. This result includes the mass polarization correction of 48.8345×10^{-6} reduced a.u., an identical value obtained with ECG and Hylleraas basis sets.

A microwave cavity has been used to measure the refractive index of helium to an accuracy of 9 ppm and the value of polarizability derived from this measurement is 1.383 59 (13) a.u. (Schmidt *et al.*, 2007). If the ^{4}He polarizability is taken as a known quantity from theory, then this experiment admits another interpretation. Taking the polarizability and diamagnetic susceptibility as known quantities, the refractive index experiment yields a value for the universal gas constant $R = 8.314\,487(76)$ J/(mol K), which in terms of the error is not far from the recommended value of 8.314 71(15) (Mohr and Taylor, 2005). Boltzmann's constant, the definition of the mol, and the universal gas constant are all interrelated through the identity $R = k_B N_A$. Further improvement in the precision of experiments measuring either the refractive index or the dielectric constant of helium could lead to a redefinition of these quantities in terms of a standard which is based on the calculated helium polarizability (Stone and Stejskal, 2004; Fellmuth, Gaiser, and Fischer, 2006).

TABLE VI. Energies (in hartree) of the singlet state of helium atom with $M = 0$, -1, and -2 as calculated with SVM and Hylleraas-like basis. The SVM calculations used 200 basis states.

β	SVM[a]	HYL[b]	CI (HYL-Gaussian)[c]
		$M = 0$	
0.0	−2.903 723 37		−2.903 71
0.1	−2.895 834 45	−2.895 83	−2.895 81
0.2	−2.872 870 76	−2.872 87	
0.4	−2.788 424 46	−2.788 42	
		$M = -1$	
0.0	−2.123 840 89		−2.123 83
0.1	−2.145 275 02	−2.145 27	−2.145 25
0.2	−2.106 157 55	−2.106 18	
0.4	−1.969 856 31	−1.970 11	
		$M = -2$	
0.0	−2.055 615 73		−2.055 619
0.1	−2.079 373 21	−2.079 49	−2.079 374
0.2	−2.032 415 90	−2.033 08	
0.4	−1.886 524 46	−1.890 21	

[a]Varga (2011).
[b]Scrinzi (1998).
[c]Wang and Qiao (2008).

TABLE VII. Energies (in hartree) of the $1s^2 2s$ $M = 0$ state of Li in a magnetic field as calculated with SVM and Hylleraas-like functions.

β	SVM[a]	HYL[b]
0.000	−7.478 058	−7.477 796
0.009	−7.527 529	−7.527 505
0.25	−7.523 784	−7.523 595
0.4	−7.486 518	−7.486 436

[a]Varga (2011).
[b]Guan and Li (2001).

Another atomic polarizability calculation with potential practical applications is that for the Be atom. ECG-type calculations have given the dipole polarizability of 37.755 a.u. for $^{\infty}$Be (Komasa, 2001). The result has implications for the new generation of atomic frequency standards based on highly forbidden optical transitions (Margolis, 2009; Mitroy, Safronova, and Clark, 2010). Frequency shifts due to temperature-dependent blackbody radiation (BBR) loom as one of the sources of uncertainty in these standards (Mitroy, Safronova, and Clark, 2010). The significance of this result lies in the coincidence that the $^1S^e \rightarrow {}^3P^o$ clock transition of neutral beryllium has the smallest BBR shift of any of the atoms that could potentially serve as frequency standards (Mitroy, 2010a). Besides having the smallest BBR shift, its small size means that first-principles calculations using ECGs permit an accurate estimate of the temperature-dependent correction due to the BBR shift. The use of ^{9}Be for an optical frequency standard is currently a theoretical curiosity since the cooling and trapping of this atom is not possible with the existing technology.

E. Positronic complexes

Apart from positronium, the first mixed electron-positron system predicted to exist was the positronium ion (Ps^- or e^-Ps) (Wheeler, 1946). Subsequently, positronium hydride (Ore, 1951) and the positronium molecule (or dipositronium) (Hylleraas and Ore, 1947) were also shown to be electronically stable. Positron binding systems are, of course, not absolutely stable due to the propensity of the positron to annihilate with the electrons.

Table VIII lists the most recent results for a number of small positron binding systems. The calculations based on ECGs give the best energies for all systems with one exception, namely, Ps^-. The positronium negative (positive) ion is a three-body system and it is accessible to calculation using Hylleraas or exponentially correlated Slater-type basis sets. The PsH system is a four-body system and is amenable to calculations using both ECG and Hylleraas basis functions. The ECG energy is clearly superior in this case. The PsH system has a Ps + H structure and the Ps cluster is not well described using Hylleraas functions with the electron-positron correlations solely represented by r_{ij}^k factors (Yan and Ho, 1999). The DMC energies (Mella, Morosi, and Bressanini, 1999; Mella, Casalegno, and Morosi, 2002) have not achieved the same level of precision as the best ECG and Hylleraas basis function calculations but are in agreement when the statistical uncertainty is taken into consideration.

One class of exotic atomic systems are those atoms or negative ions with an attached positron. The salient feature of these systems is the attractive Coulomb interaction between the positron and atomic electrons. This leads to the wave function having a component that is best characterized as a positronium cluster. As mentioned in Sec. III.I.3, it is difficult to describe such a cluster with a CI wave function and

TABLE VIII. Total energies of some exotic positron binding systems. Only the latest calculations of a given type by a particular group are listed. In all cases the nuclear masses are set to infinity. The uncertainty associated with the DMC calculations is purely statistical and does not take into consideration uncertainties in the definition of the nodal surfaces.

System	Method	Basis size	Energy (hartree)	Binding energy (hartree)
Ps^-	SVM (Krivec, Mandelzweig, and Varga, 2000)	800	−0.262 005 070 226	0.012 005 070 226
	HYL (Korobov, 2000)	2 200	−0.262 005 070 232 980 107 7(3)	0.012 005 070 232 980 107 7(3)
	HH (Krivec, Mandelzweig, and Varga, 2000)	676	−0.262 005 069 5	0.012 005 069 5
PsH	ECG (Bubin and Varga, 2011)	4 000	−0.789 196 766 900(200)	0.039 196 766 900(200)
	HYL (Yan and Ho, 1999)	5 741	−0.789 196 705 1	0.039 196 705 1
	DMC (Mella, Morosi, and Bressanini, 1999)		−0.789 15(4)	0.039 15(4)
e^+PsH	SVM (Zhang and Mitroy, 2007)	1 500	−0.810 254	0.021 057
Ps_2	ECG (Bubin *et al.*, 2007)	6 000	−0.516 003 790 455(50)	0.016 003 790 455(50)
	HYL (Ho, 1986)	400	−0.515 105	0.015 105
$(p^+, 2e^+, 4e^-)$	SVM (Varga, 1999)	800	−1.055 42	0.004 23
e^+He($^3S^e$)	SVM (Mitroy, 2005a)	1 500	−2.250 595 1	0.000 595 1
e^+Li	SVM (Mitroy, 2004)	1 200	−7.532 396	0.002 482
	DMC (Mella, Morosi, and Bressanini, 1999)		−7.532 29(2)	0.002 38(2)
	FCSVM (Mitroy, 2004)	240		0.002 479
LiPs	SVM (Mitroy, 2010b)	2 200	−7.740 431 6	0.012 371
	DMC (Mella, Casalegno, and Morosi, 2002)		−7.739 6(1)	0.011 6(1)
	FCSVM (Mitroy, 2010b)	1 000		0.012 365
e^+LiPs	ECG (Varga, 1999)	800	−7.805 10	0.009 18
e^+Be	SVM (Mitroy, 2010b)	2 200	−14.670 519	0.003 163
	DMC (Mella, Casalegno, and Morosi, 2002)		−14.668 8(4)	0.001 4(4)
	FCSVM (Mitroy, 2010b)	1 023		0.003 181
e^+Na	FCSVM (Mitroy, 2005b)	488		0.000 474
e^+ Mg	FCSVM (Bromley and Mitroy, 2006b)	1 200		0.016 930
	FCCI (Bromley and Mitroy, 2006b)	≈ 500 000		0.017 040
e^+Ca	FCCI (Bromley and Mitroy, 2006b)	≈ 500 000		0.018 930

consequently there had been no conclusive calculation demonstrating positron binding to neutral atoms until 1997 [indicative calculations did exist (Danby and Tennyson, 1988; Dzuba *et al.*, 1995)], when two calculations using ECGs established that e^+Li was electronically stable (Ryzhikh and Mitroy, 1997; Strasburger and Chojnacki, 1998) and has a structure best described as a Ps atom weakly bound to a Li^+ core. The existence of positron binding to electrically neutral atoms and molecules had long been suspected from the results of gas phase positron annihilation spectroscopy. In these experiments, high-energy positrons from a positron source are injected into a gas. After thermalization, the annihilation cross section is measured. Very large annihilation cross sections had been measured for a variety of gases. It is now believed that positrons trapped in vibrational Feshbach resonances (i.e., positrons bound to vibrationally excited states of the molecule) provide the mechanism responsible for the large annihilation cross sections (Gribakin, Young, and Surko, 2010). This mechanism did not gain widespread acceptance until the ability of positrons to form bound states with a variety of atoms (and by implication molecules) was established by variational calculations using ECG basis sets (Ryzhikh, Mitroy, and Varga, 1998b; Reich, 2004).

The stability of e^+Li was independently verified by a hyperspherical calculation (Yuan *et al.*, 1998). Subsequently positron binding to Na (Ryzhikh, Mitroy, and Varga, 1998a, 1998b; Yuan *et al.*, 1998), Be (Ryzhikh, Mitroy, and Varga, 1998b), Mg (Ryzhikh, Mitroy, and Varga, 1998b), Cu (Ryzhikh and Mitroy, 1998a), Zn (Mitroy and Ryzhikh, 1999a), and Ag (Ryzhikh and Mitroy, 1998b) was quickly established. Crucial to these results was the development of a fixed core variant of SVM (FCSVM). The FCSVM was validated by performing calculations for light atoms for which both SVM and FCSVM calculations are possible. The differences between the SVM and FCSVM binding energies for the atoms listed in Table VIII are about 1%. While DMC calculations have been used to estimate the binding energies of some of these systems, e^+Li, e^+Be, and LiPs, the DMC energies do not agree with the ECG energies within the DMC statistical uncertainty. A possible cause are imperfectly known nodal surfaces which are needed as input to DMC calculations involving fermions.

Inclusion of various core terms in the FCSVM Hamiltonian increases the amount of time required to calculate the matrix elements by at least 1 order of magnitude. In addition to the slower matrix element evaluation, the larger systems have core structures that lead to more complicated nodal structures for the valence electrons. Larger ECG expansions are needed to generate an accurate wave function. Furthermore, the strongly repulsive OPP potential leads to a loss in numerical precision, making it more difficult for the stochastic search to establish binding.

For these reasons, CI methods were also adapted to study positronic systems. The CI calculations were all done using a frozen core approximation (FCCI). They demonstrated the electronic stability of e^+Sr (Bromley and Mitroy, 2006b) and e^+Cd (Bromley and Mitroy, 2002a), as well as the stability of the $^2S^e$ ground state and the $^2P^o$ excited state of e^+Ca (Bromley and Mitroy, 2006a, 2006b, 2007b). The FCCI calculations were computationally demanding with very large orbital basis sets, e.g., with more than 100 electron and 100 positron orbitals.

Because of the importance of the positronium cluster, it was suggested (Mitroy, Bromley, and Ryzhikh, 1999, 2002) that the structure of any atom binding a positron can be written schematically as

$$\Psi = \alpha\Phi(\text{atom})\phi(e^+) + \beta\Omega(\text{atom}^+)\omega(\text{Ps}). \tag{99}$$

The first of these terms represents a positron moving in the field of a polarized atom while the second term represents a Ps cluster attached to the residual ion (or atom). The relative strength of these two configurations is determined by the ionization potential I of the atomic parent. When the ionization potential is less than 0.25 hartree (the Ps binding energy), the most loosely bound electron is attached to the positron forming a Ps cluster. However, when the ionization potential is greater than 0.250 hartree, the tendency to form a Ps cluster is disrupted by the stronger attraction of the electron to the parent atom. The electron is more strongly attracted to the nucleus and the repulsive positron-nucleus interaction breaks up the cluster.

This tendency is clearly seen in Fig. 5 where the spin-averaged annihilation rate for electron-positron annihilation is plotted as a function of I. The annihilation rate is very close to the spin-averaged Ps annihilation rate of 2.0081×10^9 s^{-1} (Mitroy, Bromley, and Ryzhikh, 2002) for e^-He($^3S^e$) and e^+Na. The annihilation rate steadily decreases as I increases.

The value of I also influences the feasibility of doing CI calculations on these systems. The e^+Li, e^+Na, and e^+He($^3S^e$) systems (with small values of I) all consist of a Ps cluster bound in the field of the residual ion and the partial wave expansion is very slowly convergent. No CI calculations giving an estimate of the binding energy even remotely close to the FCSVM energies have been reported.

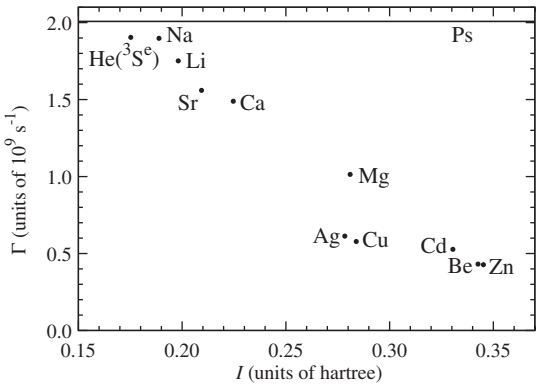

FIG. 5. The spin-averaged 2γ annihilation rate Γ (in units of 10^9 s^{-1}) as a function of the ionization potential I for a number of positronic atoms. The source of the annihilation rate for each system is as follows: He($^3S^e$) (Mitroy, 2005a), Li (Mitroy, 2004), Be (Mitroy, 2010b), Na (Ryzhikh, Mitroy, and Varga, 1998b), Mg (Bromley and Mitroy, 2006b), Ca (Bromley and Mitroy, 2006b), Cu (Mitroy, Bromley, and Ryzhikh, 2001), Zn (Mitroy *et al.*, 2008), Sr (Bromley and Mitroy, 2006b), Ag (Mitroy, Bromley, and Ryzhikh, 2001), and Cd (Bromley and Mitroy, 2010). The annihilation rates for Ca, Sr, Zn, and Cd come from FCCI calculations which have large corrections from an extrapolation procedure.

The ionization potential also has an influence on the likelihood of positron binding. The binding energy is largest when the parent atom ionization potential is closest to 0.250 hartree (the binding energy of Ps) (Mitroy, Bromley, and Ryzhikh, 1999, 2002). The atoms with the largest positron binding energies in Table VIII are e^+Mg and e^+Ca with ionization potentials of 0.280 99 and 0.224 65 hartree (Ralchenko, Kramida, and Reader, 2008), respectively.

Bound states of systems containing more than one positron have also been predicted (Varga, 1999) by SVM calculations. Some examples are listed in Table VIII. The H^- ion can bind not only one but two positrons. The binding energy of e^+PsH (0.021 057 a.u.) is comparable to that of PsH (0.039 197 a.u.).

While the e^+PsH system can be viewed as Ps^+ bound to the hydrogen atom, there are also exotic systems more akin to a charged particle bound to the Ps_2 molecule. The Ps_2 molecule cannot bind an extra electron or positron because of restrictions imposed by the Pauli principle. However, a distinguishable singly charged particle can bind to Ps_2. For example, the five-body system $Ps_2 + x^+ = (2e^+, 2e^-, x^+)$ containing a hypothetical x particle is bound for any $0 \leq m_e/m_x \leq 1$ mass ratio. An atomic example from Table VIII is the seven-body e^+LiPs system (Mitroy and Ryzhikh, 1999b; Varga, 1999; Mezei *et al.*, 2001). The structure is best described as $Li^+ + Ps_2$. The FCSVM has also been used to describe e^+LiPs and to demonstrate the electronic stability of e^+NaPs (Mitroy and Ryzhikh, 1999b).

Another seven-body bipositron system from Table VIII is the H^-Ps_2 system. This system consisting of a proton, four electrons, and two positrons has an estimated binding energy of 0.004 23 hartree (Varga, 1999). It is not clear whether this system would be best described as $H^- + Ps_2$ or as the H^- analog, $p + 2Ps^-$.

Another significant achievement of the SVM was the identification of a second bound state of the Ps_2 molecule with an orbital angular momentum $L = 1$ and a total energy of $-0.334\,408\,317\,34(81)$ a.u. (Usukura, Varga, and Suzuki, 1998; Varga, Usukura, and Suzuki, 1998; Puchalski and Czarnecki, 2008). The lowest-energy dissociation threshold is at $-0.312\,50$ a.u. The electronic dipole transition between this state and the Ps_2 ground state is an unambiguous signature of the experimental formation of Ps_2.

F. Coulomb few-body systems

There are numerous Coulombic systems that can be formed from combinations of charged mesons, baryons, and leptons. The determination of which four- (Varga, Fleck, and Richard, 1997) and five-body (Mezei *et al.*, 2001) systems are bound is reduced by application of the SVM to a largely mechanical exercise.

Coulomb few-body systems admit the possibility of Borromean binding. An N-body Borromean state is one which has no bound $(N-1)$-body subsystems (Zhukov *et al.*, 1993). The existence of Coulombic four-body Borromean systems was established (Richard, 2003) by combining results from different four-body DMC calculations (Bressanini, Mella, and Morosi, 1997) and three-body SVM calculations (Mitroy, 2000). The $(p, \bar{p}, d, \bar{d})$ system is an example of a Borromean system.

G. Outlook

Future efforts need to be focused on developing efficient theoretical and computational approaches to extend the ECG approach to larger atoms keeping the accuracy at a high level. To achieve high computational efficiency, sophisticated optimization approaches have to be developed for the nonlinear parameters of the orbital part of the basis functions. Development in this direction has already started and is showing promising results (Matyus and Reiher, 2012). Alternatively, one can explore the possible use of partially correlated basis functions (versus all-particle correlated ones) to ease the computational burden.

The ECG approach can also be used to elucidate the electronic correlations in confined atoms. There is an intense interest in studying the electronic properties of atoms trapped in fullerenes, carbon nanotubes, or nanopores (Jaskolski, 1996). Recent experiments, for example, measured the energy spectrum of Ps atoms confined in 5 nm diameter silicon nanopores (Cassidy *et al.*, 2011). Accurate ECG calculations would probably be able to explain the dependence of the measured $1S$-$2P$ transition on the radius of the cavity. ECG calculations of confined systems of Ps atoms can also be used to explore the possibility of Bose-Einstein condensation of a Ps atom.

Another area of application of the ECG approach is the calculation of energy levels and the structure of atoms in strong magnetic fields. The advance of astrophysical observations led to a growing number of data on properties of matter in magnetic stars, but the theoretical calculations are so far restricted to the H, He, and Li atoms. The ECG approach can be applied to describe the Be and B and the result can help to test the accuracy of the density functional calculations (Medin and Lai, 2006) which have been used to calculate the properties of these as well as larger atoms.

V. MOLECULAR STRUCTURE APPLICATIONS

A. Motivation

Electronic structure calculations have been enormously successful in predicting structure and properties of molecular systems and various approximate methods of this type can currently be applied to systems with hundreds of atoms. The success is, in particular, affirmed by the fact that these methods have become a tool used not only by theoreticians, but often also by experimentalists. Accuracies of calculations for very large systems are limited by several factors more severe than the reproduction of electron cusps, so that orbital basis sets used in such calculations are not a restriction. However, for few-atomic molecules the orbital approximation eventually encounters the cusp problem. Thus, the motivation for using explicitly correlated functions for molecular systems is the same as for atomic systems discussed in Sec. IV.A, i.e., to achieve accuracies needed to evaluate and guide some experimental work one has to go beyond the orbital approximation. Whereas in atomic applications ECG functions are only one of several possible explicitly correlated bases, in the case of molecules ECGs were for some time the unique basis of this type that could be applied to arbitrary molecules. Other basis sets lead to

integrals which are too difficult to compute even for many-electron diatomic molecules. The only successful applications of other explicitly correlated bases to molecules are those using the JC (James and Coolidge, 1933) and GJC (Kołos and Wolniewicz, 1965) bases for H_2 and other two-electron diatomics. Only in the late 1980s, the first successful applications of Gaussian bases with a linear r_{12} factor appeared (Kutzelnigg, 1985; Kutzelnigg and Klopper, 1991); however, in contrast to the ECG basis sets, one has to use several approximations in calculating molecular integrals. Even for the H_2 molecule, the ECGs have advantages over the JC and GJC basis sets in some types of applications. For example, the JC and GJC bases cannot be used in calculations that require Fourier transforms, such as Compton profiles and electron-scattering cross sections. In fact, the first ever applications of ECG functions accurate enough to confront experimental issues were to these types of problems (Jeziorski and Szalewicz, 1979; Kolos, Monkhorst, and Szalewicz, 1982a; Kolos, Monkhorst, and Szalewicz, 1982b). Perhaps the most significant application of ECG functions is that to interactions between helium atoms, which is currently used to formulate new thermophysical measurement standards (Cencek *et al.*, 2012).

In addition to work aimed at guiding experiments, the ECG functions provide benchmarks used to evaluate other computational approaches. One can test the convergence of orbital methods in the rank of excitations and in basis-set completeness. This can be done not only at the level of total energies, but also for several theory levels in MBPT and CC methods. Direct ECG calculations of effects neglected by the Born-Oppenheimer approximation allow evaluations of the corresponding perturbative approaches.

B. Geminals and perturbation theory

GTG functions in the framework of MBPT (see Sec. III.J for theoretical details) were pioneered for atoms at the MP2 level (Pan and King, 1970). The approach was later extended to the H_2, LiH, and BH molecules (Adamowicz, 1978; Adamowicz and Sadlej, 1978). Early applications were restricted to small basis sets because of the computationally expensive direct treatment of the strong orthogonality problem. The introduction of the more efficient weak-orthogonality second-order energy functional (Szalewicz *et al.*, 1982) resulted in MP2 (Szalewicz *et al.*, 1983a) and MP3 energies (Szalewicz *et al.*, 1983b) of He, Be, H_2, and LiH that were the most accurate ones at that time. This approach was also applied to ten-electron systems: the Ne atom (Wenzel *et al.*, 1986) and the water molecule (Bukowski *et al.*, 1995).

Considerable effort was invested over the years to find efficient techniques to optimize GTG parameters. The current method of choice is a stochastic optimization approach similar to those described in Sec. III.A.1. The computational overhead associated with the optimization means that calculations using GTGs can surpass those utilizing products of orbitals only for relatively small systems (Bukowski, Jeziorski, and Szalewicz, 2003).

The first coupled-cluster applications utilizing the GTG functions were performed in 1984, when this approach was applied at the CCD level to He, Be, H_2, and LiH (Jeziorski *et al.*, 1984). Later the formalism was extended to the CCSD level of theory, with benchmark results reported for some two-electron (He, Li^+, H_2) and four-electron (Be, Li^-, LiH) systems (Bukowski, Jeziorski, and Szalewicz, 1999).

The most significant application of coupled-cluster approaches has been to the calculation of a helium dimer potential accurate at the millikelvin level (Cencek *et al.*, 2004; Jeziorska *et al.*, 2007; Patkowski *et al.*, 2007) ($1\ \mathrm{K} = 3.166\,815\,3 \times 10^{-6}$ hartree). To calculate the dominant contribution, the CCD correlation energy, the pair functions τ^1_{11}, τ^1_{12}, τ^3_{12}, and τ^1_{22} in Eq. (94) were expanded in large GTG basis sets (up to $\mathcal{N} = 800$ terms). It was possible to eliminate basis-set superposition errors in the interaction energy (the difference in energy with respect to two non-interacting He atoms) by using the same basis set for each pair at a given $\mathcal{N}$ (Bukowski, Jeziorski, and Szalewicz, 1996). The GTG parameters were carefully optimized in MP2 calculations. Corrections going beyond the CCD level, $E_{\mathrm{CCSD}} - E_{\mathrm{CCD}}$, were obtained from calculations using orbital basis sets. At some selected distances (due to computational expense), GTG-based CCSD calculations were performed, yielding results consistent with those using orbitals. The post-CCSD contributions were calculated as $E_{\mathrm{CCSD(T)}} - E_{\mathrm{CCSD}}$ and $E_{\mathrm{FCI}} - E_{\mathrm{CCSD(T)}}$, using large orbital basis sets (FCI denotes full CI, i.e., CI with the complete set of electron excitations). The energy differences between any two levels of theory were computed, of course, using identical basis sets. At $5.6\,a_0$, the obtained interaction energy amounts to $-11.0037(31)$ K.

GTG functions have also been used in another perturbative approach, namely, symmetry-adapted perturbation theory (SAPT) (Jeziorski, Moszyński, and Szalewicz, 1994; Szalewicz, Patkowski, and Jeziorski, 2005; Szalewicz, 2012). SAPT is a perturbation theory using as the zeroth-order approximation monomers at infinite separation, i.e., it is designed to treat weak (van der Waals) intermolecular (or interatomic) interactions. In SAPT, the interaction energy is expanded in a double perturbation series with respect to the intermonomer (intermolecular) interaction operator and to the intramonomer correlation operators. The dominant (for non-polar systems) attractive component, the second-order dispersion energy, can be obtained by minimization of an appropriate Hylleraas-type functional (Chalasinski *et al.*, 1977; Szalewicz and Jeziorski, 1979; Rybak *et al.*, 1987) with a two-electron dispersion pair function. The main repulsive component, the first-order energy, can be obtained from the accurate wave functions of the monomers. Some additional second-order components can be computed using the orbital-based SAPT code (Bukowski *et al.*, 2012). The residual parts of the interaction energy, from high-order SAPT terms not coded yet, can be computed for small dimers as $E_{\mathrm{FCI}} - E_{\mathrm{SAPT}}$. Using this strategy, a complete SAPT-based helium dimer potential was obtained (Williams *et al.*, 1996; Korona *et al.*, 1997) with the interaction energy of $-11.059(30)$ K at $R = 5.6a_0$. This potential was used extensively in the next decade to predict various properties of helium (Janzen and Aziz, 1997). Recently, the SAPT calculations for the helium dimer were repeated (Jeziorska *et al.*, 2007) with much larger basis sets. The new SAPT results are

fully consistent with the coupled-cluster results discussed above but have smaller uncertainties at large distances. The current recommended helium dimer potential combines coupled-cluster and SAPT results and includes adiabatic, relativistic, and QED corrections (see Sec. V.D).

C. BO calculations

For almost 30 years after the pioneering work of James and Coolidge (1933), the GJC functions were the only explicitly correlated basis set applied to molecular systems, but such applications were limited to H_2 and isoelectronic diatomic species like HeH^+. One well-known milestone of the GJC approach was the prediction of the ground state dissociation energy of H_2 (Kolos and Wolniewicz, 1968) that later proved to be more accurate than the concurrent experimental data (Herzberg, 1970). Generalizations of the GJC approach to systems with more than two electrons resulted in prohibitively complicated integrals, although one should mention the calculations for He_2^+ and He_2 by Clary and Handy (1977). Going beyond diatomic molecules for a GJC basis seems almost impossible because of intractable many-center integrals.

The introduction of the ECG basis resulted in succession of very accurate calculations on a variety of diatomic and triatomic molecules. Calculations on the H_2 molecule using GJC and ECG have been leapfrogging each other in accuracy for a number of years (Rychlewski and Komasa, 2003; Cencek and Szalewicz, 2008). The current best estimate of the BO energy of H_2 at the equilibrium distance of $1.4011a_0$, equal to 1.174 475 931 400 216 7(3) hartree, results from extrapolated GJC expansions with up to 22 363 terms (Pachucki, 2010). The current best ECG energy of 1.174 475 931 400 21(6) hartree was obtained with shorter expansions of only 4800 terms (Cencek and Szalewicz, 2008).

The first applications of ECG functions with $N > 2$ were limited LiH studies by Karunakaran and Christoffersen (1975, 1982). This pioneering work was resumed only 15 years later with applications to He_2^+ (Cencek and Rychlewski, 1995, 2000), LiH (Cencek and Rychlewski, 1993, 2000; Tung, Pavanello, and Adamowicz, 2011), H_3 (Cencek and Rychlewski, 1993; Pavanello, Tung, and Adamowicz, 2009), H_4 (Patkowski *et al.*, 2008; Tung, Pavanello, and Adamowicz, 2010), and H_5^+ (Müller and Kutzelnigg, 2000). These calculations invariably yielded variational energies lower than those obtained by other methods.

Table IX gives a comparison of ECG energies with the best results from other methods for the LiH molecule. This table shows that only ECG-based approaches have achieved μhartree-level accuracy for this system. However, the multireference (MR)-CISD result of −8.070 792 hartree at $R = 3.000$ bohr reported by Holka *et al.* (2011) is 239 μhartree below the best ECG value and about 50 times outside its estimated uncertainty. The reasons for this discrepancy are unclear at the moment. It is possible that it is due to the size-consistency correction and (or) the extrapolation procedure used by Holka *et al.* The 5 μhartree estimate of the uncertainty from Cencek and Rychlewski (2000) is consistent, on the other hand, with the independent ECG calculation (Tung, Pavanello, and Adamowicz, 2011). The result of Cencek and Rychlewski differs by only 37 μhartree from the value obtained using the ICI approach (Nakatsuji *et al.*, 2007).

The two-electron, three-center H_3^+ molecular ion is a system particularly suitable for ECG applications. It has been the subject of numerous *ab initio* calculations (Kutzelnigg and Jaquet, 2006), but had eluded the efforts to achieve spectroscopic accuracy until 1998, when a potential energy surface (PES) based on roughly optimized 1300-term ECG expansions was obtained (Cencek *et al.*, 1998). The wave functions were used to evaluate the lowest-order relativistic corrections and the diagonal adiabatic (post-BO) correction. In a follow-up paper (Jaquet *et al.*, 1998), the total energies were fitted by a functional form and used to calculate the rovibrational frequencies for H_3^+ and D_3^+, resulting in a close agreement with experiment (on average, about 0.3 and 0.1 cm^{-1}, respectively). This PES has remained the basis for most *ab initio* investigations of the low-energy (up to about 10 000 cm^{-1}) spectrum of H_3^+ for over 10 years and was recently extended to higher energies (Bachorz *et al.*, 2009). In the same year, a new nonrelativistic BO PES for the low-energy region was published (Pavanello, Tung, and Adamowicz, 2009). They used only a 900-term ECG expansion, but performed a thorough parameter optimization which resulted in energies 0.01 to 0.02 cm^{-1} lower than those in the 1998 PES.

The helium dimer plays an important role in many areas of physics, including establishing new standards of temperature and pressure (Fischer and Fellmuth, 2005; Pitre, Moldover, and Tew, 2006; Mehl, 2009). The best current BO potential (Jeziorska *et al.*, 2007) is based on coupled-cluster GTG and SAPT GTG calculations (see Sec. V.B). However, the most

TABLE IX. The total electronic energy (in hartree) of the LiH molecule at $R = 3.015\,a_0$, except the last entry, (Holka *et al.*, 2011), which used $R = 3.000\,a_0$.

Method	E	Reference
CI, $[9s8p6d1f]$ basis set	−8.069 336	Bendazzoli and Monari (2004)
GFMC	−8.070 21(5)	Chen and Anderson (1995)
DMC	−8.070 1(4)	Ospadov, Oblinsky, and Rothstein (2011)
CCSD[T]-R12	−8.070 491	Noga *et al.* (1995)
Iterative complement interaction	−8.070 516	Nakatsuji *et al.* (2007)
ECG, 200 terms	−8.069 221	Cencek and Rychlewski (1993)
ECG, 2400 terms	−8.070 538	Cencek and Rychlewski (2000)
ECG, 2400 terms	−8.070 547 3	Tung, Pavanello, and Adamowicz (2011)
ECG, extrapolated	−8.070 553(5)	Cencek and Rychlewski (2000)
MR-CISD	−8.070 792	Holka *et al.* (2011)

accurate value of the interaction energy at the potential minimum ($R = 5.6\,a_0$) was obtained using the direct variational optimization of the full four-electron ECG function (Cencek and Szalewicz, 2008). For He_2, the linear combination of ECGs is supplemented by an additional contracted term leading to the following expansion:

$$\Psi = c_0\phi_0 + \sum_{k=1}^{K} c_k\phi_k(1, 2, \ldots, N). \tag{100}$$

The term ϕ_0 in Eq. (100) is a linear combination of ECGs that are designed to represent two noninteracting helium atoms separated by a distance of $R = 5.6\,a_0$. The helium-atom basis used in ϕ_0 consisted of 337 terms and yielded an energy of $-2.903\,724\,377\,002$ hartree. This term is included because the dimer wave function can be regarded as dominated by two helium atoms subjected to a minor perturbation. With ϕ_0 (which is kept frozen), the whole optimization effort can then be directed toward the interaction energy, which in this case constitutes only 0.0006% of the total energy of the dimer. Since the inclusion of ϕ_0 is computationally expensive, it is advisable to use a moderate size monomer contraction in the optimization and replace it with a more accurate one for the final energy evaluation. It is also possible to obtain ϕ_0 by a separate optimization of a four-electron ECG expansion. In this approach, one minimizes the expectation value of the four-electron Hamiltonian with the intermonomer terms switched off (Patkowski *et al.*, 2008). This leads to much shorter ϕ_0 expansions (compared to monomer products) without any loss of accuracy.

Table X presents the interaction energies obtained both without and with the use of the monomer contraction method. The inclusion of ϕ_0 results in a dramatic improvement of the accuracy and the extrapolated value $-11.0006(2)$ K has 15 times smaller uncertainty than the next best literature result (Patkowski *et al.*, 2007), where the dominant contributions were also obtained using ECG functions.

D. Relativistic and QED corrections for light molecules

One of the most spectacular applications of ECG functions is in predicting energy levels of light molecules to an accuracy competitive with the experiment. The precision of the measurements has reached the level at which not only nonadiabatic and relativistic but also QED effects become important (Salumbides *et al.*, 2011). This challenge has been taken up by ECG calculations on the hydrogen molecule and its isotopomers in the framework of the relativistic and QED theory described in Secs. II.F, II.G, and III.C. At the present time, the current best theoretical value of the H_2 molecule dissociation energy $D_0 = 36\,118.0695(10)$ cm^{-1} (Piszczatowski *et al.*, 2009) was obtained with a basis that used a GJC potential curve for $R \leq 6.0\,a_0$ and an ECG potential curve for $R > 6.0\,a_0$.

The good agreement between the measured and calculated values of the dissociation energy D_0 and lowest rotational energy spacing ($J = 1 \leftarrow 0$) is seen in Table XI. The accuracy of both experiment and theory is sufficiently high to enable extraction of the QED contribution from the measurements (Komasa *et al.*, 2011). Dissociation energy of all the bound levels as well as the allowed transition intensities have been computed, leading to a purely theoretical absorption spectrum of Fig. 6. The accuracy of such a model spectrum for HD has been assessed (Kassi and Campargue, 2011) on the basis of the first overtone band (2-0): the average line position deviation is $1.1(8.7) \times 10^{-4}$ cm^{-1} and the line intensity deviation is about 1%. It was recommended that the calculated rovibrational spectrum can be used as reference frequencies with uncertainties that range from 0.001 in the near infrared to 0.005 cm^{-1} at 35 000 cm^{-1} (Campargue *et al.*, 2012).

For both metrological purposes and the investigations of the sole vibrational state of He_2, it is of critical importance to account for contributions beyond the nonrelativistic BO (post-BO) level. The adiabatic, the lowest-order relativistic (of the order α^2), and the QED contributions (of the order α^3) were recently evaluated for a broad range of intermonomer distances (Przybytek *et al.*, 2010; Cencek *et al.*, 2012). The nonrelativistic ECG wave functions with up to $K = 2400$ terms [and orbital CCSD(T) and FCI wave functions at large distances] were used to calculate the appropriate expectation values. The total energies [including the BO potential (Jeziorska *et al.*, 2007)] were fitted by an asymptotically correct functional form and an appropriate component of the Casimir-Polder potential was added to account for the long-range retardation damping. The resulting dissociation energy and average separation of the helium dimer are 1.62 ± 0.03 mK and 47.1 ± 0.5 Å, respectively. The latter value has an order of magnitude tighter error bar than the current best experimental result (Grisenti *et al.*, 2000) of 52 ± 4 Å.

Apart from the interaction potential, the proposed helium-based temperature and pressure standards assume accurate knowledge of the helium-atom polarizability and helium

TABLE X. Interaction energy $E_{\rm int}$ (in kelvin) of He_2 at $R = 5.6\,a_0$ as a function of the number of expansion terms K. The interaction energy values were calculated using the exact monomer energy and are strict upper bounds to the exact value. ϕ_0 in Eq. (100) contained 56 953 terms resulting from a product of two helium-atom functions with $L = 337$ terms. During the optimization, a shorter expansion of ϕ_0 was used (40 186 terms, $L = 283$). The conversion factor is 315 774.65 K/hartree.

	Without ϕ_0		With ϕ_0	
K	$E_{\rm int}$	Reference	$E_{\rm int}$	Reference
1200	−10.9582	Cencek *et al.* (2005)	−10.998 53	Cencek and Szalewicz (2008)
2400	−10.9900	Cencek *et al.* (2005)	−11.000 12	Cencek and Szalewicz (2008)
4800	−10.9953	Cencek *et al.* (2005)	−11.000 35	Cencek and Szalewicz (2008)
Extrap.			−11.000 6(2)	Cencek and Szalewicz (2008)
CCSD using GTGs, CCSD(T) and FCI using orbitals			−11.003 7(31)	Patkowski *et al.* (2007)
SAPT using GTGs to second-order plus higher-order contributions using orbitals			−10.999 6(105)	Jeziorska *et al.* (2007)
GFMC			−10.998(5)	Anderson (2004)

TABLE XI. Comparison between the measured (Liu *et al.*, 2009, 2010; Drouin, 2011; Sprecher *et al.*, 2010; Salumbides *et al.*, 2011) and theoretically predicted (Piszczatowski *et al.*, 2009; Pachucki and Komasa, 2010; Komasa *et al.*, 2011) dissociation energy D_0 and the lowest rotational energy spacing ($J = 1 \leftarrow 0$) for H_2 and its isotopomers (all entries in cm^{-1}).

D_0	H_2	HD	D_2
Exp.	36 118.069 62(4)	36 405.783 66(4)	36 748.362 86(7)
Theo.	36 118.069 6(11)	36 405.782 8(10)	36 748.363 4(9)
Diff.	0.000 0(12)	0.000 9(11)	0.000 5(11)
$J = 1 \leftarrow 0$			
Exp.	118.486 84(10)	89.227 932 6(3)	59.781 30(95)
Theo.	118.486 812(9)	89.227 933(8)	59.780 615(3)
Diff.	0.000 03(10)	0.000 000(8)	0.000 68(95)

dimer collision-induced polarizabilities. The critical components of the former were discussed in Sec. IV.D. The benchmark values of the latter were recently obtained using four-electron ECG expansions (Cencek, Komasa, and Szalewicz, 2011).

GTG-based helium dimer potentials have been used in numerous studies of helium clusters, bulk helium, and doped helium nanodroplets. For example, this potential was applied in a thorough study of the helium trimer (Suno and Esry, 2008). In this study, the three-body problem was solved numerically in hyperspherical coordinates, with two-body interactions described by the GTG-based potential (Jeziorska *et al.*, 2007) and nonadditive three-body interactions by the (orbital-based) SAPT potential developed by Cencek *et al.* (2007).

E. Going beyond the Born-Oppenheimer approximation

Recently it became possible to perform *ab initio* calculations for small molecular systems without making the BO approximation (Kinghorn and Adamowicz, 1999b). The nuclear and electronic motion are treated on an equal footing. The nuclear-nuclear interaction is strongly repulsive and difficult to describe with a basis-set expansion. As discussed in Sec. III.D the use of ECGs with r^{2m} prefactors solves this problem.

Calculations without the BO approximation can provide an independent test of the validity of the more usual perturbative calculations of nonadiabatic effects starting from the BO level. One regime where one can expect such perturbative treatments to be unreliable occurs when the energy spacings between the rovibrational energy levels are comparable to the electronic energy spacings. Another possible regime would be when the energy shifts arising from different nuclear isotopes are comparable to the rovibrational binding energies.

HD^+ and other heteronuclear isotopologs of H_2^+ represent a simple system that, due to the difference in nuclear masses, lacks the center of symmetry. For highly excited vibrational states that lie close to the dissociation threshold, the electron can be found near the deuteron with a noticeably higher probability than near the proton. The $D + p$ configuration is energetically preferred over the $H + d$ configuration, as deuterium's ground state energy is slightly lower than that of the hydrogen. To adequately describe the charge asymmetry in those states near the dissociation threshold, an approach that treats all particles on equal footing is needed.

The asymmetry of the HD^+ wave function was investigated experimentally (Carrington *et al.*, 1991; Ben-Itzhak *et al.*, 2000). In particular, Ben-Itzhak *et al.* studied the dissociation of the electronic ground state following the ionization by fast proton impact and found that the $H^+ + D(1s)$ dissociation channel is more likely than the $H(1s) + D^+$ dissociation channel by about 7%. This asymmetry breakdown was attributed to the finite nuclear mass correction to the BO approximation, which makes the $1s\sigma$ state 3.7 meV lower than the $2p\sigma$ state at the dissociation limit.

In Table XII, a catastrophic breakdown of the BO approximation is seen to occur above the $v = 20$ vibrational level. The calculations were performed with ECGs and up to 4000 basis functions were used (Bubin, Bednarz, and Adamowicz, 2005). As one can see, in the ground vibrational state ($v = 0$) and a moderately excited state ($v = 10$) there is practically no charge asymmetry present, whereas for the highest two states with zero total angular momentum ($v = 21, 22$), the electron is essentially localized around the deuteron.

Similar to the case of atomic calculations and molecular BO calculations, a major advantage of the ECG method in the

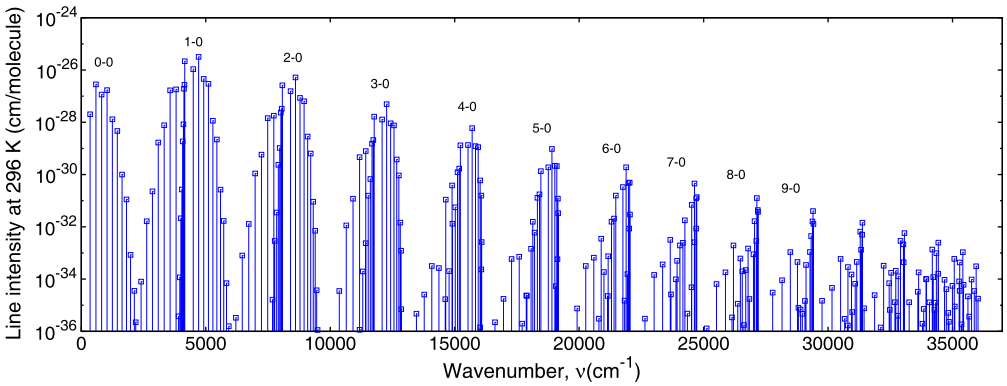

FIG. 6 (color online). Theoretical rovibrational absorption spectrum of the ground electronic ($X^1\Sigma_g^+$) state of H_2 obtained including nonadiabatic, relativistic, and QED corrections. The notation v-0 stands for a band of transitions from the $(0, J)$ states to states $(v, J \pm 2)$. The estimated accuracy of the line positions is of the order of 0.001 cm^{-1}, whereas the line intensities are accurate to about 0.1%. From Campargue *et al.*, 2012.

TABLE XII. Expectation values showing charge asymmetry in highly excited (near the dissociation threshold) rovibrational states of HD^+ versus the ground state ($v = 0$) and a moderately excited state ($v = 10$) (Bubin, Bednarz, and Adamowicz, 2005). All values are in atomic units.

v	$\langle r_{d-p}\rangle$	$\langle r_{d-e}\rangle$	$\langle r_{p-e}\rangle$	$\langle r^2_{d-p}\rangle$	$\langle r^2_{d-e}\rangle$	$\langle r^2_{p-e}\rangle$
0	2.055	1.688	1.688	4.268	3.534	3.537
10	3.489	2.445	2.448	13.48	8.250	8.272
21	12.95	2.306	12.19	176.0	12.94	168.2
22	28.62	1.600	28.55	910.0	4.266	911.4
D atom		1.500			3.002	

nonadiabatic case is the possibility to perform accurate calculations of systems containing more than just two electrons. Table XIII lists the energies of several diatomic molecules and molecular ions computed without assuming the BO approximation. The largest molecule in the table, boron hydride, is an eight-body system (two nuclei and six electrons). While the size of the basis and the accuracy for such relatively large systems are currently limited by available computational resources, the results can be improved when more powerful hardware becomes available.

Accurate BO ECG energies for the largest molecules listed in Table XIII, BeH and BH, have not yet been computed. However, the quality of the nonadiabatic energies from this table can be examined by comparison with the best literature results obtained in state-of-the-art quantum chemical calculations. Koput (2011) reported the ground state energy of BeH of −15.246 593 a.u. (at the equilibrium internuclear distance and including the FCI and diagonal adiabatic corrections) and the fundamental vibrational frequency of 1987.68 cm^{-1}. These values were obtained at the multireference averaged coupled-pair functional (MR-ACPF) level of theory in conjunction with a septuple-zeta correlation-consistent valence basis set, augmented with sets of diffuse and tight functions (aug-cc-pCV7Z) basis. Therefore, the total nonrelativistic energy of the first vibrational state of BeH from that work is −15.242 065 a.u., which agrees well with the value of −15.242 03(10) shown in Table XIII. The uncertainty in both energy values is of the same order of magnitude and its primary source is the finite size of the basis sets employed. The best current ground state BO energy of the BH molecule was obtained in a restricted coupled-cluster calculation with single, double, and triple (RCCSDT) excitations in conjunction with the quintuple-ζ quality basis set (Miliordos and Mavridis, 2008). Its value is −25.287 650 a.u. Using a fundamental vibrational frequency of 2361 cm^{-1} and estimates of the adiabatic corrections (which can be calculated from the finite and infinite mass energies of B and H atoms) the total nonrelativistic energy of the first vibrational state becomes −25.280 757 a.u., which is also in good agreement with the nonadiabatic energy given in Table XIII.

Results obtained with the variational nonadiabatic approach can be compared directly with those calculated within the BO approximation with the finite nuclear mass effects determined perturbatively by means of the methodology described in Sec. II.G. Inspection of Table XIV, which contains such a comparison for dissociation energies of molecular hydrogen and its isotopomers, allows one to conclude that at the present stage both methods yield equivalent results.

Nonrelativistic nonadiabatic calculations can be complemented with evaluation of relativistic corrections (Stanke *et al.*, 2006) as demonstrated in Table XV for some three-electron systems. The theoretical $v = 0 \rightarrow 1$ transition energy for $^3He^4He^+$ agrees with experiment when the theoretical and experimental uncertainties are taken into consideration. Table XV also shows that the relativistic corrections tend to cancel for the $v = 0$ and $v = 1$ vibrational states.

F. Outlook

The motivation for extreme-accuracy molecular calculations is the quest for first-principles predictions of molecular properties with reliability comparable to or better than that achievable by experiments. To reach this goal, the calculations must be performed in the exact numerical regime (i.e., without any time-saving approximations, for instance in the integral evaluation) and nonlinear parameters of ECGs have to be thoroughly optimized. For most applications, at least the diagonal adiabatic correction and lowest-order relativistic corrections must be taken into account, sometimes even QED and nonadiabatic contributions. Only recently a similar level of accuracy was achieved for He_2 as was possible for H_2 about 40 years ago. Four-electron molecules seem to be the current limit of spectroscopic-accuracy ECG-based applications. An extension to six-electron ones such as BH or Li_2 (as five-electron molecular systems are rare) at this level of accuracy is probably possible, but only with enormous computational resources.

The computational cost of MBPT and CC calculations with GTGs is much less, and such calculations have already been performed for ten-electron molecules, although not at a spectroscopic-accuracy level. As a future direction, the MBPT and CC GTG calculations can be used in a hybrid

TABLE XIII. Total nonadiabatic ground state energies (in hartree) of selected small diatomic molecules. In parentheses we show the estimated difference between the variational upper bound and the exact nonrelativistic energy.

System	Basis size	Energy	Reference
H_2	10 000	−1.164 025 030 84(21)	Bubin, Leonarski *et al.* (2009)
HD	10 000	−1.165 471 922 0(20)	Bubin, Stanke, and Adamowicz (2011b)
HeH^+	8 000	−2.971 078 465 9(5)	Stanke *et al.* (2008a)
LiH	7 200	−8.066 437 1(15)	Bubin, Adamowicz, and Molski (2005)
LiH^-	3 600	−8.067 382 5(50)	Bubin and Adamowicz (2004)
BeH	4 000	−15.242 03(10)	Bubin and Adamowicz (2007)
BH	2 000	−25.280 3(10)	Bubin, Stanke, and Adamowicz (2009)

TABLE XIV. The equivalence of the nonrelativistic dissociation energy D_0 obtained from the direct nonadiabatic approach (Bubin, Leonarski *et al.*, 2009; Stanke, Bubin *et al.*, 2009; Bubin, Stanke, and Adamowicz, 2011a) and the results based on the BO approximation augmented by a perturbative treatment of the finite nuclear mass effects (Pachucki and Komasa, 2009, 2010; Piszczatowski *et al.*, 2009).

	D_0 (cm^{-1})		
	H_2	HD	D_2
Perturbative	36 118.797 8(2)	36 406.510 8(2)	36 749.091 0(2)
Direct	36 118.797 74(1)	36 406.510 5(4)	36 749.091 0(0)
Diff.	0.000 06(20)	0.000 3(4)	0.000 0(2)

approach where the bulk of the notoriously difficult pair-correlation problem is treated with GTG functions (possibly only at favorably scaling levels of theory, such as the factorizable CCD) and the remaining higher excitation effects, which are relatively small, are treated with orbital methods (Patkowski *et al.*, 2007). Such a hybrid approach is currently the most promising method for establishing benchmark results for molecules with about ten electrons.

In the case of non-BO calculations, future efforts will be focused on tri- and four-atomic molecular systems. An important example is H_3^+, which is one of the key species in the interstellar medium (Oka, 2006). Neither theory nor experiment has fully elucidated the spectrum of this molecule, although recent BO calculations (Pavanello *et al.*, 2012a, 2012b), as discussed in Sec. V.C, have demonstrated progress. The main challenges in achieving truly spectroscopic accuracy for small polyatomic molecules in the BO framework are due to the multidimensional nature of the PES and the description of rotational nonadiabatic effects. Non-BO treatment avoids these difficulties, but non-BO calculations of polyatomic molecules are considerably more demanding.

Another area of future development are MBPT and CC-F12 methods (see Sec. III.J) closely related to the GTG approach. Since these methods use several numerical approximations and do not optimize nonlinear parameters, such methods cannot aim at spectroscopic accuracies, and in fact in some cases are less accurate than extrapolated orbital calculations (Patkowski and Szalewicz, 2010; Patkowski, 2012). Nevertheless, due to their efficiency, F12 methods are becoming the mainstream of computational chemistry. One may consider development of a method intermediate between MBPT and CC-GTG and MBPT and CC-F12, incorporating advantages of both approaches.

VI. APPLICATION TO NUCLEAR STRUCTURE CALCULATIONS

A. Motivation

The solution of the nuclear few-body problem is crucial for a complete description of the nuclear interaction. The nucleon-nucleon (NN) interaction is not a fundamental interaction but results from quantum chromodynamics (QCD). At present, our knowledge of the short-range behavior of the NN interaction is incomplete. In addition, the nuclear interaction also contains three- and four-body terms and their determination is somewhat ambiguous. Comparison between experimental data and results of high accuracy calculations for light nuclei helps to define and refine the most appropriate form of nuclear interactions.

The nuclear few-body problem has two additional properties that distinguish it from the atomic and molecular cases. First, in the nuclear case there is no confining potential like the electron-nuclear Coulomb interaction. Second, as the nucleons are composite particles, the nucleon-nucleon interaction contains a very strong, short-range repulsive core, which makes the solution of the nuclear few-body problem challenging.

The solution of the nuclear few-body problem is also important for the fundamental understanding of the creation of elements, the description of various astrophysical processes, the study of clustering mechanism, and of the neutron rich nuclei. The flexibility and accuracy of the ECG approach is a great advantage in investigations of loosely bound neutron halos and cluster substructures of nuclei.

B. Nuclear Hamiltonian and wave function

In nuclear physics the Hamiltonian includes the kinetic energy K_i, hard-core and noncentral two-nucleon NN potentials v_{ij}, as well as three-nucleon interactions v_{ijk}:

$$H = \sum_i K_i + \sum_{i<j} v_{ij} + \sum_{i<j<k} v_{ijk}. \tag{101}$$

Various phenomenological or field theory motivated NN potentials have been proposed (Epelbaum, Hammer, and Meißner, 2009). The most widely used and tested NN potential is the AV18 potential (Wiringa, Stoks, and Schiavilla, 1995). The AV18 is one of a class of highly accurate NN potentials that fit both pp and np scattering data up to 350 MeV. In the calculations presented in this section, the AV8′ NN potential (Pudliner *et al.*, 1997) was used, which is a simplified, reprojected version of the fully realistic AV18

TABLE XV. Nonrelativistic and relativistically corrected non-BO energies and transition frequencies for the lowest vibrational states of three-electron molecular ions: $^3He^4He^+$ and LiH^+ (Stanke, Kędziera, Bubin, Molski, and Adamowicz, 2007; Bubin, Stanke, and Adamowicz, 2010, 2011c).

System	State or transition	Nonrelativistic	Relativistic	Experiment
$^3He^4He^+$	$v = 0$ (hartree)	−4.989 719 657(30)	−4.989 926 676(30)	
	$v = 1$ (hartree)	−4.981 743 256(80)	−4.981 950 301(80)	
	$1 \rightarrow 0$ (cm^{-1})	1750.618(60)	1750.612(60)	1750.556 87(98)
LiH^+	$v = 0$ (hartree)	−7.783 247 013(40)	−7.783 882 745(40)	
	$v = 1$ (hartree)	−7.781 629 462(500)	−7.782 265 092(500)	
	$1 \rightarrow 0$ (cm^{-1})	355.011(50)	355.034(50)	

TABLE XVI. Comparison of the binding energies E_b (in MeV) and the root-mean-square radius (in fm) of the alpha particle calculated by different methods (Kamada *et al.*, 2001). The Coulomb and $3N$ interactions are turned off.

Method	Reference	E_b	$\sqrt{\langle r^2\rangle}$
FY	Glöckle and Kamada (1993)	−25.94(5)	1.485
GEM	Kamimura (1988)	−25.90	1.482
SVM	Kamada *et al.* (2001)	−25.92	1.486
HH	Viviani, Kievsky, and Rosati (1995)	−25.90(1)	1.483
GFMC	Wiringa *et al.* (2000)	−25.93(2)	1.490
NCSM	Navrátil and Barrett (1999)	−25.80(20)	1.485
EIHH	Barnea, Leidemann, and Orlandini (2000)	−25.944(10)	1.486

model, but still has most of its complexity. This potential is a sum of central, spin-spin, isospin-isospin, spin-orbit, and tensor interactions. A phenomenological interaction that reproduces the ground state energies of ^{3}H and ^{4}He was used as a three-nucleon potential v_{ijk} (Hiyama, Gibson, and Kamimura, 2004).

A total wave function with the isospin TM_T is expressed in an LS-coupled scheme as

$$\Psi^{\pi}_{JM_JTM_T} = \sum_{iLS} C^i_{LS} \Psi^{\pi}_{i(LS)JM_JTM_T}, \tag{102}$$

where the basis function is defined as

$$\Psi^{\pi}_{i(LS)JM_JTM_T} = \mathcal{A}\{[\theta^i_L(\hat{\mathbf{x}})\xi^i_{SM_S}]_{JM}\xi^i_{TM_T}\exp(-\mathbf{x}A_i\mathbf{x})\}, \tag{103}$$

where $\mathcal{A}$ is the antisymmetrizer, $\mathbf{x}$ stands for a set of $N-1$ intrinsic coordinates $(\mathbf{x}_1, \mathbf{x}_2, \ldots, \mathbf{x}_{N-1})$, and $\xi^i_{SM_S}$ ($\xi^i_{TM_T}$) is the spin (isospin) function of the N-particle system. The nonspherical (orbital) part $\theta^i_L(\hat{\mathbf{x}})$ of the trial function is represented by either a successively coupled product of spherical harmonics or by the global vector representation (see Sec. II.D.2). Equally good results have been obtained in both representations (Suzuki, Horiuchi *et al.*, 2008).

C. Alpha particle

The nuclear structure calculation will be exemplified by a complex four fermion system ^{4}He (the alpha particle). Accurate calculations for the ground state of ^{4}He were performed with various sophisticated methods including the SVM (Kamada *et al.*, 2001). Table XVI compares the binding energy and radius of the alpha particle calculated with different methods.

^{4}He has many excited (resonance) states, and some of them have the same spin and parity. The width of some of these states is relatively small and in the calculation they are treated as bound states. The wave functions of states with identical spin and parity are optimized simultaneously by SVM. Figure 7 compares the calculated energy spectrum with experiment (Horiuchi and Suzuki, 2012). The SVM calculation reproduces a sequence of the excited levels.

Besides the energy, other properties can also be accurately calculated with ECGs. One example is the coordinate-space correlation function

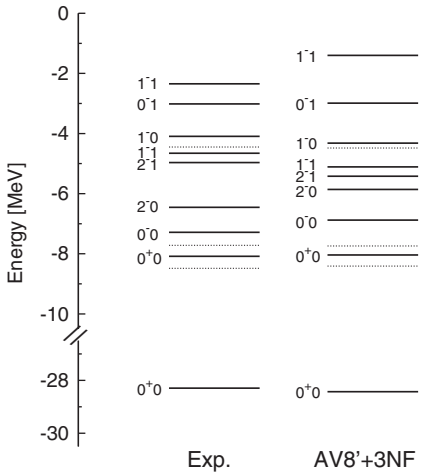

FIG. 7. Energy levels of ^{4}He labeled with $J^{\pi}T$. Dotted lines indicate the thresholds of ^{3}H + p, ^{3}He + n, and ^{2}H + ^{2}H from below. The energy is given from the $p + p + n + n$ threshold. From Horiuchi and Suzuki, 2012.

$$C(r) = \frac{1}{4\pi r^2}\frac{1}{2J+1}\sum_M \langle \Psi^{\pi}_{JM}|\delta(|\mathbf{r}_1 - \mathbf{r}_2| - r)|\Psi^{\pi}_{JM}\rangle, \tag{104}$$

which describes the short-range behavior of the NN relative motion. As displayed in Fig. 8, $C(r)$ calculated for ^{2}H, ^{3}H, and ^{4}He indeed show near vanishing amplitudes at short distances. The function $C(r)$ does not incorporate the $4\pi r^2$ volume element so the small amplitude as $r \to 0$ is a manifestation of the strong repulsion found in the NN interaction at short range. This can be accommodated to some extent by the SVM since ECGs explicitly include interparticle distances.

The peak position of $C(r)$ is about 1 fm, independent of the system. In fact, the $C(r)$ functions for $r \leq 1$ fm are found to show universal behavior (Forest *et al.*, 1996; Feldmeier *et al.*, 2011). The significance of various correlation functions for the operators $\mathcal{O}_i$ as well as of the momentum-space correlation function has been discussed by Suzuki and Horiuchi (2009).

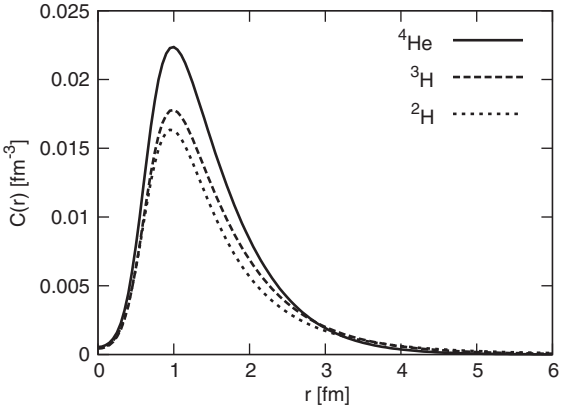

FIG. 8. Coordinate-space correlation functions for the ground states of ^{2}H, ^{3}H, and ^{4}He calculated with the AV8′ potential. From Suzuki, Horiuchi *et al.*, 2008.

D. Application to multicluster systems

Extensive applications of the ECG + SVM approach to light nuclei including halo nuclei started in the 1990s (Arai *et al.*, 2001; Suzuki *et al.*, 2003). The first careful test of SVM was actually performed in a microscopic $\alpha(^4\mathrm{He}) + n + n$ three-cluster model for a two-neutron halo nucleus ^{6}He (Varga, Suzuki, and Lovas, 1994). Here the cluster indicates a system of several nuclei, that is, ^{6}He is considered to be composed of α and two neutrons. Although the cluster model is useful and physically sound for extending the few-body approach to light nuclei, a fully microscopic cluster-model calculation that takes into account the correlations among the particles accurately is fairly involved because of the antisymmetry requirement on the wave function of the system. A simpler macroscopic model, which approximates the alpha cluster as a structureless particle, has often been used. In this model the Pauli principle is taken into account by projecting out occupied states. Such $\alpha + N + N$ model has been used for ^{6}He and ^{6}Li to describe the correlated motion of the two nucleons outside the α core (Horiuchi and Suzuki, 2007; Baye *et al.*, 2009). The α-n interaction is phenomenological in nature and constructed to fit to low-energy n-α scattering data (Kanada *et al.*, 1979). This potential supports a low-lying s-wave bound state, which was eliminated by the inclusion of an OPP potential. Figure 9 compares the momentum distribution of the two-nucleon relative motion, a momentum-space analog of $C(r)$. The distribution of ^{6}Li is similar to that of ^{2}H reflecting the effect of the tensor force, while the two neutrons in ^{6}He exhibit quite a different pattern due to the dominant s-wave motion.

A macroscopic $^{20}\mathrm{C} + n + n$ model was applied to look into two-neutron halo structure in ^{22}C (Horiuchi and Suzuki, 2006). The size of this fragile nucleus is predicted to be as large as that of a nucleus with mass number 60. The information on the structure of unstable nuclei is obtained through the analysis of interaction and breakup cross sections (Suzuki *et al.*, 2003).

The ^{12}C nucleus is often modeled as a three-α system. The soundness of this model is confirmed in a fermionic nuclear dynamics calculation (Chernykh *et al.*, 2007) that does not assume the existence of α clusters *a priori*. The first excited 0^+ state at the excitation energy of 7.65 MeV, called the Hoyle state, plays a significant role in producing a ^{12}C element in a star through triple-α reactions. It is well known that both the ground and first excited 0^+ states of ^{12}C are well reproduced by a microscopic 3α calculation (Kamimura, 1981; Matsumura and Suzuki, 2004). However, an unexpected effect occurs in macroscopic model calculations (Suzuki *et al.*, 2007). A local α-α potential, that reproduces the experimental phase shifts, leads to a ground state energy of the 3α system that is far above the experimental value (Suzuki, Matsumura *et al.*, 2008), as seen from the result with the ABd potential of Table XVII. Instead of such a model, one often uses a deep α-α potential and excludes some bound states as Pauli-forbidden states. The results of this model denoted as BFW (Buck, Friedrich, and Wheatley) in Table XVII depend on the definition of the forbidden states. When they are chosen to be harmonic-oscillator states based on the nuclear shell model, the ground state turns out to be deeply bound and the first excited state appears slightly below the 3α threshold. If the forbidden states are chosen to be bound states of the BFW potential, the result is quite different from the harmonic-oscillator case but is similar to the *ABd* case. This enigmatic result has been resolved by carefully analyzing the Pauli-forbidden states (Matsumura *et al.*, 2006). The semimicroscopic calculation in the table uses a nonlocal α-α potential V^{RGM} derived from a microscopic 2α calculation (Suzuki, Matsumura *et al.*, 2008) and reproduces both the ground and first excited 0^+ states reasonably well. The usefulness of this type of nonlocal potential is confirmed in other multicluster systems as well (Theeten *et al.*, 2007). The accuracy of the ECG calculation for this nonlocal potential has been tested by comparing with the result of the HH method (Suzuki, Horiuchi *et al.*, 2008).

The GEM approach has also been applied to the study of hypernuclei which consist of one hyperon (e.g., a Λ particle) in addition to the nucleons. For example, it has been applied to determine the energy levels of ${}^{7}_{\Lambda\Lambda}$He, ${}^{7}_{\Lambda\Lambda}$Li, ${}^{8}_{\Lambda\Lambda}$Li, ${}^{9}_{\Lambda\Lambda}$Li, ${}^{9}_{\Lambda\Lambda}$Be, and ${}^{10}_{\Lambda\Lambda}$Be in a four-body $\alpha + x + \Lambda + \Lambda$ (where $x = n$, p, ^{2}H, ^{3}H, ^{3}He, and α, respectively) cluster model (Hiyama *et al.*, 2002). Recently a five-body model was applied to ${}^{11}_{\Lambda\Lambda}$Be (Hiyama *et al.*, 2010). The ${}^{10}_{\Lambda\Lambda}$Be calculations predicted binding energies of 11.88 MeV for a $J^P = 2^+$ state and 14.74 MeV for a $J^P = 0^+$ state. The Demachi-Yanagi event, which was identified as ${}^{10}_{\Lambda\Lambda}$Be with a binding energy of

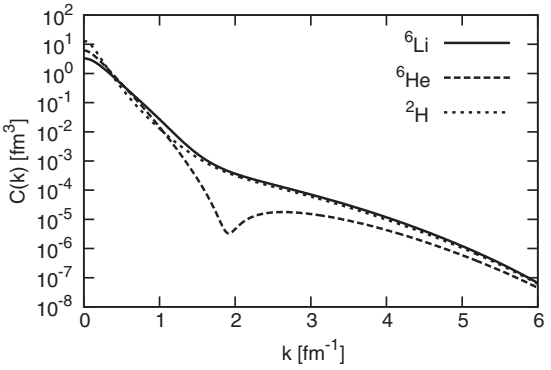

FIG. 9. Momentum distributions of the relative motion between the valence nucleons in ^{6}He and ^{6}Li. The momentum distribution of ^{2}H is also shown.

TABLE XVII. The energy E (measured in MeV) from the 3α threshold and the root-mean-square radius $\sqrt{\langle r^2\rangle}$ (fm) of the point α particle distribution for the ground state and the first excited 0^+ state of the 3α system calculated with different models and potentials. The results with the BFW potential depend on the definition of the Pauli-forbidden states: (i) harmonic-oscillator states and (ii) bound states of the BFW potential. Experimental energies are -7.27 and 0.38 MeV for the 0^+_1 and 0^+_2 states, respectively. RGM denotes the renormalization group method.

Potential	J^π	E	$\sqrt{\langle r^2\rangle}$
ABd (Ali and Bodmer, 1966)	0^+_1	-1.52	2.34
BFW (Buck *et al.*, 1977) (i)	0^+_1	-20.62	1.29
	0^+_2	-1.25	2.34
(ii)	0^+_1	-0.66	2.31
V^{RGM}	0^+_1	-9.44	1.62
	0^+_2	0.597	...

11.90 ± 0.13 MeV (Ahn *et al.*, 2001; Ichikawa, 2001), was interpreted as an observation of the 2^+ state but the angular momentum parity cannot be definitely determined from the experimental data.

E. Baryon spectroscopy

The ECG basis, due to its accuracy, is also a useful tool in baryon spectroscopy. In a seminal work proposing a chiral constituent quark model, the ECG basis with SVM has been used to predict the correct level ordering of low-lying baryons (Glozman *et al.*, 1998); see Fig. 10. ECGs have also been employed in semirelativistic potential models for three-gluon glueballs (Mathieu, Semay, and Silvestre-Brac, 2008) and to calculate the mass of a charmonium hybrid meson with a magnetic gluon (Mathieu, 2009). There are calculations going beyond the three-body problems as well. Pentaquark states in a full five-body model have been explored (Hiyama *et al.*, 2006; Matsumura and Suzuki, 2006; Nemura and Nakamoto, 2007).

F. Outlook

One of the major features of light nuclei is the tendency for the neutrons and protons to coalesce into ^{4}He clusters. It is relatively easy for ECG basis sets to represent wave functions with cluster components. *Ab initio* descriptions of systems such as ^{6}Li ($= {}^4\mathrm{He} + n + p$) or the He halo nuclei should not pose insuperable computational difficulties. It is somewhat surprising that the SVM has not already been applied to nuclei with $5 < A < 8$. One inhibiting factor is the complexity of the NN interaction which slows down the evaluation of the Hamiltonian matrix and the optimization process itself.

The importance of accurate solutions to the nuclear few-body problem is connected with incomplete knowledge of the nuclear interactions. Accurate calculations of binding energies, correlation functions, and other physical properties can be used to select the most reliable nuclear force from the variations derived from QCD-based theories. A similar approach may be used in hypernuclear physics, where the hyperon-nucleon interaction has to be tested and improved.

An ECG-based few-body nuclear model is also useful in studying nuclear correlations that are otherwise difficult to describe, such as the asymptotic behavior of the wave function of a decaying state, the spatially extended neutron halo, or the enhanced electric dipole transitions in ^{212}Po (Astier *et al.*, 2010). Most of the cluster-model calculations done to date have been using phenomenological potentials. Since it is now possible to accurately solve few-body bound-state problems, this cluster-model description should be revisited using interactions that are derived from the realistic interactions utilizing novel approaches, like the unitary correlation operator method (Roth, Neff, and Feldmeier, 2010).

An example for this approach is a systematic calculation of the rates of generating the light elements up to A around 12 in stars. The production of ^{4}He is now well understood as mentioned earlier. The next step is the ^{12}C production through triple alphas. This triple-alpha reaction rate at extremely low energies near the three-alpha threshold poses a challenging three-body problem. There are a number of interesting reactions that need a realistic calculation even for a small mass number.

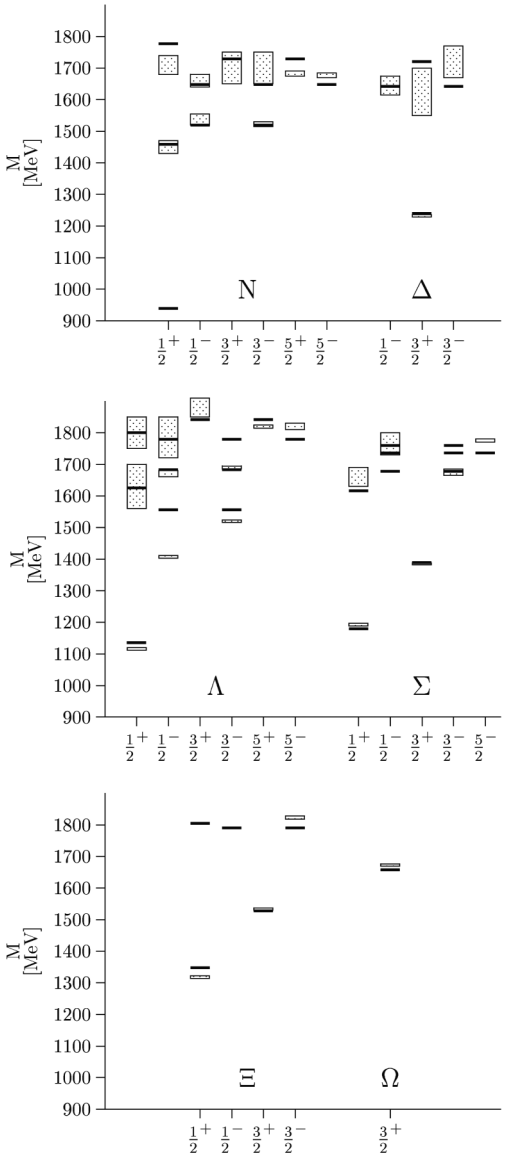

FIG. 10. Energy levels of the lowest light- and strange-baryon states with total angular momentum and parity J^P. The nucleon ground state is 939 MeV. The shadowed boxes represent the experimental values with their uncertainties. Adapted from Glozman *et al.*, 1998.

VII. FEW-BODY SYSTEMS IN CONDENSED MATTER

A. Motivation

Condensed matter physics traditionally deals with infinite systems and the interest in few-body problems is relatively new. The possibility of fabrication of nanoscale devices for electronic and optical applications has dramatically changed this situation. The physical properties of quantum dots, quantum wells, nanowires, nanotubes, and other nanoscale and mesoscale structures are often determined by quantum effects of few-electron systems. While in general these nanostructures contain tens of thousands of electrons, the interaction of these electrons and nuclei determines only the geometric structure of the system and establishes a mean-field potential. This mean-field potential can be a confining potential in which electrons or electrons and holes are trapped and the

quantum mechanical few-body wave function of these particles is responsible for the physical properties of the nanostructure.

The geometry and atomic composition of these structures determines the confining potential, and the confining potential can be changed in various ways essentially tuning the properties of the quantum mechanical systems. This possibility has led to envisioning applications ranging from nanoelectronic devices (e.g., transistors) to quantum computation using entangled few-electron systems confined in quantum dots (Kouwenhoven, Austing, and Tarucha, 2001; Hanson *et al.*, 2007).

Beside electrons, electrons and holes can also be confined in nanostructures. The creation and recombination of excitons and excitonic complexes is one of the principal mechanisms by which light interacts with semiconductors (Snoke, 2002; Rapaport *et al.*, 2004; Hammack *et al.*, 2006). The possibility of engineering these interactions (e.g., emission of light with a desired frequency) leads to a range of applications, including optical sources and detectors (Li *et al.*, 2003; Erementchouk and Leuenberger, 2010).

The common theme of these few-body problems is that the physical properties are determined by quantum mechanical few-particle correlations which cannot be described by single-particle models. ECG approaches with flexible basis functions that can approximate the correlated wave function in various (weak or strong, spherically symmetric or deformed, etc.) confining potentials are indispensable tools to tackle such systems.

B. Excitonic complexes

Electrons and holes in semiconductors combine to form hydrogenlike bound states called excitons. These excitons can also form hydrogen-molecule-like bound states with each other or charged excitons by binding electrons or holes.

The constituents of these systems are electrons and holes with effective masses m_e^* and m_h^* interacting via the Coulomb potential. In crystalline materials, the electrons occupy the valence and conduction bands. The concept of holes is introduced to keep track of the missing electrons in the valence band. The electrons do not freely move in the bands and that restriction is modeled by the introduction of the concept of the effective mass. The effective mass depends on the actual band the electrons or holes occupy; therefore the effective masses of the electrons and holes are different. The properties of the systems strongly depend on the mass ratio $\sigma = m_e^*/m_h^*$. Previous calculations of the binding energy of biexcitons include quantum Monte Carlo (Bressanini, Mella, and Morosi, 1998; Lee, Drummond, and Needs, 2009), boson representation (Okumura and Ogawa, 2001), and variational (Kleinman, 1983; Usukura, Suzuki, and Varga, 1999; Riva *et al.*, 2002) approaches.

The binding energies in two- and three-dimensional excitonic complexes have been studied using SVM (Usukura, Suzuki, and Varga, 1999). The results of these calculations for the energies $E(\sigma)$ at the two limiting cases ($\sigma = 0$ and $\sigma = 1$) are collected in Table XVIII for 2D and 3D systems. The energies are in perfect agreement with other theoretical results in 3D for H_2^+, H^-, H_2 ($\sigma = 0$) and Ps^-, Ps_2 ($\sigma = 1$).

TABLE XVIII. SVM energies of 2D and 3D excitonic complexes in hartree (Usukura, Suzuki, and Varga, 1999).

	2D		3D	
System	$E(\sigma = 0)$	$E(\sigma = 1)$	$E(\sigma = 0)$	$E(\sigma = 1)$
eh	−2.000	−1.000	−0.500	−0.250
eeh	−2.240	−1.121	−0.527	−0.262
ehh	−2.818	−1.121	−0.602	−0.262
eehh	−5.33	−4.385	−1.174	−0.516
eeehh	Unbound	Unbound	Unbound	Unbound
eehhh	−6.82	Unbound	−1.343	Unbound

In both 2D and 3D cases, the charged excitons *eeh* and *ehh* and the biexciton *eehh* are bound for any mass ratio. The *eeehh* complex is not bound for any σ while *eehhh*, a semiconductor analog of H_3^+, is bound for small σ values. The behavior of the energies as a function of σ is quite similar in 2D and 3D except that the energies are much larger in 2D due to the reduced dimensionality.

Figure 11 displays the Haynes factor $f_H = B_{X_2}/B_X$, where B_X and B_{X_2} are the binding energies of the exciton and the biexciton, respectively. The SVM values for f_H are significantly larger than those of a variational calculation using exponential basis functions (Kleinman, 1983). The Haynes factor predicted in the SVM 2D calculation is 0.20 at $\sigma = 0.68$ GaAs, which is in good agreement with the experimental value $f_H = 0.2$ (Birkedal *et al.*, 1996).

C. 2D and 3D quantum dots and quantum wells

Quantum dots (Kouwenhoven, Austing, and Tarucha, 2001; Zumbühl *et al.*, 2004; Fasth *et al.*, 2007; Hanson *et al.*, 2007) are small, nanometer size structures in a solid. Current advances in nanotechnology allow for precise control over the size and shape of these dots. The electronic properties of dots are similar to those of atoms, e.g., the confinement of electrons results in a quantized energy spectrum. It is possible to vary the exact number of electrons in the quantum dot and one can create an entire periodic table of artificial elements.

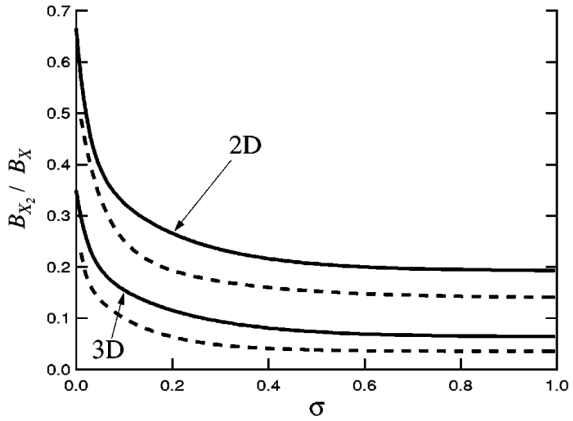

FIG. 11. The SVM binding energy of the biexciton X_2 (*eehh*) compared to the binding energy of the exciton X as a function of the mass ratio σ [adapted from Fig. 5 of Usukura, Suzuki, and Varga (1999)]. The dashed curves show the results of an earlier variational calculation of Kleinman (1983).

Theoretical calculations for quantum dot systems are based on the effective mass approximation: the electrons move in an external confining potential $V_{\rm conf}$ and interact via the Coulomb interaction,

$$H=\sum_{i=1}^{N}\left(-\frac{\hbar^2}{2m_i^*}\nabla_i^2+V_{\rm conf}(\mathbf{r}_i)\right)+\frac{1}{\epsilon}\sum_{i<j}^{N}\frac{q_iq_j}{|\mathbf{r}_i-\mathbf{r}_j|}, \tag{105}$$

where m_i^* is the mass, q_i is the charge of the ith particle, N is the number of electrons, and ϵ is the dielectric constant. The confining potential is often modeled by a harmonic-oscillator potential,

$$V_{\rm conf}(\mathbf{r}_i)=\tfrac{1}{2}m^*\omega^2r_i^2. \tag{106}$$

The apparent similarity of "natural" atoms and quantum dots has motivated the application of sophisticated theoretical methods borrowed from atomic physics and quantum chemistry to calculate the properties of quantum dots, such as exact diagonalization (Maksym and Chakraborty, 1990; Hawrylak and Pfannkuche, 1993), HF approximations (Fujito, Natori, and Yasunaga, 1996; Müller and Koonin, 1996; Yannouleas and Landman, 1999), and density functional approaches (Koskinen, Manninen, and Reimann, 1997; Hirose and Wingreen, 1999). QMC techniques have also been used for 2D (Bolton, 1996; Egger *et al.*, 1999; Harju *et al.*, 1999; Pederiva, Umrigar, and Lipparini, 2000) as well as 3D structures (Taut, 1993; Thompson and Alavi, 2002; Cioslowski and Buchowiecki, 2005; Cioslowski and Pernal, 2006; Ryabinkin and Staroverov, 2010).

The two-electron problem in a harmonic-oscillator potential in 3D is analytically solvable for certain harmonic-oscillator frequencies (Taut, 1993) making it an ideal test ground to study the Coulomb correlation. For more than two electrons, the electronic wave functions can be calculated accurately for various special cases, e.g., at the strong-correlation ($\omega\rightarrow 0$) limit, where the electrons form Wigner molecules with the shapes of an equilateral triangle ($N=3$), a regular tetrahedron ($N=4$), etc. (Cioslowski and Pernal, 2006). Results of accurate configuration interaction (Cioslowski and Matito, 2011), QMC (Amovilli and March, 2011), and SVM (Varga *et al.*, 2001) calculations can be used as benchmark tests for density functional and other quantum chemistry approaches.

The SVM naturally lends itself as a powerful approach to study N-particle quantum dots (Varga *et al.*, 2001). In Table XIX, the SVM energies are compared with the energies of the "exact diagonalization" (Hawrylak and Pfannkuche, 1993; Wojs and Hawrylak, 1996) and the QMC methods (Bolton, 1996; Harju *et al.*, 1999; Pederiva, Umrigar, and Lipparini, 2000) for $N=3$ electron systems. The different methods give energies for both the ground and excited states that typically agree to about 0.1%. The SVM energy is lower than the exact diagonalization one indicating that it is probably more reliable.

In Table XX, a similar comparison is presented for $N=2-6$ electron systems. The SVM results are in agreement with the DMC predictions (Pederiva, Umrigar, and Lipparini, 2000).

To explore the spatial structure of the wave function, a pair-correlation function is defined as

TABLE XIX. SVM energies of a three-electron system. The electrons are harmonically confined in 2D, the oscillator parameter is $\omega=0.2841$ H* [in atomic units which corresponds to $\hbar\omega=3.37$ meV (Varga *et al.*, 2001)]. All values are in meV except those in square brackets, which are in effective hartree (1.0 H* = 11.86 meV for the GaAs system). Results from the "exact" diagonalization, DIAG (Hawrylak and Pfannkuche, 1993) and three DMC calculations DMC1 (Bolton, 1996), DMC2 (Pederiva, Umrigar, and Lipparini, 2000), and DMC3 (Harju *et al.*, 1999) are shown for comparison.

(M, S)	SVM	DIAG	DMC1	DMC2	DMC3
(1,1/2)	26.7827 [2.2582]	26.82	26.77	26.8214(36)	26.88
(2,1/2)	28.2443 [2.3814]	28.27	28.30		28.35
(3,3/2)	30.0101 [2.5304]	30.02	30.04		30.03

$$P(\mathbf{r},\mathbf{r}_0)=\frac{2}{N(N-1)}\times\langle\Psi|\sum_{i<j}\delta(\mathbf{r}_i-\mathbf{R}-\mathbf{r})\delta(\mathbf{r}_j-\mathbf{R}-\mathbf{r}_0)|\Psi\rangle. \tag{107}$$

Here $\mathbf{r}_0$ is a fixed vector and its magnitude is chosen to be equal to $\langle\Psi|\sum_i|\mathbf{r}_i-\mathbf{R}||\Psi\rangle/N$ and $\mathbf{R}$ is the position of the center of mass. This correlation function defines the probability of finding an electron at position $\mathbf{r}$ provided that an electron is at position $\mathbf{r}_0$. Figure 12 shows the pair-correlation functions for the ground state $(M, S)=(1, 1/2)$ of the $N=5$ electron system. For $\omega=1$, the confinement potential is strong and the contribution of the single-particle energies to the total energy is larger than that of the Coulomb potential. The electrons are confined in a rather compact region so that the contour map does not show four peaks clearly. On the contrary, for $\omega=0.1$ (in atomic units) the effect of the confinement becomes weak and the contribution of the Coulomb potential is larger than that of the harmonic-oscillator part. The spatial extent of the system increases and a well-separated pentagonlike structure is seen. The Wigner moleculelike structures formed in this case are in good qualitative agreement with the results from a HF calculation (Yannouleas and Landman, 1999). The SVM calculation is expected to be more accurate.

D. Outlook

The recent surge in nanotechnology has led to the discovery and investigation of numerous nanostructures whose properties

TABLE XX. Comparison of the energies (in units of effective hartree = 11.86 meV) of harmonically confined 2D electron systems ($\omega=0.28$, $\hbar\omega=3.32$ meV).

N	(M, S)	DMC[a]	SVM[b]
2	(0,0)	1.021 62(7)	1.021 64
3	(1,1/2)	2.233 9(3)	2.232 0
4	(0,1)	3.715 7(4)	3.713 0
4	(2,0)	3.754 5(1)	3.752 5
4	(0,0)	3.713 5(6)	3.778 3
5	(1,1/2)	5.533 6(3)	5.531 0
6	(0,0)	7.599 6(8)	7.602 0

[a]Pederiva, Umrigar, and Lipparini (2000).
[b]Varga *et al.* (2001).

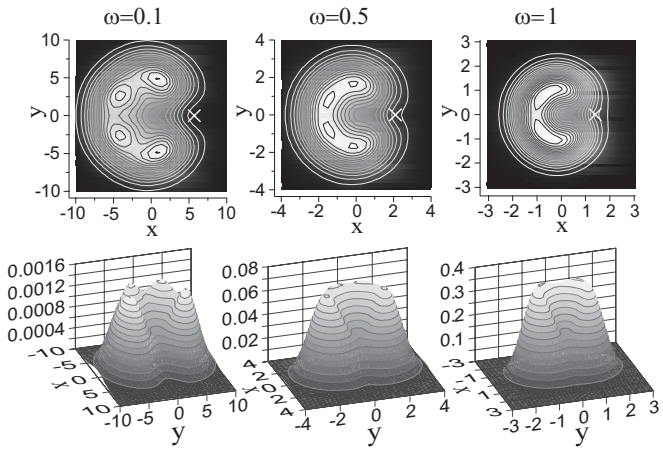

FIG. 12. Pair-correlation function of the ground state $(M, S) = (1, 1/2)$ of the 2D five-electron system as a function of the frequency ω of the harmonically confining potential. The white crosses denote $\mathbf{r}_0$. Atomic units are used. Adapted from Varga *et al.*, 2001.

are determined by quantum mechanical few-body systems. Carbon nanotubes, for example, offer a novel challenge for few-body approaches where the electrons and holes move on the surface of a cylinder (Pedersen *et al.*, 2005; Kammerlander *et al.*, 2007; Roy and Maksym, 2012). This is a "fractional dimensional" few-body system where the 2D problem is embedded into 3D space and one has to use either an appropriate confining potential or an appropriately constrained ECG basis. The studies of properties of excitonic complexes in carbon nanotubes are important, because such complexes determine the linear and nonlinear properties of these materials.

New experiments also revealed many hitherto unknown properties of few-electron systems in quantum dots. Low density, almost localized few-electron systems exhibit peculiar rovibrational modes of an electron molecular state (Kalliakos *et al.*, 2008). The spectra of low-lying excitations associated with changes of the relative-motion wave function are the analogs of the vibration modes of a conventional molecule but do not depend on the rotational state. Theoretical calculations studying the connection between these molecular excitations and short-range correlation are necessary to explore the underlying physical mechanism.

Calculations for quantum dots of various shapes (Fuechsle *et al.*, 2010), including quantum wires (Björk *et al.*, 2004), double quantum dots, and quantum dot molecules, are also important future directions. Recent experiments provided access not only to accurate spectroscopic properties, but they also allow imaging of correlated wave functions of electrons (Rontani *et al.*, 2007). This presents new challenges for few-body calculations and calls for accurate descriptions of the electron-electron correlation and Coulomb blockade in confined systems.

VIII. ULTRACOLD BOSONIC AND FERMIONIC FEW-BODY SYSTEMS

A. Motivation

The study of dilute ultracold atomic and molecular systems is presently at the forefront of modern physics (Dalfovo *et al.*, 1999; Braaten and Hammer, 2006; Bloch, Dalibard, and Zwerger, 2008; Giorgini, Pitaevskii, and Stringari, 2008; Chin *et al.*, 2010). In the ultracold regime, the thermal de Broglie wavelength λ_{dB} (Chin *et al.*, 2010), $\lambda_{\mathrm{dB}} = h/\sqrt{2mk_BT}$, becomes comparable to the average interparticle distance (here m denotes the atom mass, T the temperature, and k_B Boltzmann's constant). Imagine that two atoms collide at room temperature. In this case, λ_{dB} is small and the collision outcome depends on the details of the underlying interaction potential, i.e., a proper description of the collision process involves many partial waves. Imagine, in contrast, that two atoms, which interact through a spherically symmetric interaction potential, collide at an ultracold temperature. In this case, λ_{dB} is large compared to the effective range of the underlying interaction potential and the collision outcome is governed by the lowest partial wave allowed by symmetry. For identical bosons or distinguishable particles, this is the s wave. For identical fermions, in contrast, this is the p wave since s-wave scattering is forbidden by symmetry (Chin *et al.*, 2010).

B. Two-component Fermi gases

The model Hamiltonian for two-component s-wave interacting Fermi gases under external spherically symmetric harmonic confinement reads

$$H = \sum_{j=1}^{N_1}\sum_{k=N_1+1}^{N} V_{\mathrm{tb}}(r_{jk}) + \sum_{j=1}^{N_1}\left(\frac{-\hbar^2}{2m_1}\nabla^2_{\mathbf{r}_j} + \frac{1}{2}m_1\omega^2\mathbf{r}_j^2\right) + \sum_{j=N_1+1}^{N}\left(\frac{-\hbar^2}{2m_2}\nabla^2_{\mathbf{r}_j} + \frac{1}{2}m_2\omega^2\mathbf{r}_j^2\right), \quad (108)$$

where N_1 denotes the number of fermions of species 1 with mass m_1. We denote by N_2 the number of fermions of species 2 with mass m_2 ($N = N_1 + N_2$). In Eq. (108), the unlike atoms interact through a sum of central two-body potentials $V_{\mathrm{tb}}(r_{jk})$, where r_{jk} denotes the distance between particles j and k, $r_{jk} = |\mathbf{r}_j - \mathbf{r}_k|$; here $\mathbf{r}_j$ ($j = 1, \ldots, N$) denotes the position vector of the jth fermion measured with respect to the trap center. Throughout this section, we assume that the atoms of components 1 and 2 occupy two different internal hyperfine states of the same species (implying $m = m_1 = m_2$). If the harmonic-oscillator length a_{ho} that characterizes the external confinement [$a_{ho} = \sqrt{\hbar/(m\omega)}$, where ω denotes the angular trapping frequency] and the absolute value of the interspecies two-body s-wave scattering length $|a_s|$ are much larger than the range r_0 and the effective range r_e of V_{tb}, then the two-component Fermi gas behaves universally, i.e., its properties are fully determined by the dimensionless quantities a_s/a_{ho}, N_1, and N_2.

The ECG approach is extremely well suited to describe universal aspects of small two-component Fermi gases for two primary reasons: (i) Since low-energy observables are, in general, independent of the details of the interaction potential V_{tb} (Giorgini, Pitaevskii, and Stringari, 2008), the true atom-atom potential, which typically supports several tens or hundreds of bound states, can be replaced by a simple Gaussian model potential V_g, $V_g(r) = -V_0 \exp[-r^2/(2r_0^2)]$, whose depth V_0 and range r_0 are adjusted such as to reproduce the desired s-wave scattering length a_s and so that V_g supports no

or one two-body s-wave bound state in free space. The advantage of the Gaussian model potential over, say, a square well model potential is that the matrix elements associated with the interaction potential are readily evaluated (Suzuki and Varga, 1998). Extrapolation of the energy and other observables to the $r_0 \to 0$ limit allows one to simulate zero-range interacting systems. (ii) The functional form of the basis functions employed in the ECG approach is sufficiently flexible to describe short-range correlations that occur at length scales of the order of the range of the interaction potential and long-range correlations that occur at length scales of the order of the external confining potential (Blume, von Stecher, and Greene, 2007; von Stecher and Greene, 2007; von Stecher, Greene, and Blume, 2008).

When a_s is negative and $|a_s|$ small, the N-fermion system behaves like a weakly attractive atomic Fermi gas. When a_s is small and positive, the system can be described as consisting of N_2 repulsively interacting composite bosonic molecules and $|N_1 - N_2|$ unpaired fermions. These small $|a_s|$ regimes are, as has been shown through comparison with results obtained by the ECG and MC approaches, quite well described perturbatively (von Stecher, Greene, and Blume, 2007, 2008). When $|a_s|/a_{ho}$ becomes of the order of 1, nonperturbative approaches are needed. The ECG approach has been applied to determine the energies, structural properties, and dynamics of small trapped gases described by the Hamiltonian given in Eq. (108) as a function of the s-wave scattering length with up to $N = 6$ (Blume, von Stecher, and Greene, 2007; von Stecher and Greene, 2007, 2009; von Stecher, Greene, and Blume, 2007, 2008; Blume and Daily, 2009, 2011; Daily and Blume, 2010; Rittenhouse *et al.*, 2011). For the $(N_1, N_2) = (2, 2)$ system, for example, the ECG formalism was used to model the molecule formation rate in ramp experiments throughout the BCS-BEC crossover (von Stecher and Greene, 2007).

In the unitary regime, i.e., in the regime where the s-wave scattering length diverges, the system is strongly correlated. In this regime, the s-wave scattering length does not define a meaningful length scale and the system is—when $r_0 \to 0$ (i.e., in the zero-range limit)—characterized by the same number of length scales as the noninteracting system (Werner and Castin, 2006a; Giorgini, Pitaevskii, and Stringari, 2008). Like the noninteracting system, the unitary system is scale invariant and possesses ladders of states whose energies are separated by $2\hbar\omega$ (Werner and Castin, 2006a) and are associated with excitations along the hyperradial coordinate (see Sec. III.K for the definition of the hyperradius). The relative energy of the system at unitarity can be written as $E_{\rm rel} = (s_\nu + 2q + 1)\hbar\omega$ (Werner and Castin, 2006a), where s_ν is determined by the eigenvalues of the hyperangular Schrödinger equation (see also below) and q, $q = 0, 1, \ldots$, denotes the hyperradial quantum number. The first numerical verification of the $2\hbar\omega$ spacing for $N > 3$ was obtained by applying the ECG approach (Blume, von Stecher, and Greene, 2007).

Circles and squares in Fig. 13 show the energy of the $(N_1, N_2) = (3, 2)$ system with $1/a_s = 0$ as a function of r_0 for the lowest and third lowest states with $L^\pi = 1^-$ symmetry. In anticipation of the $2\hbar\omega$ spacing, the energy of the third lowest state is shifted down by $2\hbar\omega$. The basis sets contain

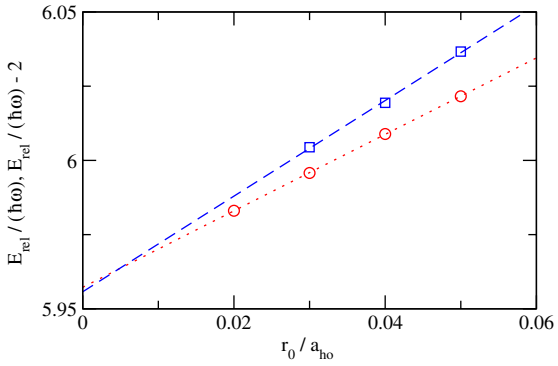

FIG. 13 (color online). Relative energy $E_{\rm rel}$ of harmonically trapped equal-mass two-component Fermi gas with $(N_1, N_2) = (3, 2)$ and $L^\pi = 1^-$ at unitarity as a function of r_0. Circles and squares show $E_{\rm rel}$ (energetically lowest lying state) and $E_{\rm rel} - 2\hbar\omega$ (third lowest state), respectively. Dotted and dashed lines show linear fits to the ECG energies.

between 2400 to 3000 properly antisymmetrized basis functions. The ECG energies shown in Fig. 13 have not been extrapolated to the infinite basis-set limit; the difference between the energies for the largest basis set considered and those for the infinite basis-set limit is of the order of $0.002\hbar\omega$. Dotted and dashed lines show linear fits to the finite-range energies. In the $r_0 \to 0$ limit, the energies of the lowest and third lowest states are $5.957(3)\hbar\omega$ and $7.956(5)\hbar\omega$, respectively, where the number in parentheses indicates the combined basis-set extrapolation and $r_0 \to 0$ extrapolation errors; thus, the $2\hbar\omega$ spacing is verified to within the numerical accuracy of the extrapolated zero-range energies. For the $(N_1, N_2) = (3, 3)$ system [see Fig. 1 in Blume, von Stecher, and Greene (2007)], the hyperradial densities determined from the ECG wave functions were found to be in good agreement with analytic predictions (Werner and Castin, 2006a), thereby confirming the scale invariance of the trapped equal-mass two-component Fermi gas at unitarity.

Table XXI summarizes the zero-range energies of the energetically lowest-lying gaslike state of various trapped (N_1, N_2) systems at unitarity. While analytical results exist for the two- and three-body systems, no analytical results are presently available for $N > 3$. The ECG energies for $L^\pi \neq 0^+$ reported in Table XXI have been obtained using basis functions that are written in terms of one or more global vectors (see Sec. II.D.2) and by extrapolating the energies to the $r_0 \to 0$ limit. These energies constitute the most precise energies for trapped two-component Fermi gases with $N = 4 - 6$ to date.

C. Hyperspherical ECG approach

The previous section considered bound states of trapped few-fermion systems. While some scattering properties such as the atom-dimer and dimer-dimer scattering lengths can be extracted from the energy spectrum of the harmonically trapped system (von Stecher, Greene, and Blume, 2007, 2008), an alternative approach, the hyperspherical ECG (HECG) approach (von Stecher and Greene, 2009; Rittenhouse *et al.*, 2011) (note that they refer to their method as the correlated Gaussian hyperspherical method, or CGHS),

TABLE XXI. Relative energies for trapped two-component Fermi gas with equal masses in the zero-range limit at unitarity. Calculations performed by the ECG approach are marked by * (the numbers in parentheses in the third column indicate the combined basis set and zero-range extrapolation errors).

(N_1, N_2)	L^π	$E_{\rm rel}/(\hbar\omega)$	Reference
(1,1)	0^+	1/2	Busch *et al.* (1998)
(2,1)	1^-	2.772 724	Werner and Castin (2006b)
(3,1)	1^+	5.081 86(10)	Rakshit, Daily, and Blume (2012)*
(4,1)	0^-	7.45(9)	Blume and Daily (2010b)*
(2,2)	0^+	3.509 2(4)	von Stecher and Greene (2009)*
(3,2)	1^-	5.957(3)	Blume and Daily (2011)*
(3,3)	0^+	6.84(9)	Blume and Daily (2011)*

combined with, e.g., an R-matrix calculation allows for the description of multichannel scattering processes. The HECG approach is distinctly different from the ECG-based scattering applications described in Sec. IX. It solves the Schrödinger equation in a two-step process by first considering the hyperangular degrees of freedom and then considering the hyperradial degree of freedom. The key advantage of the HECG approach over, say, the HH expansion approach (see Sec. III.K) is that the ECG functions provide, at least in the low-energy regime considered here, a more flexible basis set than HH.

We consider an N-particle system in three-dimensional space with position vectors $\mathbf{r}_j$ and masses m_j ($j = 1, \ldots, N$) with the interaction potentials of Eq. (3) dependent only on the relative distance coordinates. No external confining potential is considered and the center-of-mass degrees of freedom have been separated.

The starting point of the HECG approach is the hyperspherical representation (Rittenhouse *et al.*, 2011), which expands the relative wave function Ψ in terms of a complete set of channel functions $\Phi_\nu(\mathbf{\Omega}; R)$ which depend parametrically on the hyperradius R and weight functions $F_{\nu q}(R)$ as defined by Eq. (95). The idea of the HECG approach (von Stecher and Greene, 2009) is to expand the channel functions Φ_ν of Eq. (95) in terms of the basis functions given in Eq. (2). Such an expansion requires transformation of the basis functions to hyperspherical coordinates and evaluation of the overlap matrix elements, the hyperangular kinetic energy matrix elements, and the interaction potential matrix elements by integrating over all hyperangles while keeping the hyperradius R fixed. Once $U_\nu(R)$ and $\Phi_\nu(\mathbf{\Omega}; R)$ are known, the coupling matrix elements $P_{\nu'\nu}(R)$ and $Q_{\nu'\nu}(R)$ can be computed and the solutions of the coupled set of one-dimensional radial equations can be obtained using standard techniques. It is important to note that the coupled set of hyperradial equations can be solved using boundary conditions appropriate for bound or scattering states; in the latter case, single-channel and multichannel scattering processes can be treated, i.e., the number of open and closed channels can be adjusted as needed.

To date, the HECG approach has been applied primarily to $N = 3$ and 4 systems with $L^\pi = 0^+$ symmetry. For states with this symmetry, compact expressions for the fixed R matrix elements have been obtained for $N = 3$, while expressions that involve $N - 3$ numerical angular integrations have been obtained for $N > 3$ (von Stecher and Greene, 2009; Rittenhouse *et al.*, 2011). Application of the HECG approach to five-body systems seems possible but application of the HECG approach to six-body systems may be beyond current computational resources. Extensions of the HECG approach to higher angular momentum states appear feasible.

Figure 14 shows the scaled hyperangular eigenvalues or effective potential curves $2\mu R^2 U_\nu(R)/\hbar^2$ for the (2, 2) system, described by the Hamiltonian given in Eq. (108) with $m_1 = m_2$, $\omega = 0$, $L^\pi = 0^+$ symmetry, and infinitely large interspecies scattering length a_s as functions of R/r_0, where r_0 is the range of the Gaussian model potential (von Stecher and Greene, 2009). In the small R region (i.e., for $R/r_0 \lesssim 1$), the hyperradial potential curves are dominated by the hyperangular kinetic energy, resulting in potential curves whose degeneracies coincide with those of the noninteracting system. In the intermediate R region, in contrast, the behavior of the potential curves is governed by a competition between the hyperangular kinetic energy and the interaction energy. In the large R region (i.e., for $R/r_0 \gtrsim 20$), the hyperradial potential curves are dominated by the interaction energy. The large R potential curves at unitarity can be written as $2\mu R^2 U_\nu(R) = \hbar^2(s_\nu^2 - 1/4)$, where s_ν is R independent. The horizontal lines in Fig. 14 show the asymptotic behavior of the three lowest scaled hyperradial potential curves, obtained by extracting s_ν from the relative ECG energies at unitary (see discussion in Sec. VIII.B). The fact that the scaled hyperradial potential curves in the small and large R regions agree with the expected behavior shows that the basis sets employed in the HECG approach are flexible enough to describe the hyperangular dynamics. The next section discusses applications of the HECG approach to the four-boson system.

D. Bose systems and Efimov physics

Section VIII.B discussed the behavior of two-component Fermi gases with equal masses, whose behavior is, for $|a_s| \gg r_0$, fully governed by the s-wave scattering length. For these systems, there are no weakly bound three-body states and the

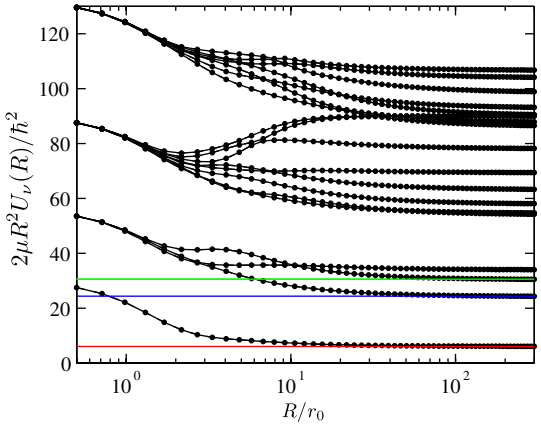

FIG. 14 (color online). Scaled hyperradial potential curves $2\mu R^2 U_\nu/\hbar^2$ as functions of R/r_0 for the (2, 2) system with $L^\pi = 0^+$ symmetry and infinitely large interspecies scattering length a_s. The horizontal lines show the expected asymptotic large-R behavior of the lowest three scaled hyperradial potential curves. Adapted from von Stecher and Greene, 2009.

atom-dimer scattering length a_{ad} is directly proportional to a_s (Giorgini, Pitaevskii, and Stringari, 2008). For the three-boson system with large scattering length and zero-range interactions, the situation is different (Efimov, 1970, 1973). The lowest effective hyperradial potential curve with $L^\pi = 0^+$ symmetry is supercritical, i.e., the problem is undetermined unless augmented by the so-called Efimov or three-body parameter that determines the behavior of the hyperradial wave function in the small R region where all three particles are close together (Braaten and Hammer, 2006). It follows that the equal-mass three-boson system with infinitely large s-wave scattering length supports an infinite number of geometrically spaced three-body bound states (or Efimov trimers) with energy $E_{3,n}$, $E_{3,n+1} \approx E_{3,n}/515$ ($n = 1, 2, \ldots$), where $E_{3,1}$ is determined by the small R boundary condition. Solid lines in Fig. 15 schematically show the three-body Efimov spectrum as a function of $1/a_s$.

Since the early 1970s, when Efimov put this intriguing three-boson scenario forward (Efimov, 1970, 1973), the question "What happens in the four-body sector?" has been asked (Amado and Greenwood, 1973; Kröger and Perne, 1980). Is the behavior of the four-boson system fully determined by the s-wave scattering length and the three-body parameter, or is a four-body parameter needed? Answers to these questions have come from a number of analytical and numerical techniques (Platter, Hammer, and Meissner, 2004; Hammer and Platter, 2007; D'Incao, von Stecher, and Greene, 2009; von Stecher, D'Incao, and Greene, 2009; Deltuva, 2011a, 2011b; Hadizadeh *et al.*, 2011). Using the HECG approach, the effective hyperradial potential curves of the four-boson system were calculated and it was found (von Stecher, D'Incao, and Greene, 2009), in agreement with earlier predictions

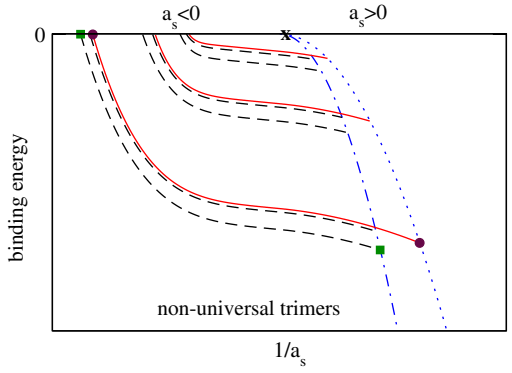

FIG. 15 (color online). Schematic of the extended Efimov scenario for equal-mass boson system as a function of $1/a_s$ ($|a_s|$ large). The solid lines show the energy of three Efimov trimers (the accumulation of infinitely many bound states for slightly negative energy is not shown). Dashed lines show the energy of the two four-body states attached to each Efimov trimer. The dotted and dash-dotted lines show the energy of the weakly bound two-body state and twice the energy of that state, respectively. The scattering lengths at which the most strongly bound Efimov trimer dissociates into three free atoms or a dimer and a free atom are marked by circles. The scattering lengths at which the more deeply bound tetramer attached to the most strongly bound Efimov trimer dissociates into four free atoms or two dimers are marked by squares. The point $(1/a_s, E) = (0, 0)$ is marked by an x.

(Hammer and Platter, 2007), that there are two weakly bound four-body states with energies $E^{(1)}_{4,n}$ and $E^{(2)}_{4,n}$ "attached" to each Efimov trimer state with energy $E_{3,n}$: $E^{(1)}_{4,n} \approx 4.58E_{3,n}$ and $E^{(2)}_{4,n} \approx 1.01E_{3,n}$ (see dashed lines in Fig. 15). The proportionality constants 4.58 and 1.01 are universal, i.e., they are the same for all Efimov trimers and independent of the details of the underlying two-body potential. The fact that the energies $E^{(1)}_{4,n}$ and $E^{(2)}_{4,n}$ are universally linked to the energy of the nth Efimov trimer suggests that a four-body parameter is not needed, i.e., that the short-range behavior of the four-body hyperradial potential curves is not supercritical. We note that alternative interpretations exist (Hadizadeh *et al.*, 2011).

Furthermore, the application of the HECG approach showed that the s-wave scattering lengths $a^{(1),-}_{4,n}$ and $a^{(2),-}_{4,n}$ at which the four-body states dissociate into four free atoms are universally related to the scattering lengths $a^-_{3,n}$ at which the Efimov trimers dissociate into three free atoms, $a^{(1),-}_{4,n} \approx 0.43a^-_{3,n}$ and $a^{(2),-}_{4,n} \approx 0.90a^-_{3,n}$ (von Stecher, D'Incao, and Greene, 2009). On the positive scattering length side, the HECG calculations predicted that the scattering lengths $a^{(1),+}_{4,n}$ and $a^{(2),+}_{4,n}$ at which the tetramers dissociate into two dimers are universally related to the scattering lengths $a^+_{3,n}$ at which the trimers dissociate into a dimer and a free atom (D'Incao, von Stecher, and Greene, 2009). Recent scattering calculations (Deltuva, 2011a, 2011b) based on momentum-space equations confirmed these findings and significantly improved upon the numerical accuracy of the proportionality constants.

The extended Efimov scenario for equal-mass boson systems with $N > 4$ is presently less well understood. Recent ECG calculations suggest that there also exist two five-body states that are attached to each Efimov trimer (von Stecher, 2010, 2011). Indeed, preliminary experimental results show evidence for enhanced loss features at the expected s-wave scattering lengths (Zenezini *et al.*, 2012). The ECG and HECG results for the four- and five-body energy spectra are in agreement with an earlier approximate hyperspherical MC study (Blume and Greene, 2000), which found two bound states for $N = 4 - 10$ for an interaction model that supports one weakly bound trimer state, and with a ground state DMC study (Hanna and Blume, 2006), which found evidence that four- or higher-body parameters are not needed to describe the low-energy states of bosonic systems with $N > 3$. Altogether, these results point toward a unified picture of the low-energy behavior of few-boson systems with large s-wave scattering length ($N > 3$), namely, that the low-energy observables of the N-body system are universally linked to two- and three-body observables.

In addition to the equal-mass s-wave interacting boson system, Efimov physics plays a role in the three-boson system with anisotropic dipolar interactions (Wang, D'Incao, and Greene, 2011) and in unequal-mass two-component Fermi gases with sufficiently large mass ratio (Petrov, 2003). It is expected that applications of the ECG and HECG approaches contribute to the construction of extended Efimov scenarios that include three- and four-body physics for these systems in the future. In the regime where Efimov physics is absent, the ECG approach has already been applied to investigate three- and four-body resonances of trapped unequal-mass

two-component Fermi gases (Blume and Daily, 2010a, 2010b).

E. Outlook

As mentioned in the Introduction, the ECG approach is most powerful if applied to four- and higher-body systems where a variety of other numerical approaches have limitations because of their unfavorable scaling with increasing numbers of degrees of freedom. The study of few-body phenomena for systems with more than three constituents in the ultracold has just started. Tremendous experimental progress has paved the way for measurements of observables that have been attributed to four-body physics (Ferlaino *et al.*, 2009; Pollack, Dries, and Hulet, 2009; Zaccanti *et al.*, 2009). As experiment and theory continue to mature, it is expected that the ECG approach, with its variants, will play an increasingly prominent role in the study of low-energy bound-state and scattering observables of systems consisting of more than three particles. For example, there are presently many open questions related to the extended Efimov scenario of the five-boson system, of unequal-mass two-component Fermi systems, and of dipolar systems. Furthermore, the study of N-body resonances in three dimensions or in effectively low-dimensional geometries promises rich physics, with direct consequences for possible pairing scenarios that involve N-body clusters.

Indeed, the ECG approach has already been applied to dipolar systems in effectively low-dimensional confining geometries (Volosniev *et al.*, 2011). A key motivation behind these studies is the tremendous experimental progress in cooling polar molecules down to the near-degenerate regime (Ni *et al.*, 2008). The dipole-dipole interaction is long range and anisotropic and couples different angular momentum states. Generally speaking, "head-to-tail collisions" of aligned dipoles are attractive and can lead to detrimental losses. The application of effectively low-dimensional confining geometries has been shown theoretically and experimentally to significantly stabilize dipolar systems (Lahaye *et al.*, 2009; de Miranda *et al.*, 2011). In one set of ECG applications (Volosniev *et al.*, 2011), the system wave functions have been expanded in terms of shifted Gaussians. The emergence of weakly bound few-body states (involving, e.g., aligned dipoles located in two different layers) is of particular interest, as the few-body spectra provide crucial insights into the many-body behavior of these highly nontrivial and strongly correlated systems.

IX. SCATTERING AND RESONANCES

A. Motivation

While the possibility of employing bound-state methods to treat scattering states has always been desirable, there have been few applications of ECG technologies to collision physics (Ivanov, Mitroy, and Varga, 2001, 2002a; Hiyama, Kino, and Kamimura, 2003; Matsumoto *et al.*, 2003; Hiyama *et al.*, 2006; Mitroy, Zhang, and Varga, 2008; Zhang, Mitroy, and Varga, 2008; Zhang and Mitroy, 2011; Aoyama *et al.*, 2012). However, the few scattering calculations that have been done have often been on systems that would be difficult to treat by other means.

The diversity of scattering problems can be divided into two classes. First one has a class of low-energy systems in which only elastic scattering is possible. Such systems can be treated as quasi-bound-state systems with an *ad hoc* procedure used to impose the scattering boundary conditions. The other class of systems has multiple open channels, which are best treated by embedding ECG basis functions into an established scattering theory.

B. Single channel elastic scattering systems

1. Confining potentials

While the overall goal is the determination of the scattering wave function, it is useful to divide the calculation into two stages. The first stage of the calculation is to generate a basis that gives a good representation of the dynamics when the projectile and target are close together. The next step involves using this basis to calculate the scattering information.

The first stage can be achieved by adding a confining potential to the Hamiltonian. Two forms have so far been adopted. In initial applications, the form was

$$V_{\mathrm{CP}}(r) = \lambda r^n. \tag{109}$$

One choice adopted was $\lambda \approx 10^{-19}$ hartree$/a_0^{12}$ and $n = 12$ (Zhang and Mitroy, 2008). This gave a potential that was small in the interaction region for the system under consideration. A more refined version was

$$V_{\mathrm{CP}}(r) = G\Theta(r - R_0)(r - R_0)^2, \tag{110}$$

where Θ is the Heaviside function and G is the strength parameter of the potential.

With these potentials, the generation of the interaction region basis reduces to a standard bound-state calculation. So far, the confining potential concept has been applied only to systems with an infinitely heavy scattering center. It has not been applied to systems where the projectile and scattering particle are of comparable mass. It should be noted that the initial ECG-based calculations on atomic systems did not use confining potentials. In this case, confinement was achieved by constraining the α_{ij} coefficients in Eq. (2) to be positive and to not fall below a critical minimum size (Ivanov, Mitroy, and Varga, 2001, 2002a, 2002b).

2. The asymptotic basis

A linear combination of ECGs is not a particularly efficient way to represent the wave function in the asymptotic region since the wave function takes a simple product form at large separations. For example, the asymptotic wave function for e^--He scattering would be written (with implied antisymmetrization) as

$$\Psi = \psi_{\mathrm{He}}(\mathbf{r}_1, \mathbf{r}_2)\phi(\mathbf{r}_3). \tag{111}$$

This part of the wave function can be best incorporated by adding basis functions of the form (Zhang, Mitroy, and Varga, 2008)

$$\Psi_{i,\text{out}} = \psi_{\text{He}}(\mathbf{r}_1, \mathbf{r}_2)\psi_i(\mathbf{r}_3),$$
$$\psi_{\text{He}}(\mathbf{r}_1, \mathbf{r}_2) = \sum_k d_k \exp(-\beta_{k1} r_1^2 - \beta_{k2} r_2^2 - \beta_{k12} r_{12}^2),$$
$$\psi_i(\mathbf{r}_3) = \exp(-\alpha_i r_3^2) \tag{112}$$

to the three-electron ECGs resulting from the optimization of the energy within the confining potential. The target wave function can be represented as a linear combination of ECGs and the α_i are chosen as a geometric progression obeying $\alpha_i = \alpha_1/T^{i-1}$ (where T is typically set to be about 1.45). Each asymptotic basis function is actually composed of a linear combination of ECGs.

The utility of the asymptotic basis can be seen by reference to the e^--He ($^2S^e$) phase shift. A basis of 800 three-electron ECGs supplemented by 40 additional asymptotic basis functions given by Eq. (112) gave a phase shift that was closer to convergence than a basis of 1600 three-electron ECGs without any asymptotic basis function (Zhang, Mitroy, and Varga, 2008).

3. Calculations of cross sections

Once a good basis for the interaction region has been generated, there are a number of methods that can be used to extract the scattering information. For example, it is possible to determine the phase shifts directly from the energies of the system confined by Eq. (110) (Mitroy, Zhang, and Varga, 2008; Zhang, Mitroy, and Varga, 2008). In addition, in terms of increasing complexity, one can use stabilization ideas (Hazi and Taylor, 1970), the Harris variational method (Harris, 1967; Kievsky *et al.*, 2010), the Kohn variational method (Burke and Joachain, 1995), or a Green's function method (Suzuki, Horiuchi, and Arai, 2009). Some of these methods will be discussed in the sections that follow.

4. Stabilization calculations

Two types of states occur when a large square-integrable basis is diagonalized in a potential. The first class of states are those with negative energies that approximate the exact bound states of the potential. Another class of states have positive energy but do not have the long-range character of true continuum states. However, the shape of the wave function for these positive energy states often resembles that of the true continuum state over a finite range of coordinates at that energy (Hazi and Taylor, 1970). This is demonstrated in Fig. 16 where the pseudostate with energy E obtained by diagonalizing the free particle Hamiltonian in a basis of Laguerre-type orbitals is compared to $\sin(\sqrt{2mE/\hbar}r)$. Phase shifts accurate to about 1% can be determined by making a least squares fit of the square-integrable wave function to the known asymptotic form outside the interaction region (Ivanov, Mitroy, and Varga, 2001, 2002a).

Stabilization calculations utilizing ECGs have been applied to a number of difficult to solve few-body systems. One of the first series of stabilization calculations was an application to the Ps-H, Ps-He (and other rare gases), and Ps-Ps systems. These represent difficult to treat systems since both projectile and target are composite systems with internal structures (Ivanov, Mitroy, and Varga, 2001, 2002a, 2002b).

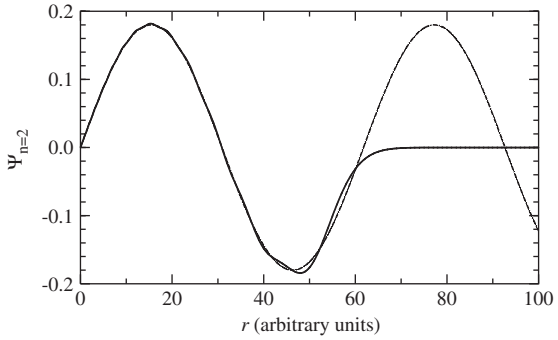

FIG. 16. Comparison between $\sin(kr)$ and a pseudostate (first excited state) obtained by diagonalization of the free particle Hamiltonian in a large basis of Laguerre-type orbitals. The value of k is taken to be $\sqrt{2E}$, where E is the energy of the pseudostate.

One of the key results of this early work was an estimate of the scattering length for ^{3}Ps-^{3}Ps scattering. A stabilization SVM calculation gave a scattering length of 8.44 a_0 (Ivanov, Mitroy, and Varga, 2002b). The only other first-principles estimates of the scattering length, namely, 9.15(4) a_0, came from the QMC calculations (Shumway and Ceperley, 2001). The interest in this system is derived from proposals to form a BEC made up of triplet positronium (Platzman and Mills, Jr., 1994) (the lifetime of ^{3}Ps is 0.125×10^{-7} s). The light mass means the critical temperature will lie between 20 and 30 K and the positive scattering length means the BEC would be stable.

The five-body Ps-He system is an example of a calculation that is technically challenging since both the target and the projectile are composite particles. The only observable that has been directly measured with any reliability is the *pickoff* annihilation rate $_1Z_{\text{eff}}$. This quantity is related to the cross section for the annihilation of the positron due to contact with the target electrons (Charlton, 1985). It can be calculated for positrons colliding with an N-electron target using

$$_1Z_{\text{eff}} = \sum_{i=1}^{N} \int d^3\tau d^3 r_0 |\Psi(\mathbf{r}_1, \ldots, \mathbf{r}_N; \mathbf{r}_0)|^2 \delta(\mathbf{r}_i - \mathbf{r}_0), \tag{113}$$

where $\Psi(\mathbf{r}_1, \ldots, \mathbf{r}_N; \mathbf{r}_0)$ is the scattering wave function, $d^3\tau$ represents the integration of electron coordinates $\mathbf{r}_1$ to $\mathbf{r}_N$, and $\mathbf{r}_0$ is the positron coordinate. Despite being one of the standard observables extracted from positron annihilation experiments (Charlton, 1985; Charlton and Humberston, 2001), there has never been a first-principles calculation of $_1Z_{\text{eff}}$ for any physical system that could be expected to be accurate to within a factor of 2. The attractive electron-positron force leads to a localization of the positron within the vicinity of the target electrons which significantly increases the annihilation rate. Incorporating this localization of the wave function is straightforward with ECG-based wave functions.

The variation of $_1Z_{\text{eff}}$ as a function of k for $k < 0.30\ a_0^{-1}$ is shown in Fig. 17 as an effective range fit to the calculated values (Zhang and Mitroy, 2008). The value of $_1Z_{\text{eff}}$ at thermal energies was found to be 0.1157. The agreement with experiment is acceptable when the uncertainties in

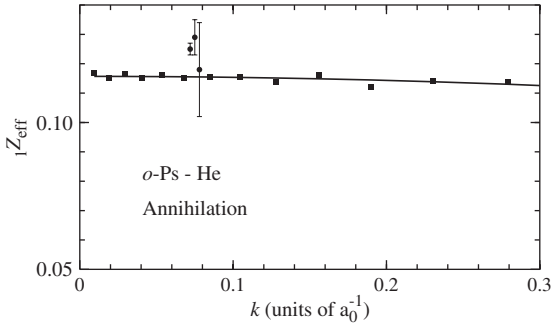

FIG. 17. The *s*-wave pickoff annihilation parameter for Ps-He scattering as a function of k (in units of a_0^{-1}) [adapted from Fig. 7 of Zhang and Mitroy (2008)]. The solid line is the fit to the *ab initio* data using effective range theory while the data points with the error bars are experimental (Duff and Heymann, 1962; Canter, McNutt, and Roellig, 1975; Coleman *et al.*, 1975).

extracting $_1Z_{\rm eff}$ from the experimental lifetime spectrum are taken into consideration.

5. Kohn variational calculations

The Kohn variational method is a well-established approach to calculating low-energy scattering information (Burke and Joachain, 1995). However, it presents additional complications due to the existence of matrix elements involving the continuum. The only ECG-based Kohn variational calculations in atomic physics involved the positron as a projectile (Zhang and Mitroy, 2011). The most complicated matrix elements have two continuum functions, e.g.,

$$\langle \psi(\mathbf{r})\Phi(\mathbf{R})|(H-E)|\psi(\mathbf{r})\Psi(\mathbf{R})\rangle. \tag{114}$$

In this expression, $\Psi(\mathbf{R})$ is a target many-body wave function expressed in terms of ECGs and $\psi(\mathbf{r})$ is a continuum function. One can integrate over the collective set of target coordinates, i.e., $\mathbf{R}$, leaving a numerical integral over the last coordinate.

Potentially more complicated problems appear when there is an exchange interaction between the projectile and target (e.g., electron-atom scattering). One has to deal with integrals of the type

$$\langle \psi(\mathbf{r})\Psi(\mathbf{r}',\mathbf{R}')|(H-E)|\psi(\mathbf{r}')\Psi(\mathbf{r},\mathbf{R})\rangle, \tag{115}$$

which in general can be complicated. However, the exchange interaction is a short-range interaction and there are a number of ways for evaluating such integrals, for example, by separable expansion, or by replacing the continuum function at short distances by a linear combination of Gaussians (Kamimura, 1977; Rescigno and Orel, 1981; Rescigno and Schneider, 1988).

One recent landmark calculation was the application of SVM to e^+-H_2 scattering (Zhang, Mitroy, and Varga, 2009; Zhang and Mitroy, 2011). The strong electron-positron interactions mandate the use of a correlated basis. Calculations of the low-energy cross section with Hylleraas basis sets (Armour and Baker, 1986; Cooper, Armour, and Plummer, 2008) had not been able to achieve convergence due to difficulties in calculating the matrix elements. However, matrix element evaluation of the ECG basis did not pose any insuperable problems in a recent calculation of zero-energy e^+-H_2 scattering. The strategy of the calculation was to optimize the energies of the two lowest states of the e^+-H_2 system inside a confining potential. The resulting ECG basis was then used in a Kohn variational calculation.

Figure 18 shows the scattering length as a function of internuclear distance. The interesting feature is the deep minimum in the scattering length near $R = 3.4\,a_0$ which was completely unexpected. The large negative scattering length indicates that the positron is close to being bound to H_2 at this internuclear distance. The zero-energy cross section for elastic e^+-H_2 scattering can be determined by integrating over the H_2 internuclear distances corresponding to the vibrational ground state.

The most important observable for low-energy e^+-H_2 scattering is the annihilation parameter $_1Z_{\rm eff}$ for positrons annihilating at thermal energies. Experimental values are 14.7(2) (McNutt, Sharma, and Brisbon, 1979), 14.61(14) (Laricchia *et al.*, 1987), and 16.02(8) (Wright *et al.*, 1983). The differences between the experimental values can be ascribed to variations in how the positrons achieve thermal energies in the different experiments (Zhang and Mitroy, 2011). The Kohn variational calculation using ECGs generated in a confining potential gave $_1Z_{\rm eff} = 15.7$ (Zhang and Mitroy, 2011) and is supportive of the experiment giving the large $_1Z_{\rm eff}$. The ECG basis can easily represent the localization of the electron density around the positron which is essential in positron annihilation calculations. Kohn variational calculations based on Hylleraas basis functions (Armour and Baker, 1986; Cooper, Armour, and Plummer, 2008, 2009; Armour *et al.*, 2010) gave values ranging from 10 to 13 with some uncertainty about which value to adopt.

The Kohn variational method has also been used with GEM wave functions to investigate the nucleon-K meson system treated as a five-quark system (Hiyama *et al.*, 2006). Two resonances at 500 and 520 MeV were identified (Hamaguchi *et al.*, 2007) with this approach.

C. Multichannel scattering

1. Continuum discretized coupled-channel method

The continuum discretized coupled-channel (CDCC) method can be used to study breakup reactions in nuclear physics (Yahiro *et al.*, 1982; Austern *et al.*, 1987). The GEM

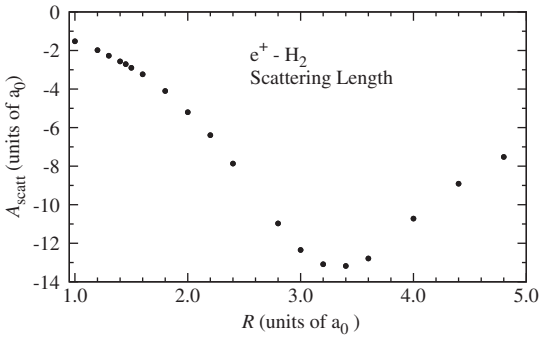

FIG. 18. The scattering length (in units of a_0) as a function of the internuclear distance R for positron scattering from H_2. Adapted from Zhang, Mitroy, and Varga, 2009.

approach was used to construct CDCC wave functions for three-body (Yahiro *et al.*, 1982; Matsumoto *et al.*, 2003; Egami *et al.*, 2004) and four-body (Matsumoto *et al.*, 2006) breakup.

The ^{6}He nucleus is a very weakly bound halo nucleus. As such, breakup reactions involving this nucleus and a heavy nuclei (X) have a contribution from the four-body $^6\mathrm{He} + X \rightarrow n + n + \alpha + X$ continuum (Matsumoto *et al.*, 2004, 2006). In the three-body model for describing this reaction, the two neutrons are treated as a single di-neutron, i.e., as $^2n + \alpha + X$. Figure 19 shows the impact of the four-body continuum on the differential cross section for $^6\mathrm{He} + ^{209}\mathrm{Bi}$ *elastic* scattering (Matsumoto *et al.*, 2006). The four-body continuum leads to an increase in the differential cross section for center-of-mass scattering angles larger than 30°. The inclusion of the four-body continuum has larger impact on the *total reaction* cross section. The three-body CDCC calculation overestimated an optical potential analysis (Aguilera *et al.*, 2000) by 180% while the four-body calculation overestimated by 35%.

2. *R*-matrix calculations of few-nucleon reactions

Because of the complexity of the *NN* interaction, only a few approaches (Nollett *et al.*, 2007; Quaglioni and Navrátil, 2008; Suzuki, Horiuchi, and Arai, 2009; Viviani *et al.*, 2011) have been applied to the *ab initio* study of nuclear scattering and reactions for $A > 3$ using realistic nuclear interactions. A common theme underpinning these approaches is to divide the configuration space into internal and external regions with the dynamical interactions confined to the internal region.

ECGs have recently been used to construct the interaction region basis in a microscopic *R*-matrix treatment of few-body nuclear scattering (Descouvemont and Baye, 2010; Arai *et al.*, 2011; Aoyama *et al.*, 2012). The total wave function in the internal region $\Psi^{\pi}_{\mathrm{int}JM}$, where J is the angular momentum and π is the parity, is expanded in terms of the channel functions defined as

$$\Phi^{\pi}_{\alpha JM} = [[\Psi_{I_a}\Psi_{I_b}]_I F_{aI_abI_b}(r_\alpha)Y_\ell(\hat{\mathbf{r}}_\alpha)]_{JM}. \tag{116}$$

The channel wave functions are eigenstates of the total angular momentum of the system and couple the internal wave functions Ψ_{I_a} and Ψ_{I_b} of the fragments with a function describing the radial and angular dependences of the relative motion (vector $\mathbf{r}_\alpha$ connects the center of mass of the fragments). The internal channel wave functions are represented by a linear combination of ECGs that are generated by diagonalizing the appropriate realistic *NN* potential. The wave function $F_{aI_abI_b}(r_\alpha)$ is represented in the interaction region as a set of Gaussians. Outside the interaction region (e.g., outside the *R*-matrix boundary), the wave function is represented by the appropriate asymptotic form that satisfies a prescribed asymptotic boundary condition.

The equation of motion for the internal region is

$$(H + \mathcal{L} - E)\Psi^{\pi}_{\mathrm{int}JM} = \mathcal{L}\Psi^{\pi}_{\mathrm{ext}JM}, \tag{117}$$

with the Bloch operator

$$\mathcal{L} = \sum_\alpha \frac{\hbar^2}{2\mu_\alpha R}|\Phi^{\pi}_{\alpha JM}\rangle\delta(r_\alpha - R)\left(\frac{\partial}{\partial r_\alpha} - \frac{b_\alpha}{r_\alpha}\right)r_\alpha\langle\Phi^{\pi}_{\alpha JM}|, \tag{118}$$

where b_α are arbitrary constants. The Bloch operator acts only at the surface R and ensures that the logarithmic derivative of the wave function is continuous at R. A solution of Eq. (117) determines the S matrix from which cross sections can be computed.

The first few-body system investigated with the *R*-matrix or ECG approach consisted of reactions related to the four-nucleon α-particle system (Descouvemont and Baye, 2010; Arai *et al.*, 2011; Aoyama *et al.*, 2012). The total wave function included the physical channels $d(^2\mathrm{H}) + d$, $t(^3\mathrm{H}) + p$, and $^3\mathrm{He} + n$. The d, t, and ^{3}He ground states and excited pseudostates were included in the expansion. Pseudostates describing nn and pp channels were also added.

The particle transfer reactions for d-d collisions and the radiative capture of deuterons during these collisions are fundamental to an understanding of nuclear fusion. The three most important reactions are $^2\mathrm{H}(d,\gamma)^4\mathrm{He}$, $^2\mathrm{H}(d,n)^3\mathrm{He}$, and $^2\mathrm{H}(d,p)^3\mathrm{H}$. The latter two reactions can be directly calculated from the S matrix coming from a solution of Eq. (117). The first reaction involves an electromagnetic transition matrix element between the scattering state and the ^{4}He ground state, which can be calculated by using first-order perturbation theory.

Below the Coulomb barrier, the cross section is strongly dependent on energy-dependent kinematic factors. To reduce this energy dependence, it is usual to convert the cross sections into the astrophysical S factors, defined as

$$S_{J_f\pi_f}(E) = E\exp(2\pi\eta)\sigma_{J_f\pi_f}(E), \tag{119}$$

where $\eta = Z_1Z_2e^2/k$ is the Sommerfeld parameter.

Figure 20 displays the calculated astrophysical S factor for the $^2\mathrm{H}(d,\gamma)^4\mathrm{He}$ (Arai *et al.*, 2011) reaction. The angular

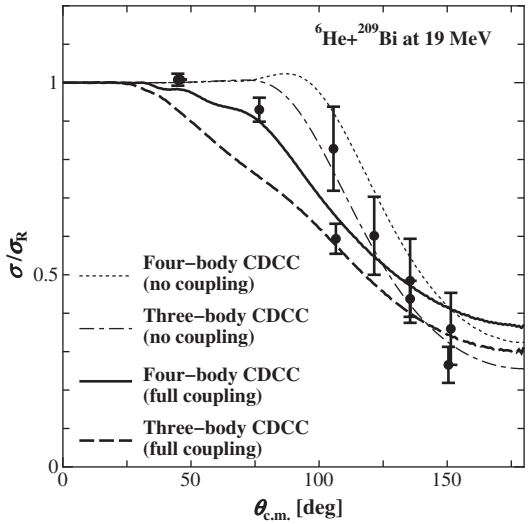

FIG. 19. Angular distribution of the ratio of the elastic differential cross section to the Rutherford cross section for $^6\mathrm{He} + ^{209}\mathrm{Bi}$ scattering at 19 MeV. The solid (dashed) and dotted (dot-dashed) lines show the results of the four-body (three-body) CDCC calculation with and without breakup effects, respectively. The experimental data are at laboratory frame energies of 19.0 MeV (Aguilera *et al.*, 2000) and 19.1 MeV (Aguilera *et al.*, 2001) Adapted from Matsumoto *et al.*, 2006.

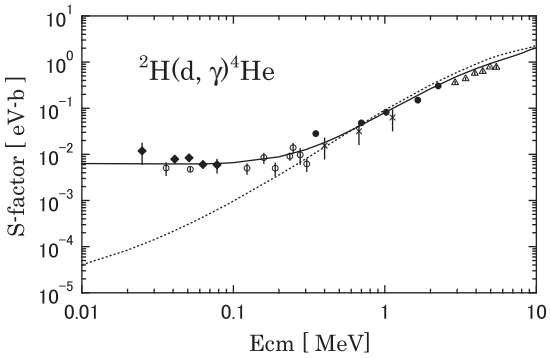

FIG. 20. Astrophysical S factor of the ^{2}H(d, γ)^{4}He reaction. Results with AV8′ + 3NF (solid line) and Minnesota interaction (Thompson, Lemere, and Tang, 1977) (dotted line) are compared to experiment (Angulo *et al.*, 1999). Adapted from Arai *et al.*, 2011.

momentum of the deuteron is 1. The radiative capture reaction to the ground state of ^{4}He proceeds from an incoming $d + d$ channel ($^{2I+1}\ell_J$) by particular electromagnetic multipole transitions: $E1$ for $^3P_1$, $M1$ for $^5D_1$, $E2$ for $^5S_2$, $^1D_2$, and $^5D_2$, etc. Because only the $^5S_2$ channel contains an s-wave scattering wave function, the radiative capture is expected to proceed predominantly via an $E2$ transition at least at low energies. Results with the AV8′ + 3NF potential reproduce the experimental data very well. The simple Minnesota potential, which does not include the tensor interaction, grossly underestimates $S_{J_f\pi_f}(E)$ at the lowest $E_{\text{c.m.}}$ since the scattering wave function does not have an s wave at low energies. Figure 21 shows the contributions of the $^5S_2$, $^1D_2$, and $^5D_2$ incoming dd channels to the S factor. The first two channels give equal contributions at about 0.3 MeV. Below that energy, the $^5S_2$ channel overwhelms the $^1D_2$ channel as expected, yielding the flat behavior. Above 0.3 MeV, the $^1D_2$ channel contributes more than the $^5S_2$ channel. The contribution of the $^5D_2$ channel is negligible at low energies.

Figure 22 shows the astrophysical S factors for the particle transfer reactions ^{2}H(d, p)^{3}H and ^{2}H(d, n)^{3}He (Arai *et al.*, 2011). All states with $J^\pi = 0^\pm, 1^\pm, 2^\pm$ are taken into account in the calculation. The results obtained with the realistic AV8′ + 3NF potential are in good agreement with experiment. The simpler Minnesota potential grossly underestimated the

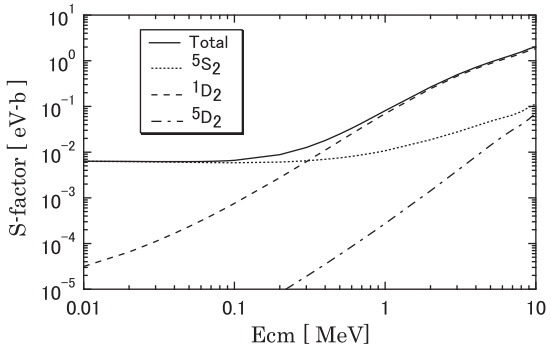

FIG. 21. Contributions of three incoming $d + d$ channels, $^5S_2$, $^1D_2$, and $^5D_2$, to the astrophysical S factor of the ^{2}H(d, γ)^{4}He reaction calculated with AV8′ + 3NF potential. Adapted from Arai *et al.*, 2011.

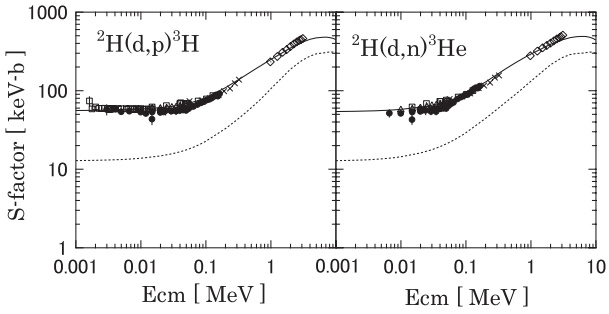

FIG. 22. Astrophysical S factors of the ^{2}H(d, p)^{3}H and ^{2}H(d, n)^{3}He reactions. Results with AV8′ + 3NF (solid line) and Minnesota interaction (dotted line) are compared to experiment (Angulo *et al.*, 1999; Leonard *et al.*, 2006). Adapted from Arai *et al.*, 2011.

capture cross section. The cross section at very low energies is found to be dominated by the 2^+ state that contains the transition from the initial $^5S_2$ to the final $^3D_2$ channel.

The R-matrix or ECG model is sufficiently flexible to permit the inclusion of important dynamical interactions in the description of the collision. It also permits the use of a modern realistic NN interaction. Excellent agreement with experiment suggests that further applications to other few-body systems might be worthwhile.

D. Complex rotation calculations of resonances

There have been relatively few calculations of resonances with ECG-based wave functions. Most of the calculations have been performed with the complex rotation method (Nuttal and Cohen, 1969; Moiseyev, Certain, and Weinhold, 1978; Ho, 1983; Moiseyev, 1998) called also the complex scaling method (CSM). In this method, the Hamiltonian and wave function are transformed by a coordinate rotation

$$\mathbf{r} \rightarrow \exp(i\theta)\mathbf{r}. \tag{120}$$

Rotation of the coordinates sufficiently far into the complex plane leads to the resonant wave function which is square integrable and accessible to a basis-set expansion. When the interactions are purely Coulombic, the complex scaled Hamiltonian can be written as

$$H_\theta = \exp(-2i\theta)T + \exp(-i\theta)V_C, \tag{121}$$

where the complex scaling parameter θ is an arbitrary real parameter satisfying the inequality $0 < \theta < \pi/2$. A generalized variational principle (Ho, 1983; Moiseyev, 1998) can be applied to the complex scaled Hamiltonian. Resonant states can be identified by adjusting the θ parameter. The complex energies of scattering states rotate in an approximately circular trajectory on the complex plane as θ is varied, while resonant state energies show relatively little change as θ changes. The variational principle for the complex scaled Hamiltonian, Eq. (121), is only a stationary principle. There is no guarantee that the calculated position of the resonance is a lower or upper bound for the true value. The energies of scattering states can also slide through the resonance energy during optimization. For these reasons, some of the first complex scaling calculations of resonances using ECGs

were performed with the GEM approach without extensive optimization process.

1. Antiprotonic helium

One application of the ECG-based GEM has been to the metastable states of the exotic $\bar{p}\mathrm{He}^+$ system (Hayano *et al.*, 2007). Such states have the antiproton trapped with a large angular momentum ($L \sim 30$). The states are metastable since the system can undergo an Auger decay resulting in the $\bar{p}\mathrm{He}^{2+}$ state, which quickly annihilates. The transition frequencies between optical transitions provide limits on the accuracy of the antiproton mass.

Table XXII lists the frequencies from the GEM calculation (Kino, Kudo, and Kamimura, 2003) for some selected transitions of the $\bar{p}\mathrm{He}^+$ system and compares them with Hylleraas type (Korobov, 2006) calculations and experiment (Hori *et al.*, 2006). The theoretical transition frequencies include relativistic corrections. Comparison between theory and experiment yielded an estimate of the antiproton to electron mass ratio of 1836.152 674(5) (Hori *et al.*, 2006).

The energies obtained with the Hylleraas-type basis are a couple of orders of magnitude more precise than the GEM calculation. This is expected since $\bar{p}\mathrm{He}^+$ is a three-body system. The GEM calculations were performed in double precision arithmetic and it is possible to improve the accuracy by adopting quadruple precision arithmetic as done in the Hylleraas-type calculations.

2. Complex scaling calculations with SVM

Recently a modified and more sophisticated SVM optimization process was developed to improve resonance parameters as the basis set increases (Mezei, Kruppa, and Varga, 2007). Test calculations of the lowest resonances for the Ps^-, H^-, (p, p, μ^-), and the two-dimensional He atoms using the modified SVM gave resonance energies and widths that were in good agreement with the best calculations in the literature.

This approach was applied to study the mass dependence of resonance energies and width of excitonic complexes. The study of bound-state properties of these systems was described in Sec. VII. Knowing that these Coulombic systems have an infinite number of resonances accumulating at thresholds, in order to perform the study of mass dependence, the resonance closest to the $N = 1$ threshold has been chosen. The position of this resonance for the $X^- = (m_h^*, m_e^*, m_e^*)$ system as the function of the mass ratio is shown in Fig. 23. The $n = 2$ thresholds (both 2D and 3D) are also shown. The position of the resonance E_R shows a very smooth behavior; it runs almost parallel with the threshold.

TABLE XXII. Selected frequencies for transitions between states of $\bar{p}^4\mathrm{He}^+$. The experimental frequencies (Hori *et al.*, 2006) and frequencies from a Hylleraas-type (HYL) calculation (Korobov, 2008) and a GEM calculation (Kino, Kudo, and Kamimura, 2003) are listed. Numbers in parentheses are the estimated experimental uncertainties at the 1σ level.

Transition $(n, \ell) \rightarrow (n', \ell')$	Method	Transition frequency (MHz)
(36, 34) → (35, 33)	Exp.	717 474 004(10)
	HYL	717 474 001.1
	GEM	717 473 893.0
(35, 33) → (34, 32)	Exp.	804 633 059(8)
	HYL	804 633 058.1
	GEM	804 633 026.0
(32, 31) → (31, 30)	Exp.	1 132 609 209(15)
	HYL	1 132 609 223.5
	GEM	1 132 609 194.0

3. Electric dipole response of ^{4}He

Another application of the ECG and GVR approach to continuum problems was the electric dipole response of ^{4}He computed using the complex scaling method (Horiuchi, Suzuki, and Arai, 2012). Application of the complex scaling method in nuclear physics is not trivial (Witała and Glöckle, 1999), because the NN potential contains an exponential factor $e^{-\rho r}$. This transforms to $e^{-\rho r(\cos\theta + i\sin\theta)}$ upon coordinate rotation extending to large distances as θ increases.

The response function due to the electric dipole operator $\mathcal{E}_{1\mu}$ acting on the initial state Ψ^+_{00} is given by

$$S(E) = \sum_{\mu f} |\langle \Psi^-_{J_f M_f} | \mathcal{E}_{1\mu} | \Psi^+_{00} \rangle|^2 \delta(E_f - E_0 - E)$$
$$= -\frac{1}{\pi} \sum_{\mu} \mathrm{Im} \langle \Psi^+_{00} | \mathcal{E}^\dagger_{1\mu} \frac{1}{E - H + E_0 + i\epsilon} \mathcal{E}_{1\mu} | \Psi^+_{00} \rangle, \tag{122}$$

where $\sum_f$ represents a sum over all bound states and an integration over the continuum over all possible final states with energy E_f and magnetic projection M_f. The summation over the final states is performed using the closure relation, resulting in the resolvent $1/(E - H + E_0 + i\epsilon)$. After the rotation $U(\theta)$ of the coordinate and momentum in the complex plane by the angle θ, the resolvent can be expanded in terms of the eigenfunctions of the rotated Hamiltonian $H(\theta) = U(\theta) H U^{-1}(\theta)$ (Aoyama *et al.*, 2006; Suzuki, Horiuchi, and Baye, 2010).

The observed photoabsorption cross section is related to $S(E)$ by

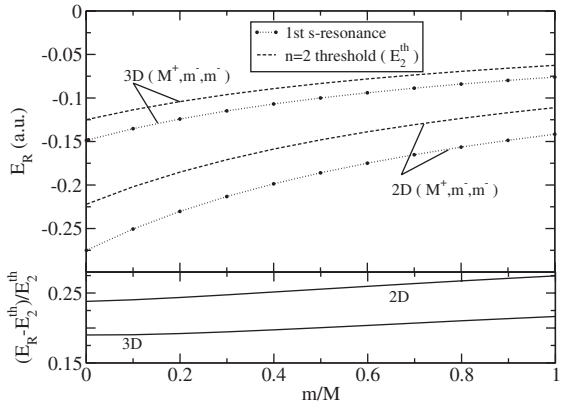

FIG. 23. The position (real part of the energy) of the resonance state as the function of the mass ratio for negatively charged trions in 2D and 3D. The resonance energy is given by $E_R - i\Gamma/2$. The second thresholds are also shown for both 2D and 3D systems. M^+ denotes the mass of the positively charged heavy hole and m^- is the mass of the electron. Adapted from Mezei, Kruppa, and Varga, 2007.

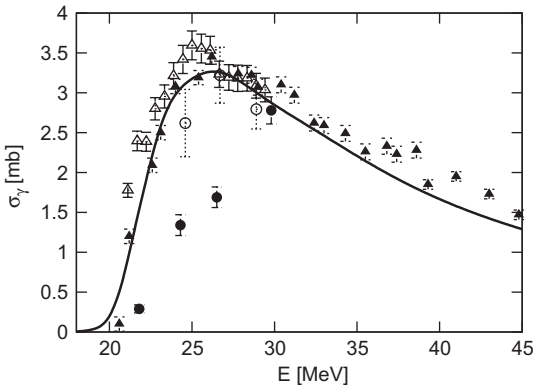

FIG. 24. Photoabsorption cross section of ^{4}He computed with CSM using $\theta = 17°$ (Horiuchi, Suzuki, and Arai, 2012). The AV8′ + 3NF potential is used. The experimental data are taken from Arkatov *et al.* (1979) (solid triangle), Shima *et al.* (2005) (solid circle), Nilsson *et al.* (2007) (open circle), and Tornow (2011) (open triangle). The last two data are obtained by doubling the (γ, n) and (γ, p) cross sections, respectively.

$$\sigma_\gamma(E) = \frac{4\pi^2}{3\hbar c} ES(E). \tag{123}$$

Figure 24 compares results of the CSM calculation with experiment for $\sigma_\gamma(E)$. The agreement between theory and experiment is satisfactory. The calculation reproduces the energy and height of the peak of most of the data, with one exception (Shima *et al.*, 2005). The ECG-based calculation gives results that are consistent with other calculations using different methods (Gazit *et al.*, 2006; Quaglioni and Navrátil, 2007). This *ab initio* type of calculations has very recently been applied to study the spin-dipole responses of ^{4}He (Horiuchi and Suzuki, 2013). It is found that all peaks of the spin-dipole and electric dipole response functions well explain the resonance properties of the observed negative parity states of ^{4}He.

E. Outlook

So far there have been fewer applications of ECG basis sets to scattering problems than to bound-state calculations. One common feature of these applications has been that they have generally been to scattering systems that would be difficult to describe by other methods, for example, having a target and projectile with internal structure. The embedding of ECGs into a conventional scattering theory such as the R matrix for four-nucleon systems constitutes a significant achievement.

A possibility exists for accurate calculations of low-energy nuclear reactions and scattering for systems with $N < 8$ using microscopic NN interactions. The target and projectile internal wave functions can be described with ECGs while the relative motion between the fragments can be described by Gaussian orbitals. This will assist in one of the overarching goals of theoretical nuclear physics, namely, the description of nuclear scattering starting from first-principles calculations.

X. CONCLUSIONS

Quantum mechanical few-body systems have been studied in nearly all areas of physics and chemistry since the early days of quantum mechanics. Over the years, a large number of analytical and numerical approaches have been developed to solve few-body bound-state and scattering problems of various complexity. A subset of approaches, including ECG-based ones, uses the variational principle and expands the nonrelativistic or relativistic few-body wave function in terms of a conveniently chosen basis set. Other approaches are based on the propagation of wave functions in imaginary time, semiclassical ideas, or on effective low-energy Hamiltonian derived within the many-body framework or using effective-field theory.

We have described significant applications of ECG-based approaches to atomic structure, exotic atoms, molecules, nuclear structure, soft condensed matter physics, cold atom physics, and few-body collision physics. The reason for this success over such a variety of different quantum systems relies on three features inherent to ECGs. First, the center-of-mass motion of the system is easily removed. Next, the matrix elements of any one- or two-body operator reduce at most to a one-dimensional numerical integral multiplied by a factor that can be obtained by standard matrix operations. Finally, the ECG approach is ''democratic'' in nature in that the interactions between all pairs of particles are given equal prominence. The inherent flexibility of the ECG basis means that it is capable of adapting to accommodate different particle masses and almost all interactions. The major

TABLE XXIII. Relative performance of selected approaches for various few-body systems.

System	Hylleraas	CI	Hyperspherical	QMC	ECG methods
Atomic systems $N \leq 3$	Extreme precision	Good	Good	Good	High precision
Atomic systems $4 \leq N \leq 6$	Not used	Very good	Hardly used	Good	Excellent
Cluster systems	Fair	Poor	Good	Very good	Excellent
Small molecular systems	Only two-electron diatomic	Good	Hardly used	Good	Excellent
Scattering	Excellent for resonances	Very good	Excellent	Good for difficult systems	Good for difficult systems
Cold atoms	Hardly used	Hardly used	Excellent	Excellent	Excellent
Electronic quantum dots	Hardly used	Very good	Hardly used	Very good	Very good
Excitons and related systems	Hardly used	Hardly used	Hardly used	Very good	Excellent
Nuclear and subnuclear systems ($N \leq 5$)	Hardly used	Very good	Hardly used	Very good	Very good
All systems ($N > 6$)	Not used	Very good	Not used	Excellent	Rarely used

computational limitations at present are the factorial growth in the time taken to evaluate matrix elements with identical particles and the increasingly more difficult optimization as the system becomes strongly correlated or the total number of particles increases.

ECG basis sets have been applied to generate very accurate wave functions for systems with $N = 3$–7. They have not achieved the hyperaccuracy possible with Hylleraas techniques for $N = 3$ Coulombic systems, but reaching 12 significant figures for the helium ground state energy is certainly very respectable. The real advantage of ECGs becomes apparent for $N = 4$. For example, calculations for the H_2 molecule without using the BO approximation allowed a unique validation of the method based on the perturbative treatment of nonadiabatic effects. Another significant achievement of ECGs were calculations for He_2, which have been used to set *ab initio*-based standards in thermophysical metrology. Looking at $N = 5$, SVM was used to demonstrate that e^+Li was electronically stable and therefore solved a long-standing problem in positron physics. Currently the only other *ab initio* calculation for this system is a DMC calculation which underestimates the binding energy by 5%.

In general, scattering calculations are more challenging than bound-state calculations, and there have been relatively few applications of ECG-based approaches in this field until recently. However, ECGs have now been embedded into scattering methodology based on the regular and hyperspherical-harmonic R-matrix approaches. These are significant developments since ECG basis sets can now be utilized in general treatments of reactive and rearrangement collisions for systems with $N = 3$ and 4. For three-body scattering systems, ECG-based approaches are not, at least not in general, competitive with discrete variable representation, finite-element, or B-spline-based approaches. ECG-based approaches have, however, proven to be competitive for certain four-body scattering systems. A recent ECG-based development, for example, formulated the four-body scattering problem within the hyperspherical framework and has helped in many instances to elucidate the underlying physical mechanisms. In the future, it will be interesting to further refine ECG-based scattering calculations for four-body systems, within the regular R-matrix and hyperspherical frameworks, and to extend the formalisms to treating five- and six-body scattering problems.

Table XXIII gives an evaluation of merits of various computational approaches applied to different classes of few-body problems. Hylleraas methods give superb precision for small Coulombic systems, but cannot be applied to larger systems. Monte Carlo methods give moderate accuracy, but can handle large systems as the computational complexity grows slowly. CI-type methods do not achieve high precision, but are a good tool when such precision is not critical since CI calculations can be performed at low computational costs. The convergence of CI methods is particularly slow for systems with components that tend to form clusters so that this method is not recommended in such cases. Hyperspherical approaches can deal effectively with cluster systems, and there has also been a number of applications to scattering problems. The complexity of hyperspherical methods increases markedly for $N > 4$. One aspect of ECG methods that stands out is the ease with which it can handle clustering, which means that it can be usefully applied to practically any few-body system. This adaptability of the ECG basis to describe practically any few-body configuration should lead to an increase in applications of ECGs in the coming years.

LIST OF SYMBOLS AND ABBREVIATIONS

AV8	Argonne nucleon-nucleon interaction with eight operators
AV18	Argonne nucleon-nucleon interaction with 18 operators
BEC	Bose-Einstein condensate
BO	Born-Oppenheimer
CDCC	Continuum discretized coupled channels
CCSD(T)	Coupled-cluster method with single, double, and noniterative triple excitations
CI	Configuration interaction
CI-R12	Configuration interaction with r_{ij} correlation factors
CSM	Complex scaling method
DMC	Diffusion Monte Carlo
ECG	Explicitly correlated Gaussian
EIHH	Effective interaction hyperspherical harmonics
EVI	Expectation value identities (for evaluation of singular operators)
FCCI	Fixed core configuration interaction
FCSVM	Fixed core stochastic variational method
FY	Faddeev-Yakubovsky
GEM	Gaussian expansion method
GFMC	Green's function Monte Carlo
GJC	Generalized James-Coolidge
GTG	Gaussian-type geminals
GVR	Global vector representation
HECG	Hyperspherical ECG
HYL	Hylleraas basis functions
HYL-LOG	Hylleraas basis functions with logarithmic factors
HF	Hartree-Fock
HH	Hyperspherical harmonic
IT	Integral transform approach for evaluation of singular operators
MP2	Second-order perturbation theory with Møller-Plesset partition of the Hamiltonian
NCSM	No-core shell model
OPP	Orthogonalizing pseudopotential
PES	Potential energy surface
PWE	Partial wave expansion
QED	Quantum electrodynamics
QMC	Quantum Monte Carlo
SO	Strong orthogonality
SAPT	Symmetry-adapted perturbation theory
SVM	Stochastic variational method
VMC	Variational Monte Carlo

ACKNOWLEDGMENTS

W. H. and Y. S. thank S. Aoyama and K. Arai for discussions and help that were vital to complete the manuscript.

J. M. thanks Dr. G. G. Ryzhikh for correcting his prejudices regarding the use of exponential basis functions with arguments consisting of quadratic factors in the interparticle distances. The work of J. M. was supported in part by the Australian Research Council Discovery Project No. DP-1092620. The work of Y. S. is in part supported by a Grant-in-Aid for Scientific Research (No. 21540261) of the Japan Society for the Promotion of Science. The work of W. C. and K. S. was supported by the National Science Foundation Grant No. CHE-0848589. J. K. acknowledges support by NCN Grant No. N204 015338, and by a computing grant from Poznań Supercomputing and Networking Center. D. B. gratefully acknowledges support by the NSF through Grant No. PHY-0855332.

REFERENCES

Adamowicz, L., 1978, Int. J. Quantum Chem. **13**, 265.
Adamowicz, L., and A. J. Sadlej, 1978, J. Chem. Phys. **69**, 3992.
Adler, T. B., G. Knizia, and H.-J. Werner, 2007, J. Chem. Phys. **127**, 221106.
Aguilera, E. F., *et al.*, 2001, Phys. Rev. C **63**, 061603.
Aguilera, E. F., *et al.*, 2000, Phys. Rev. Lett. **84**, 5058.
Ahn, K., *et al.*, 2001, in *Hadron and Nuclei*, edited by II-Tong Cheon , AIP Conf. Proc. No. 594 (AIP, New York), p. 180.
Alexander, S. A., H. J. Monkhorst, R. D. Roeland, and K. Szalewicz, 1990, J. Chem. Phys. **93**, 4230.
Alexander, S. A., H. J. Monkhorst, and K. Szalewicz, 1986, J. Chem. Phys. **85**, 5821.
Alexander, S. A., H. J. Monkhorst, and K. Szalewicz, 1988, J. Chem. Phys. **89**, 355.
Al-Hujaj, O.-A., and P. Schmelcher, 2003, Phys. Rev. A **67**, 023403.
Ali, S., and A. R. Bodmer, 1966, Nucl. Phys. **80**, 99.
Almora-Diaz, C. X., and C. F. Bunge, 2010, Int. J. Quantum Chem. **110**, 2982.
Amado, R. D., and F. C. Greenwood, 1973, Phys. Rev. D **7**, 2517.
Amovilli, C., and N. H. March, 2011, Phys. Rev. A **83**, 044502.
Anderson, J. B., 2004, J. Chem. Phys. **120**, 9886.
Angel, J. R. P., E. F. Borra, and J. D. Landstreet, 1981, Astrophys. J. **45**, 457.
Angulo, C., *et al.*, 1999, Nucl. Phys. **A656**, 3.
Aoyama, S., K. Arai, Y. Suzuki, P. Descouvemont, and D. Baye, 2012, Few-Body Syst. **52**, 97.
Aoyama, S., T. Myo, K. Katō, and K. Ikeda, 2006, Prog. Theor. Phys. **116**, 1.
Arai, K., S. Aoyama, Y. Suzuki, P. Descouvemont, and D. Baye, 2011, Phys. Rev. Lett. **107**, 132502.
Arai, K., Y. Ogawa, Y. Suzuki, and K. Varga, 2001, Prog. Theor. Phys. Suppl. **142**, 97.
Araki, H., 1957, Prog. Theor. Phys. **17**, 619.
Arkatov, Yu. M., *et al.*, 1979, Yad. Konst. **4**, 55.
Armour, E. A. G., and D. J. Baker, 1986, J. Phys. B **19**, L871.
Armour, E. A. G., J. N. Cooper, M. R. Gregory, S. Jonsell, M. Plummer, and A. C. Todd, 2010, J. Phys. Conf. Ser. **199**, 012007.
Astier, A., P. Petkov, M.-G. Porquet, D. S. Delion, and P. Schuck, 2010, Phys. Rev. Lett. **104**, 042701.
Austern, N., Y. Iseri, M. Kamimura, M. Kawai, G. Rawitscher, and M. Yahiro, 1987, Phys. Rep. **154**, 125.
Bachorz, R., W. Cencek, R. Jaquet, and J. Komasa, 2009, J. Chem. Phys. **131**, 024105.
Barnea, N., W. Leidemann, and G. Orlandini, 2000, Phys. Rev. C **61**, 054001.
Bartlett, R. J., and M. Musiał, 2007, Rev. Mod. Phys. **79**, 291.
Baye, D., P. Capel, P. Descouvemont, and Y. Suzuki, 2009, Phys. Rev. C **79**, 024607.
Bendazzoli, G. L., and A. Monari, 2004, Chem. Phys. **306**, 153.
Ben-Itzhak, I., E. Wells, K. D. Carnes, V. Krishnamurthi, O. L. Weaver, and B. D. Esry, 2000, Phys. Rev. Lett. **85**, 58.
Bethe, H. A., and E. E. Salpeter, 1977, *Quantum Mechanics of One- and Two-electron Atoms* (Plenum, New York).
Birkedal, D., J. Singh, V. G. Lyssenko, J. Erland, and J. M. Hvam, 1996, Phys. Rev. Lett. **76**, 672.
Björk, M. T., C. Thelander, A. E. Hansen, L. E. Jensen, M. W. Larsson, L. R. Wallenberg, and L. Samuelson, 2004, Nano Lett. **4**, 1621.
Blanco, M., and E. J. Heller, 1983, J. Chem. Phys. **78**, 2504.
Blankenbecler, R., D. J. Scalapino, and R. L. Sugar, 1981, Phys. Rev. D **24**, 2278.
Bloch, I., J. Dalibard, and W. Zwerger, 2008, Rev. Mod. Phys. **80**, 885.
Blume, D., and K. M. Daily, 2009, Phys. Rev. A **80**, 053626.
Blume, D., and K. M. Daily, 2010a, Phys. Rev. Lett. **105**, 170403.
Blume, D., and K. M. Daily, 2010b, Phys. Rev. A **82**, 063612.
Blume, D., and K. M. Daily, 2011, C.R. Physique **12**, 86.
Blume, D., and C. H. Greene, 2000, J. Chem. Phys. **112**, 8053.
Blume, D., J. von Stecher, and C. H. Greene, 2007, Phys. Rev. Lett. **99**, 233201.
Bolton, F., 1996, Phys. Rev. B **54**, 4780.
Bonifacic, V., and J. Huzinga, 1974, J. Chem. Phys. **60**, 2779.
Boninsegni, M., N. V. Prokof'ev, and B. V. Svistunov, 2006, Phys. Rev. E **74**, 036701.
Boys, S. F., 1950, Proc. R. Soc. A **200**, 542.
Boys, S. F., 1960, Proc. R. Soc. A **258**, 402.
Braaten, E., and H.-W. Hammer, 2006, Phys. Rep. **428**, 259.
Bressanini, D., M. Mella, and G. Morosi, 1997, Phys. Rev. A **55**, 200.
Bressanini, D., M. Mella, and G. Morosi, 1998, Phys. Rev. A **57**, 4956.
Brinkmann, K., and H. Kleindienst, 1991, J. Math. Chem. **6**, 267.
Bromley, M. W. J., and J. Mitroy, 2002a, Phys. Rev. A **65**, 062506.
Bromley, M. W. J., and J. Mitroy, 2002b, Phys. Rev. A **66**, 062504.
Bromley, M. W. J., and J. Mitroy, 2006a, Phys. Rev. Lett. **97**, 183402.
Bromley, M. W. J., and J. Mitroy, 2006b, Phys. Rev. A **73**, 032507.
Bromley, M. W. J., and J. Mitroy, 2007a, Int. J. Quantum Chem. **107**, 1150.
Bromley, M. W. J., and J. Mitroy, 2007b, Phys. Rev. A **75**, 042506.
Bromley, M. W. J., and J. Mitroy, 2010, Phys. Rev. A **81**, 052708.
Bubin, S., and L. Adamowicz, 2004, J. Chem. Phys. **121**, 6249.
Bubin, S., and L. Adamowicz, 2006, J. Chem. Phys. **124**, 224317.
Bubin, S., and L. Adamowicz, 2007, J. Chem. Phys. **126**, 214305.
Bubin, S., and L. Adamowicz, 2008, J. Chem. Phys. **128**, 114107.
Bubin, S., and L. Adamowicz, 2009, Phys. Rev. A **79**, 022501.
Bubin, S., and L. Adamowicz, 2011a, J. Chem. Phys. **135**, 214104.
Bubin, S., and L. Adamowicz, 2011b, Phys. Rev. A **83**, 022505.
Bubin, S., L. Adamowicz, and M. Molski, 2005, J. Chem. Phys. **123**, 134310.
Bubin, S., E. Bednarz, and L. Adamowicz, 2005, J. Chem. Phys. **122**, 041102.
Bubin, S., M. Cafiero, and L. Adamowicz, 2005, Adv. Chem. Phys. **131**, 377.
Bubin, S., J. Komasa, M. Stanke, and L. Adamowicz, 2009, J. Chem. Phys. **131**, 234112.

Bubin, S., J. Komasa, M. Stanke, and L. Adamowicz, 2010a, Phys. Rev. A **81**, 052504.

Bubin, S., J. Komasa, M. Stanke, and L. Adamowicz, 2010b, J. Chem. Phys. **132**, 114109.

Bubin, S., F. Leonarski, M. Stanke, and L. Adamowicz, 2009, Chem. Phys. Lett. **477**, 12.

Bubin, S., M. Stanke, and L. Adamowicz, 2009, J. Chem. Phys. **131**, 044128.

Bubin, S., M. Stanke, and L. Adamowicz, 2010, Chem. Phys. Lett. **500**, 229.

Bubin, S., M. Stanke, and L. Adamowicz, 2011a, J. Chem. Phys. **135**, 074110.

Bubin, S., M. Stanke, and L. Adamowicz, 2011b, Phys. Rev. A **83**, 042520.

Bubin, S., M. Stanke, and L. Adamowicz, 2011c, J. Chem. Phys. **134**, 024103.

Bubin, S., M. Stanke, D. Kędziera, and L. Adamowicz, 2007, Phys. Rev. A **75**, 062504.

Bubin, S., and K. Varga, 2011, Phys. Rev. A **84**, 012509.

Buck, B., H. Friedrich, and C. Wheatley, 1977, Nucl. Phys. **A275**, 246.

Bukowski, R., *et al.*, 2012, "SAPT2012: An *ab initio* program for many-body symmetry-adapted perturbation theory calculations of intermolecular interaction energies," University of Delaware and University of Warsaw, http://www.physics.udel.edu/~szalewic/SAPT/SAPT.html.

Bukowski, R., B. Jeziorski, R. Moszyński, and W. Kołos, 1992, Int. J. Quantum Chem. **42**, 287.

Bukowski, R., B. Jeziorski, S. Rybak, and K. Szalewicz, 1995, J. Chem. Phys. **102**, 888.

Bukowski, R., B. Jeziorski, and K. Szalewicz, 1994, J. Chem. Phys. **100**, 1366.

Bukowski, R., B. Jeziorski, and K. Szalewicz, 1996, J. Chem. Phys. **104**, 3306.

Bukowski, R., B. Jeziorski, and K. Szalewicz, 1999, J. Chem. Phys. **110**, 4165.

Bukowski, R., B. Jeziorski, and K. Szalewicz, 2003, in *Explicitly Correlated Functions in Chemistry and Physics*, edited by J. Rychlewski (Kluwer, Dordrecht), pp. 185–248.

Bunge, C. F., 2010, Theor. Chem. Acc. **126**, 139.

Burke, P. G., and C. J. Joachain, 1995, *Theory of Electron-Atom Collisions, Part 1: Potential Scattering* (Plenum, New York).

Busch, T., B.-G. Englert, K. Rzążewski, and M. Wilkens, 1998, Found. Phys. **28**, 549.

Cafiero, M., and L. Adamowicz, 2001, Int. J. Quantum Chem. **82**, 151.

Campargue, A., S. Kassi, K. Pachucki, and J. Komasa, 2012, Phys. Chem. Chem. Phys. **14**, 802.

Canter, K. F., J. D. McNutt, and L. O. Roellig, 1975, Phys. Rev. A **12**, 375.

Carrington, A., I. R. McNab, C. A. Montgomerie-Leach, and R. A. Kennedy, 1991, Mol. Phys. **72**, 735.

Carroll, D. P., H. J. Silverstone, and R. P. Metzger, 1979, J. Chem. Phys. **71**, 4142.

Cassidy, D. B., M. W. J. Bromley, L. C. Cota, T. H. Hisakado, H. W. K. Tom, and A. P. Mills, 2011, Phys. Rev. Lett. **106**, 023401.

Caswell, W. E., and G. P. Lepage, 1986, Phys. Lett. **167B**, 437.

Cencek, W., M. Jeziorska, O. Akin-Ojo, and K. Szalewicz, 2007, J. Phys. Chem. A **111**, 11 311.

Cencek, W., M. Jeziorska, R. Bukowski, M. Jaszuński, B. Jeziorski, and K. Szalewicz, 2004, J. Phys. Chem. A **108**, 3211.

Cencek, W., J. Komasa, K. Pachucki, and K. Szalewicz, 2005, Phys. Rev. Lett. **95**, 233004.

Cencek, W., J. Komasa, and J. Rychlewski, 1995, Chem. Phys. Lett. **246**, 417.

Cencek, W., J. Komasa, and K. Szalewicz, 2011, J. Chem. Phys. **135**, 014301.

Cencek, W., and W. Kutzelnigg, 1996, J. Chem. Phys. **105**, 5878.

Cencek, W., M. Przybytek, J. Komasa, J. B. Mehl, B. Jeziorski, and K. Szalewicz, 2012, J. Chem. Phys. **136**, 224303.

Cencek, W., and J. Rychlewski, 1993, J. Chem. Phys. **98**, 1252.

Cencek, W., and J. Rychlewski, 1995, J. Chem. Phys. **102**, 2533.

Cencek, W., and J. Rychlewski, 2000, Chem. Phys. Lett. **320**, 549.

Cencek, W., J. Rychlewski, R. Jaquet, and W. Kutzelnigg, 1998, J. Chem. Phys. **108**, 2831.

Cencek, W., and K. Szalewicz, 2008, Int. J. Quantum Chem. **108**, 2191.

Cencek, W., K. Szalewicz, and B. Jeziorski, 2001, Phys. Rev. Lett. **86**, 5675.

Ceperley, D., and B. Alder, 1986, Science **231**, 555.

Ceperley, D. M., 1995, Rev. Mod. Phys. **67**, 279.

Chakravorty, S. J., S. R. Gwaltney, E. R. Davidson, F. A. Parpia, and C. F. P. Fischer, 1993, Phys. Rev. A **47**, 3649.

Chalasinski, G., B. Jeziorski, J. Andzelm, and K. Szalewicz, 1977, Mol. Phys. **33**, 971.

Challacombe, M., and J. Cioslowski, 1994, J. Chem. Phys. **100**, 464.

Charlton, M., 1985, Rep. Prog. Phys. **48**, 737.

Charlton, M., and J. W. Humberston, 2001, *Positron Physics* (Cambridge University Press, Cambridge, England).

Chen, B., and J. B. Anderson, 1995, J. Chem. Phys. **102**, 4491.

Chernykh, M., H. Feldmeier, T. Neff, P. von Neumann-Cosel, and A. Richter, 2007, Phys. Rev. Lett. **98**, 032501.

Chin, C., R. Grimm, P. Julienne, and E. Tiesinga, 2010, Rev. Mod. Phys. **82**, 1225.

Cioslowski, J., and M. Buchowiecki, 2005, J. Chem. Phys. **122**, 084102.

Cioslowski, J., and R. Lopez-Boada, 1998, J. Chem. Phys. **109**, 1230.

Cioslowski, J., and E. Matito, 2011, J. Chem. Theory Comput. **7**, 915.

Cioslowski, J., and K. Pernal, 2006, J. Chem. Phys. **125**, 064106.

Cizek, J., 1966, J. Chem. Phys. **45**, 4256.

Clary, D. C., and N. C. Handy, 1977, Chem. Phys. Lett. **51**, 483.

Coleman, P. G., T. C. Griffith, G. R. Heyland, and T. L. Killeen, 1975, J. Phys. B **8**, L185.

Cooper, J. N., E. A. G. Armour, and M. Plummer, 2008, J. Phys. B **41**, 245201.

Cooper, J. N., E. A. G. Armour, and M. Plummer, 2009, J. Phys. A **42**, 095207.

Dahle, P., T. Helgaker, D. Jonsson, and P. R. Taylor, 2007, Phys. Chem. Chem. Phys. **9**, 3112.

Daily, K. M., and D. Blume, 2010, Phys. Rev. A **81**, 053615.

Dalfovo, F., S. Giorgini, L. P. Pitaevskii, and S. Stringari, 1999, Rev. Mod. Phys. **71**, 463.

Danby, G., and J. Tennyson, 1988, Phys. Rev. Lett. **61**, 2737.

Deltuva, A., 2011a, Europhys. Lett. **95**, 43002.

Deltuva, A., 2011b, Phys. Rev. A **84**, 022703.

de Miranda, M. H. G., A. Chotia, B. Neyenhuis, D. Wang, G. Quemener, S. Ospelkaus, J. L. Bohn, J. Ye, and D. S. Jin, 2011, Nat. Phys. **7**, 502.

Descouvemont, P., and D. Baye, 2010, Rep. Prog. Phys. **73**, 036301.

D'Incao, J. P., J. von Stecher, and C. H. Greene, 2009, Phys. Rev. Lett. **103**, 033004.

Drachman, R. J., 1981, J. Phys. B **14**, 2733.

Drake, G. W. F., 1987, Phys. Rev. Lett. **59**, 1549.

Drake, G. W. F., 1996, *Handbook of Atomic, Molecular and Optical Physics* (American Institute of Physics, New York).
Drake, G. W. F., M. M. Cassar, and R. A. Nistor, 2002, Phys. Rev. A **65**, 054501.
Drouin, B. J., S. Yu, J. C. Pearson, and H. Gupta, 2011, J. Mol. Struct. **1006**, 2.
Duff, B. G., and F. F. Heymann, 1962, Proc. R. Soc. A **270**, 517.
Dzuba, V. A., V. V. Flambaum, G. F. Gribakin, and W. A. King, 1995, Phys. Rev. A **52**, 4541.
Efimov, V., 1970, Phys. Lett. **33B**, 563.
Efimov, V. N., 1973, Nucl. Phys. **A210**, 157.
Egami, T., K. Ogata, T. Matsumoto, Y. Iseri, M. Kamimura, and M. Yahiro, 2004, Phys. Rev. C **70**, 047604.
Egger, R., W. Häusler, C. H. Mak, and H. Grabert, 1999, Phys. Rev. Lett. **82**, 3320.
Epelbaum, E., H.-W. Hammer, and U.-G. Meißner, 2009, Rev. Mod. Phys. **81**, 1773.
Erementchouk, M., and M. N. Leuenberger, 2010, Phys. Rev. B **81**, 195308.
Fabre de La Ripelle, M., 1983, Ann. Phys. (N.Y.) **147**, 281.
Fasth, C., A. Fuhrer, L. Samuelson, V. N. Golovach, and D. Loss, 2007, Phys. Rev. Lett. **98**, 266801.
Feldmeier, H., W. Horiuchi, T. Neff, and Y. Suzuki, 2011, Phys. Rev. C **84**, 054003.
Fellmuth, B., C. Gaiser, and J. Fischer, 2006, Meas. Sci. Technol. **17**, R145.
Ferlaino, F., S. Knoop, M. Berninger, W. Harm, J. P. D'Incao, H.-C. Nägerl, and R. Grimm, 2009, Phys. Rev. Lett. **102**, 140401.
Fischer, J., and B. Fellmuth, 2005, Rep. Prog. Phys. **68**, 1043.
Fletcher, R., 1987, *Practical Methods of Optimization* (Wiley, New York), 2nd ed., Vol. I.
Forest, J., V. Jandharipande, S. Pieper, R. Wiringa, R. Schiavilla, and A. Arriaga, 1996, Phys. Rev. C **54**, 646.
Frolov, A. M., and V. H. Smith, Jr., 1995, J. Phys. B **28**, L449.
Fuechsle, M., S. Mahapatra, F. A. Zwanenburg, M. Friesen, M. A. Eriksson, and M. Y. Simmons, 2010, Nat. Nanotechnol. **5**, 502.
Fujito, M., A. Natori, and H. Yasunaga, 1996, Phys. Rev. B **53**, 9952.
Gazit, D., S. Bacca, N. Barnea, W. Leidemann, and G. Orlandini, 2006, Phys. Rev. Lett. **96**, 112301.
Giorgini, S., L. P. Pitaevskii, and S. Stringari, 2008, Rev. Mod. Phys. **80**, 1215.
Glöckle, W., and H. Kamada, 1993, Phys. Rev. Lett. **71**, 971.
Glozman, L. Y., W. Plessas, K. Varga, and R. F. Wagenbrunn, 1998, Phys. Rev. D **58**, 094030.
Gribakin, G. F., J. A. Young, and C. M. Surko, 2010, Rev. Mod. Phys. **82**, 2557.
Grisenti, R. E., W. Schöllkopf, J. P. Toennies, G. C. Hegerfeldt, T. Köhler, and M. Stoll, 2000, Phys. Rev. Lett. **85**, 2284.
Guan, X., and B. Li, 2001, Phys. Rev. A **63**, 043413.
Hadizadeh, M. R., M. T. Yamashita, L. Tomio, A. Delfino, and T. Frederico, 2011, Phys. Rev. Lett. **107**, 135304.
Hamaguchi, K., T. Hatsuda, M. Kamimura, Y. Kino, and T. T. Yanagida, 2007, Phys. Lett. B **650**, 268.
Hammack, A. T., M. Griswold, L. V. Butov, L. E. Smallwood, A. L. Ivanov, and A. C. Gossard, 2006, Phys. Rev. Lett. **96**, 227402.
Hammer, H. W., and L. Platter, 2007, Eur. Phys. J. A **32**, 113.
Hammond, B. L., W. A. Lester, Jr., and P. J. Reynolds, 1994, *Monte Carlo Methods in ab initio Quantum Chemisty* (World Scientific, Singapore).
Handy, N. C., 1973, Mol. Phys. **26**, 169.
Hanna, G. J., and D. Blume, 2006, Phys. Rev. A **74**, 063604.
Hanson, R., L. P. Kouwenhoven, J. R. Petta, S. Tarucha, and L. M. K. Vandersypen, 2007, Rev. Mod. Phys. **79**, 1217.
Harju, A., V. A. Sverdlov, R. M. Nieminen, and V. Halonen, 1999, Phys. Rev. B **59**, 5622.
Harris, F. E., 1967, Phys. Rev. Lett. **19**, 173.
Harris, F. E., and H. J. Monkhorst, 2006, Int. J. Quantum Chem. **106**, 3186.
Hawrylak, P., and D. Pfannkuche, 1993, Phys. Rev. Lett. **70**, 485.
Hayano, R. S., M. Hori, D. Horváth, and E. Widmann, 2007, Rep. Prog. Phys. **70**, 1995.
Hazi, A. U., and H. S. Taylor, 1970, Phys. Rev. A **1**, 1109.
Head-Gordon, M., and J. A. Pople, 1988, J. Chem. Phys. **89**, 5777.
Helgaker, T., W. Klopper, and D. P. Tew, 2008, Mol. Phys. **106**, 2107.
Herzberg, G., 1970, J. Mol. Spectrosc. **33**, 147.
Hibbert, A., 1975, Rep. Prog. Phys. **38**, 1217.
Hill, R. N., 1985, J. Chem. Phys. **83**, 1173.
Hill, R. N., 1998, Int. J. Quantum Chem. **68**, 357.
Hiller, J., J. Sucher, and G. Feinberg, 1978, Phys. Rev. A **18**, 2399.
Hirose, K., and N. S. Wingreen, 1999, Phys. Rev. B **59**, 4604.
Hiyama, E., B. F. Gibson, and M. Kamimura, 2004, Phys. Rev. C **70**, 031001.
Hiyama, E., M. Kamimura, A. Hosaka, H. Toki, and M. Yahiro, 2005, Nucl. Phys. **A755**, 411.
Hiyama, E., M. Kamimura, A. Hosaka, H. Toki, and M. Yahiro, 2006, Phys. Lett. B **633**, 237.
Hiyama, E., M. Kamimura, T. Motoba, T. Yamada, and Y. Yamamoto, 2002, Phys. Rev. C **66**, 024007.
Hiyama, E., M. Kamimura, Y. Yamamoto, and T. Motoba, 2010, Phys. Rev. Lett. **104**, 212502.
Hiyama, E., Y. Kino, and M. Kamimura, 2003, Prog. Part. Nucl. Phys. **51**, 223.
Ho, Y. K., 1983, Phys. Rep. **99**, 1.
Ho, Y. K., 1986, Phys. Rev. A **33**, 3584.
Holka, F., P. G. Szalay, J. Fremont, M. Rey, K. A. Peterson, and V. G. Tyuterev, 2011, J. Chem. Phys. **134**, 094306.
Hori, M., *et al.*, 2006, Phys. Rev. Lett. **96**, 243401.
Horiuchi, W., and Y. Suzuki, 2006, Phys. Rev. C **74**, 034311.
Horiuchi, W., and Y. Suzuki, 2007, Phys. Rev. C **76**, 024311.
Horiuchi, W., and Y. Suzuki, 2012, Few-Body Syst. (in press).
Horiuchi, W., and Y. Suzuki, 2013, Phys. Rev C **87**, 034001.
Horiuchi, W., Y. Suzuki, and K. Arai, 2012, Phys. Rev. C **85**, 054002.
Hylleraas, E. A., 1928, Z. Phys. **48**, 469.
Hylleraas, E. A., 1929a, Naturwissenschaften **17**, 982.
Hylleraas, E. A., 1929b, Z. Phys. **54**, 347.
Hylleraas, E. A., 1930a, Z. Phys. **63**, 291.
Hylleraas, E. A., 1930b, Z. Phys. **65**, 759.
Hylleraas, E. A., 1963, Rev. Mod. Phys. **35**, 421.
Hylleraas, E. A., and A. Ore, 1947, Phys. Rev. **71**, 493.
Ichikawa, A., 2001, Ph.D. thesis (Kyoto University).
Ivanov, I. A., J. Mitroy, and K. Varga, 2001, Phys. Rev. Lett. **87**, 063201.
Ivanov, I. A., J. Mitroy, and K. Varga, 2002a, Phys. Rev. A **65**, 032703.
Ivanov, I. A., J. Mitroy, and K. Varga, 2002b, Phys. Rev. A **65**, 022704.
James, H. M., and A. S. Coolidge, 1933, J. Chem. Phys. **1**, 825.
Janzen, A. R., and R. A. Aziz, 1997, J. Chem. Phys. **107**, 914.
Jaquet, R., W. Cencek, W. Kutzelnigg, and J. Rychlewski, 1998, J. Chem. Phys. **108**, 2837.
Jaskolski, W., 1996, Phys. Rep. **271**, 1.

Jeziorska, M., W. Cencek, K. Patkowski, B. Jeziorski, and K. Szalewicz, 2007, J. Chem. Phys. **127**, 124303.

Jeziorski, B., R. Bukowski, and K. Szalewicz, 1997, Int. J. Quantum Chem. **61**, 769.

Jeziorski, B., H. J. Monkhorst, K. Szalewicz, and J. G. Zabolitzky, 1984, J. Chem. Phys. **81**, 368.

Jeziorski, B., R. Moszyński, and K. Szalewicz, 1994, Chem. Rev. **94**, 1887.

Jeziorski, B., and K. Szalewicz, 1979, Phys. Rev. A **19**, 2360.

Jitrik, O., and C. Bunge, 1997, Phys. Rev. A **56**, 2614.

Jones, M. D., G. Ortiz, and D. M. Ceperley, 1996, Phys. Rev. A **54**, 219.

Jones, M. D., G. Ortiz, and D. M. Ceperley, 1997, Phys. Rev. E **55**, 6202.

Kalliakos, S., M. Rontani, V. Pellegrini, C. P. Garcia, A. Pinczuk, G. Goldoni, E. Molinari, L. N. Pfeiffer, and K. W. West, 2008, Nat. Phys. **4**, 467.

Kamada, H., *et al.*, 2001, Phys. Rev. C **64**, 044001.

Kameyama, H., M. Kamimura, and Y. Fukushima, 1989, Phys. Rev. C **40**, 974.

Kamimura, M., 1977, Prog. Theor. Phys. Suppl. **62**, 236.

Kamimura, M., 1981, Nucl. Phys. **A351**, 456.

Kamimura, M., 1988, Phys. Rev. A **38**, 621.

Kammerlander, D., D. Prezzi, G. Goldoni, E. Molinari, and U. Hohenester, 2007, Phys. Rev. Lett. **99**, 126806.

Kanada, H., T. Kaneko, S. Nagata, and M. Nomoto, 1979, Prog. Theor. Phys. **61**, 1327.

Karunakaran, K. M., and R. E. Christoffersen, 1975, J. Chem. Phys. **62**, 1992.

Karunakaran, K. M., and R. E. Christoffersen, 1982, Int. J. Quantum Chem. **22**, 11.

Kassi, S., and A. Campargue, 2011, J. Mol. Spectrosc. **267**, 36.

Kato, T., 1957, Commun. Pure Appl. Math. **10**, 151.

Kellner, D. W., 1927, Z. Phys. **44**, 91.

Kemp, J. C., J. B. Swedlund, J. D. Landstreet, and J. R. P. Angel, 1970, Astrophys. J. Lett. **161**, L77.

Kievsky, A., M. Viviani, P. Barletta, C. Romero-Redondo, and E. Garrido, 2010, Phys. Rev. C **81**, 034002.

King, F. W., D. Quicker, and J. Langer, 2011, J. Chem. Phys. **134**, 124114.

King, H. F., 1967, J. Chem. Phys. **46**, 705.

Kinghorn, D. B., 1996, Int. J. Quantum Chem. **57**, 141.

Kinghorn, D. B., and L. Adamowicz, 1997, J. Chem. Phys. **106**, 4589.

Kinghorn, D. B., and L. Adamowicz, 1999a, J. Chem. Phys. **110**, 7166.

Kinghorn, D. B., and L. Adamowicz, 1999b, Phys. Rev. Lett. **83**, 2541.

Kinghorn, D. B., and R. D. Poshusta, 1993, Phys. Rev. A **47**, 3671.

Kino, Y., H. Kudo, and M. Kamimura, 2003, Mod. Phys. Lett. A **18**, 388.

Kleinman, D. A., 1983, Phys. Rev. B **28**, 871.

Klopper, W., and J. Noga, 2003, in *Explicitly Correlated Wave Functions in Chemistry and Physics*, edited by J. Rychlewski (Kluwer, Dordrecht), p. 149.

Kohn, A., 2009, J. Chem. Phys. **130**, 131101.

Kolos, W., H. J. Monkhorst, and K. Szalewicz, 1982a, J. Chem. Phys. **77**, 1323.

Kolos, W., H. J. Monkhorst, and K. Szalewicz, 1982b, J. Chem. Phys. **77**, 1335.

Kolos, W., and J. Rychlewski, 1993, J. Chem. Phys. **98**, 3960.

Kolos, W., and L. Wolniewicz, 1968, J. Chem. Phys. **49**, 404.

Kołos, W., and L. Wolniewicz, 1964a, J. Chem. Phys. **41**, 3663.

Kołos, W., and L. Wolniewicz, 1964b, J. Chem. Phys. **41**, 3674.

Kołos, W., and L. Wolniewicz, 1965, J. Chem. Phys. **43**, 2429.

Komasa, J., 2001, Phys. Rev. A **65**, 012506.

Komasa, J., W. Cencek, and J. Rychlewski, 1995, Phys. Rev. A **52**, 4500.

Komasa, J., K. Piszczatowski, G. Lach, M. Przybytek, B. Jeziorski, and K. Pachucki, 2011, J. Chem. Theory Comput. **7**, 3105.

Komasa, J., and J. Rychlewski, 2001, Chem. Phys. Lett. **342**, 185.

Komasa, J., J. Rychlewski, and K. Jankowski, 2002, Phys. Rev. A **65**, 042507.

Komasa, J., and A. J. Thakkar, 1995, J. Mol. Struct. Theochem **343**, 43.

Koput, J., 2011, J. Chem. Phys. **135**, 244308.

Korobov, V. I., 2000, Phys. Rev. A **61**, 064503.

Korobov, V. I., 2002, Phys. Rev. A **66**, 024501.

Korobov, V. I., 2006, Phys. Rev. A **73**, 022509.

Korobov, V. I., 2008, Phys. Rev. A **77**, 042506.

Korona, T., H. L. Williams, R. Bukowski, B. Jeziorski, and K. Szalewicz, 1997, J. Chem. Phys. **106**, 5109.

Koskinen, M., M. Manninen, and S. M. Reimann, 1997, Phys. Rev. Lett. **79**, 1389.

Kosztin, I., B. Faber, and K. Schulten, 1996, Am. J. Phys. **64**, 633.

Kouwenhoven, L. P., D. G. Austing, and S. Tarucha, 2001, Rep. Prog. Phys. **64**, 701.

Kozlowski, P. M., and L. Adamowicz, 1992, J. Chem. Phys. **96**, 9013.

Kozlowski, P. M., and L. Adamowicz, 1995, Int. J. Quantum Chem. **55**, 367.

Kramida, A., and W. C. Martin, 1997, J. Phys. Chem. Ref. Data **26**, 1185.

Krasnopol'skii, V. M., and V. I. Kukulin, 1974, Yad. Fiz. (USSR) **20**, 883 [Sov. J. Nucl. Phys. **20**, 883 (1974)].

Krivec, R., 1998, Few-Body Syst. **25**, 199.

Krivec, R., V. B. Mandelzweig, and K. Varga, 2000, Phys. Rev. A **61**, 062503.

Kröger, H., and R. Perne, 1980, Phys. Rev. C **22**, 21.

Kuang, J., and C. D. Lin, 1997, J. Phys. B **30**, 2529.

Kukulin, V. I., and V. M. Krasnopol'skii, 1977, J. Phys. G **3**, 795.

Kukulin, V. I., and V. N. Pomerantsev, 1978, Ann. Phys. (N.Y.) **111**, 330.

Kutzelnigg, W., 1985, Theor. Chim. Acta **68**, 445.

Kutzelnigg, W., and R. Jaquet, 2006, Phil. Trans. R. Soc. A **364**, 2855.

Kutzelnigg, W., and W. Klopper, 1991, J. Chem. Phys. **94**, 1985.

Łach, G., B. Jeziorski, and K. Szalewicz, 2004, Phys. Rev. Lett. **92**, 233001.

Lahaye, T., C. Menotti, L. Santos, M. Lewenstein, and T. Pfau, 2009, Rep. Prog. Phys. **72**, 126401.

Laricchia, G., M. Charlton, C. D. Beling, and T. C. Griffith, 1987, J. Phys. B **20**, 1865.

Lee, R. M., N. D. Drummond, and R. J. Needs, 2009, Phys. Rev. B **79**, 125308.

Leonard, D. S., H. J. Karwowski, C. R. Brune, B. M. Fisher, and E. J. Ludwig, 2006, Phys. Rev. C **73**, 045801.

Lepage, G. P., 1997, arXiv:nucl-th/9706029.

Lester, Jr., W. A., and M. Krauss, 1964, J. Chem. Phys. **41**, 1407.

Lester, Jr., W. A., S. M. Rothstein, and S. Tanaka, 2002, *Recent Advances in Quantum Monte Carlo Methods, Part II* (World Scientific, Singapore).

Li, X., Y. Wu, D. Steel, D. Gammon, T. H. Stievater, D. S. Katzer, D. Park, C. Piermarocchi, and L. J. Sham, 2003, Science **301**, 809.

Lin, C. D., 1995, Phys. Rep. **257**, 1.

Liu, J., E. J. Salumbides, U. Hollenstein, J. C. J. Koelemeij, K. S. E. Eikema, W. Ubachs, and F. Merkt, 2009, J. Chem. Phys. **130**, 174306.

Liu, J., D. Sprecher, C. Jungen, W. Ubachs, and F. Merkt, 2010, J. Chem. Phys. **132**, 154301.

Longstaff, J. V. L., and K. Singer, 1960, Proc. R. Soc. A **258**, 421.

Longstaff, J. V. L., and K. Singer, 1964, Theor. Chim. Acta **2**, 265.

Longstaff, J. V. L., and K. Singer, 1965, J. Chem. Phys. **42**, 801.

MacDonald, J. K., 1933, Phys. Rev. **43**, 830.

Maksym, P. A., and T. Chakraborty, 1990, Phys. Rev. Lett. **65**, 108.

Margolis, H. S., 2009, J. Phys. B **42**, 154017.

Mathieu, V., 2009, Phys. Rev. D **80**, 014016.

Mathieu, V., C. Semay, and B. Silvestre-Brac, 2008, Phys. Rev. D **77**, 094009.

Matsumoto, T., T. Egami, K. Ogata, Y. Iseri, M. Kamimura, and M. Yahiro, 2006, Phys. Rev. C **73**, 051602.

Matsumoto, T., E. Hiyama, K. Ogata, Y. Iseri, M. Kamimura, S. Chiba, and M. Yahiro, 2004, Phys. Rev. C **70**, 061601.

Matsumoto, T., T. Kamizato, K. Ogata, Y. Iseri, E. Hiyama, M. Kamimura, and M. Yahiro, 2003, Phys. Rev. C **68**, 064607.

Matsumura, H., M. Orabi, Y. Suzuki, and Y. Fujiwara, 2006, Nucl. Phys. **A776**, 1.

Matsumura, H., and Y. Suzuki, 2004, Nucl. Phys. **A739**, 238.

Matsumura, H., and Y. Suzuki, 2006, Nucl. Phys. **A772**, 55.

Matyus, E., and M. Reiher, 2012, J. Chem. Phys. **137**, 024104.

May, A., E. Valeev, R. Polly, and F. R. Manby, 2005, Phys. Chem. Chem. Phys. **7**, 2710.

May, A. J., and F. R. Manby, 2004, J. Chem. Phys. **121**, 4479.

McNutt, J. D., S. C. Sharma, and R. D. Brisbon, 1979, Phys. Rev. A **20**, 347.

McWeeny, R., 1950, Nature (London) **166**, 21.

Medin, Z., and D. Lai, 2006, Phys. Rev. A **74**, 062507.

Mehl, J. B., 2009, C.R. Physique **10**, 859.

Mella, M., M. Casalegno, and G. Morosi, 2002, J. Chem. Phys. **117**, 1450.

Mella, M., G. Morosi, and D. Bressanini, 1999, J. Chem. Phys. **111**, 108.

Mezei, J. Z., A. T. Kruppa, and K. Varga, 2007, Few-Body Syst. **41**, 233.

Mezei, J. Z., J. Mitroy, R. G. Lovas, and K. Varga, 2001, Phys. Rev. A **64**, 032501.

Miliordos, E., and A. Mavridis, 2008, J. Chem. Phys. **128**, 144308.

Mitroy, J., 2000, J. Phys. B **33**, 5307.

Mitroy, J., 2004, Phys. Rev. A **70**, 024502.

Mitroy, J., 2005a, Phys. Rev. A **72**, 032503.

Mitroy, J., 2005b, Phys. Rev. Lett. **94**, 033402.

Mitroy, J., 2010a, Phys. Rev. A **82**, 052516.

Mitroy, J., 2010b, J. At. Mol. Sci. **1**, 275.

Mitroy, J., 2011 (private communication).

Mitroy, J., M. W. J. Bromley, and G. G. Ryzhikh, 1999, J. Phys. B **32**, 2203.

Mitroy, J., M. W. J. Bromley, and G. G. Ryzhikh, 2001, in *New Directions in Antimatter Physics and Chemistry*, edited by C. M. Surko, and F. A. Gianturco (Kluwer Academic Publishers, The Netherlands), p. 199.

Mitroy, J., M. W. J. Bromley, and G. G. Ryzhikh, 2002, J. Phys. B **35**, R81.

Mitroy, J., and G. G. Ryzhikh, 1999a, J. Phys. B **32**, 1375.

Mitroy, J., and G. G. Ryzhikh, 1999b, J. Phys. B **32**, L621.

Mitroy, J., and G. G. Ryzhikh, 1999c, Comput. Phys. Commun. **123**, 103.

Mitroy, J., M. S. Safronova, and C. W. Clark, 2010, J. Phys. B **43**, 202001.

Mitroy, J., J. Y. Zhang, M. W. J. Bromley, and S. I. Young, 2008, Phys. Rev. A **78**, 012715.

Mitroy, J., J. Y. Zhang, and K. Varga, 2008, Phys. Rev. Lett. **101**, 123201.

Mohr, P. J., and B. N. Taylor, 2005, Rev. Mod. Phys. **77**, 1.

Moiseyev, N., 1998, Phys. Rep. **302**, 212.

Moiseyev, N., P. Certain, and F. Weinhold, 1978, Mol. Phys. **36**, 1613.

Møller, C., and M. S. Plesset, 1934, Phys. Rev. **46**, 618.

Müller, H., and W. Kutzelnigg, 2000, Phys. Chem. Chem. Phys. **2**, 2061.

Müller, H.-M., and S. E. Koonin, 1996, Phys. Rev. B **54**, 14 532.

Nakashima, H., and H. Nakatsuji, 2007, J. Chem. Phys. **127**, 224104.

Nakashima, H., and H. Nakatsuji, 2010, Astrophys. J. **725**, 528.

Nakatsuji, H., H. Nakashima, Y. Kurokawa, and A. Ishikawa, 2007, Phys. Rev. Lett. **99**, 240402.

Navrátil, P., and B. R. Barrett, 1999, Phys. Rev. C **59**, 1906.

Navrátil, P., S. Quaglioni, I. Stetcu, and B. R. Barrett, 2009, J. Phys. G **36**, 083101.

Nemura, H., and C. Nakamoto, 2007, Prog. Theor. Phys. Suppl. **168**, 115.

Ni, K.-K., S. Ospelkaus, M. H. G. de Miranda, A. Pe'er, B. Neyenhuis, J. J. Zirbel, S. Kotochigova, P. S. Julienne, D. S. Jin, and J. Ye, 2008, Science **322**, 231.

Nilsson, B., *et al.*, 2007, Phys. Rev. C **75**, 014007.

Noga, J., D. Tunega, W. Klopper, and W. Kutzelnigg, 1995, J. Chem. Phys. **103**, 309.

Nollett, K. M., S. C. Pieper, R. B. Wiringa, J. Carlson, and G. M. Hale, 2007, Phys. Rev. Lett. **99**, 022502.

Nuttal, J., and H. L. Cohen, 1969, Phys. Rev. **188**, 1542.

Obara, S., and A. Saika, 1986, J. Chem. Phys. **84**, 3963.

Oka, T., 2006, Proc. Natl. Acad. Sci. U.S.A. **103**, 12 235.

Okumura, S., and T. Ogawa, 2001, Phys. Rev. B **65**, 035105.

Ore, A., 1951, Phys. Rev. **83**, 665.

Ospadov, E., D. G. Oblinsky, and S. M. Rothstein, 2011, Phys. Chem. Chem. Phys. **13**, 8031.

Ottschofski, E., and W. Kutzelnigg, 1997, J. Chem. Phys. **106**, 6634.

Pachucki, K., 1997, Phys. Rev. A **56**, 297.

Pachucki, K., 2005, Phys. Rev. A **71**, 012503.

Pachucki, K., 2006a, Phys. Rev. A **74**, 022512.

Pachucki, K., 2006b, Phys. Rev. A **74**, 062510.

Pachucki, K., 2007, Phys. Rev. A **76**, 059906.

Pachucki, K., 2010, Phys. Rev. A **82**, 032509.

Pachucki, K., W. Cencek, and J. Komasa, 2005, J. Chem. Phys. **122**, 184101.

Pachucki, K., and J. Komasa, 2003, Phys. Rev. A **68**, 042507.

Pachucki, K., and J. Komasa, 2004a, Chem. Phys. Lett. **389**, 209.

Pachucki, K., and J. Komasa, 2004b, Phys. Rev. Lett. **92**, 213001.

Pachucki, K., and J. Komasa, 2004c, Phys. Rev. A **70**, 022513.

Pachucki, K., and J. Komasa, 2006a, J. Chem. Phys. **125**, 204304.

Pachucki, K., and J. Komasa, 2006b, Phys. Rev. A **73**, 052502.

Pachucki, K., and J. Komasa, 2008, J. Chem. Phys. **129**, 034102.

Pachucki, K., and J. Komasa, 2009, J. Chem. Phys. **130**, 164113.

Pachucki, K., and J. Komasa, 2010, Phys. Chem. Chem. Phys. **12**, 9188.

Pachucki, K., and J. Sapirstein, 2000, Phys. Rev. A **63**, 012504.

Pan, K. C., and H. F. King, 1970, J. Chem. Phys. **53**, 4397.

Pan, K. C., and H. F. King, 1972, J. Chem. Phys. **56**, 4667.

Patkowski, K., 2012, J. Chem. Phys. **137**, 034103.

Patkowski, K., W. Cencek, P. Jankowski, K. Szalewicz, J. B. Mehl, G. Garberoglio, and A. H. Harvey, 2008, J. Chem. Phys. **129**, 094304.

Patkowski, K., W. Cencek, M. Jeziorska, B. Jeziorski, and K. Szalewicz, 2007, J. Phys. Chem. A **111**, 7611.

Patkowski, K., and K. Szalewicz, 2010, J. Chem. Phys. **133**, 094304.

Pavanello, M., L. Adamowicz, A. Alijah, N. F. Zobov, I. I. Mizus, O. L. Polyansky, J. Tennyson, T. Szidarovszky, and A. G. Császár, 2012a, J. Chem. Phys. **136**, 184303.

Pavanello, M., *et al.*, 2012b, Phys. Rev. Lett. **108**, 023002.

Pavanello, M., W. C. Tung, and L. Adamowicz, 2009, J. Chem. Phys. **131**, 184106.

Pederiva, F., C. J. Umrigar, and E. Lipparini, 2000, Phys. Rev. B **62**, 8120.

Pedersen, T. G., K. Pedersen, H. D. Cornean, and P. Duclos, 2005, Nano Lett. **5**, 291.

Peierls, R. E., and J. Yoccoz, 1957, Proc. Phys. Soc. London Sect. A **70**, 381.

Persson, B. J., and P. R. Taylor, 1996, J. Chem. Phys. **105**, 5915.

Petersson, T., and B. Hellsing, 2010, Eur. J. Phys. **31**, 37.

Petrov, D. S., 2003, Phys. Rev. A **67**, 010703(R).

Piela, L., 2007, *Ideas of Quantum Chemistry* (Elsevier, Amsterdam).

Piszczatowski, K., G. Lach, M. Przybytek, J. Komasa, K. Pachucki, and B. Jeziorski, 2009, J. Chem. Theory Comput. **5**, 3039.

Pitre, L., M. R. Moldover, and W. L. Tew, 2006, Metrologia **43**, 142.

Platter, L., H. W. Hammer, and U. G. Meissner, 2004, Phys. Rev. A **70**, 052101.

Platzman, P. M., and A. P. Mills, Jr., 1994, Phys. Rev. B **49**, 454.

Pollack, S. E., D. Dries, and R. G. Hulet, 2009, Science **326**, 1683.

Poshusta, R. D., 1979, Int. J. Quantum Chem., Quantum Chem. Symp. **16**, 59.

Powell, M. J. D., 1964, Comput. J. **7**, 155.

Press, W. H., B. P. Flannery, S. A. Teukolsky, and W. T. Vetterling, 1992, *Numerical Recipes in Fortran* (Cambridge University Press, Cambridge, England), 2nd ed.

Proschel, P., W. Rosner, G. Wunner, H. Ruder, and H. Herold, 1982, J. Phys. B **15**, 1959.

Przybytek, M., W. Cencek, J. Komasa, G. Łach, B. Jeziorski, and K. Szalewicz, 2010, Phys. Rev. Lett. **104**, 183003.

Przybytek, M., B. Jeziorski, and K. Szalewicz, 2009, Int. J. Quantum Chem. **109**, 2872.

Puchalski, K., D. Kedziera, and K. Pachucki, 2011, Phys. Rev. A **84**, 052518.

Puchalski, M., and A. Czarnecki, 2008, Phys. Rev. Lett. **101**, 183001.

Puchalski, M., D. Kędziera, and K. Pachucki, 2009, Phys. Rev. A **80**, 032521.

Puchalski, M., and K. Pachucki, 2006, Phys. Rev. A **73**, 022503.

Puchalski, M., and K. Pachucki, 2008, Phys. Rev. A **78**, 052511.

Pudliner, B. S., V. R. Pandharipande, J. Carlson, S. C. Pieper, and R. B. Wiringa, 1997, Phys. Rev. C **56**, 1720.

Quaglioni, S., and P. Navrátil, 2007, Phys. Lett. B **652**, 370.

Quaglioni, S., and P. Navrátil, 2008, Phys. Rev. Lett. **101**, 092501.

Rakshit, D., K. M. Daily, and D. Blume, 2012, Phys. Rev. A **85**, 033634.

Ralchenko, Y., A. Kramida, J. Reader, and NIST ASD Team, 2008, "NIST Atomic Spectra Database Version 3.1.5," http://physics.nist.gov/asd3.

Rapaport, R., G. Chen, D. Snoke, S. H. Simon, L. Pfeiffer, K. West, Y. Liu, and S. Denev, 2004, Phys. Rev. Lett. **92**, 117405.

Rassolov, V. A., and D. M. Chipman, 1996, J. Chem. Phys. **105**, 1470.

Regier, P. E., and A. J. Thakkar, 1985, J. Phys. B **18**, 3061.

Reich, E. S., 2004, New Sci. **182**, 34.

Rescigno, T. N., and A. E. Orel, 1981, Phys. Rev. A **24**, 1267.

Rescigno, T. N., and B. I. Schneider, 1988, Phys. Rev. A **37**, 1044.

Reynolds, P. J., D. M. Ceperley, B. J. Alder, and W. A. Lester, Jr., 1982, J. Chem. Phys. **77**, 5593.

Richard, J. M., 2003, Phys. Rev. A **67**, 034702.

Rittenhouse, S. T., J. von Stecher, J. P. D'Incao, N. P. Mehta, and C. H. Greene, 2011, J. Phys. B **44**, 172001.

Riva, C., F. Peeters, K. Varga, and V. Schweigert, 2002, Phys. Status Solidi B **234**, 50.

Riva, C., F. M. Peeters, and K. Varga, 2000, Phys. Rev. B **61**, 13 873.

Riva, C., F. M. Peeters, and K. Varga, 2001, Phys. Rev. B **64**, 235301.

Rontani, M., E. Molinari, G. Maruccio, M. Janson, A. Schramm, C. Meyer, T. Matsui, C. Heyn, W. Hansen, and R. Wiesendanger, 2007, J. Appl. Phys. **101**, 081714.

Roth, R., T. Neff, and H. Feldmeier, 2010, Prog. Part. Nucl. Phys. **65**, 50.

Roy, M., and P. A. Maksym, 2012, Phys. Rev. B **85**, 205432.

Ryabinkin, I. G., and V. N. Staroverov, 2010, Phys. Rev. A **81**, 032509.

Rybak, S., K. Szalewicz, and B. Jeziorski, 1989, J. Chem. Phys. **91**, 4779.

Rybak, S., K. Szalewicz, B. Jeziorski, and M. Jaszunski, 1987, J. Chem. Phys. **86**, 5652.

Rychlewski, J., and J. Komasa, 2003, *Explicitly Correlated Wave Functions in Chemistry and Physics: Theory and Applications*, edited by Rychlewski, J. (Kluwer Academic Publishers, The Netherlands), pp. 91–148.

Rychlewski, J., W. Cencek, and J. Komasa, 1994, Chem. Phys. Lett. **229**, 657.

Ryzhikh, G. G., and J. Mitroy, 1997, J. Phys. B **30**, 5545.

Ryzhikh, G. G., and J. Mitroy, 1998a, J. Phys. B **31**, 4459.

Ryzhikh, G. G., and J. Mitroy, 1998b, J. Phys. B **31**, 5013.

Ryzhikh, G. G., J. Mitroy, and K. Varga, 1998a, J. Phys. B **31**, L265.

Ryzhikh, G. G., J. Mitroy, and K. Varga, 1998b, J. Phys. B **31**, 3965.

Saito, S., 1969, Prog. Theor. Phys. **41**, 705.

Saito, S. L., and Y.-I. Suzuki, 2001, J. Chem. Phys. **114**, 1115.

Salmon, L., and R. D. Poshusta, 1973, J. Chem. Phys. **59**, 3497.

Salumbides, E. J., G. D. Dickenson, T. I. Ivanov, and W. Ubachs, 2011, Phys. Rev. Lett. **107**, 043005.

Schmidt, J. W., R. M. Gavioso, E. F. May, and M. R. Moldover, 2007, Phys. Rev. Lett. **98**, 254504.

Schwartz, C., 1962, Phys. Rev. **126**, 1015.

Schwartz, C., 2006a, Int. J. Mod. Phys. E **15**, 877.

Schwartz, C., 2006b, arXiv:math-ph/0605018.

Schwegler, E., P. M. Kozlowski, and L. Adamowicz, 1993, J. Comput. Chem. **14**, 566.

Scrinzi, A., 1998, Phys. Rev. A **58**, 3879.

Seth, P., P. L. Ríos, and R. J. Needs, 2011, J. Chem. Phys. **134**, 084105.

Sharkey, K. L., S. Bubin, and L. Adamowicz, 2011a, J. Chem. Phys. **134**, 044120.

Sharkey, K. L., S. Bubin, and L. Adamowicz, 2011b, Phys. Rev. A **83**, 012506.

Sharkey, K. L., S. Bubin, and L. Adamowicz, 2011c, J. Chem. Phys. **134**, 194114.

Shima, T., S. Naito, Y. Nagai, T. Baba, K. Tamura, T. Takahashi, T. Kii, H. Ohgaki, and H. Toyokawa, 2005, Phys. Rev. C **72**, 044004.

Shiozaki, T., M. Kamiya, S. Hirata, and E. F. Valeev, 2009, J. Chem. Phys. **130**, 054101.

Shumway, J., and D. M. Ceperley, 2001, Phys. Rev. B **63**, 165209.

Silvestre-Brac, B., and V. Mathieu, 2007, Phys. Rev. E **76**, 046702.

Silvestre-Brac, B., and V. Mathieu, 2008, Phys. Rev. E **77**, 036706.

Sims, J. S., and S. Hagstrom, 1971, Phys. Rev. A **4**, 908.

Sims, J. S., and S. A. Hagstrom, 2011, Phys. Rev. A **83**, 032518.
Singer, K., 1960, Proc. R. Soc. A **258**, 412.
Snoke, D., 2002, Science **298**, 1368.
Spall, J. C., 2003, *Introduction to Stochastic Search and Optimization* (Wiley, New York).
Sprecher, D., J. Liu, C. Jungen, W. Ubachs, and F. Merkt, 2010, J. Chem. Phys. **133**, 111102.
Stanke, M., S. Bubin, M. Molski, and L. Adamowicz, 2009, Phys. Rev. A **79**, 032507.
Stanke, M., D. Kędziera, S. Bubin, and L. Adamowicz, 2007a, Phys. Rev. A **75**, 052510.
Stanke, M., D. Kędziera, S. Bubin, and L. Adamowicz, 2007b, Phys. Rev. Lett. **99**, 043001.
Stanke, M., D. Kędziera, S. Bubin, and L. Adamowicz, 2008a, Phys. Rev. A **77**, 022506.
Stanke, M., D. Kędziera, S. Bubin, M. Molski, and L. Adamowicz, 2007, Phys. Rev. A **76**, 052506.
Stanke, M., D. Kędziera, M. Molski, S. Bubin, M. Barysz, and L. Adamowicz, 2006, Phys. Rev. Lett. **96**, 233002.
Stanke, M., J. Komasa, S. Bubin, and L. Adamowicz, 2009, Phys. Rev. A **80**, 022514.
Stanke, M., J. Komasa, D. Kędziera, S. Bubin, and L. Adamowicz, 2008a, Phys. Rev. A **77**, 062509.
Stanke, M., J. Komasa, D. Kędziera, S. Bubin, and L. Adamowicz, 2008b, Phys. Rev. A **78**, 052507.
Stone, J. A., and A. Stejskal, 2004, Metrologia **41**, 189.
Strasburger, K., and H. Chojnacki, 1998, J. Chem. Phys. **108**, 3218.
Sucher, J., 1958, Phys. Rev. **109**, 1010.
Sundholm, D., 1995, J. Chem. Phys. **102**, 4895.
Suno, H., and B. D. Esry, 2008, Phys. Rev. A **78**, 062701.
Suzuki, Y., Y. Fujiwara, W. Horiuchi, H. Matsumura, and M. Orabi, 2007, Nucl. Phys. **A790**, 223c.
Suzuki, Y., and W. Horiuchi, 2009, Nucl. Phys. **A818**, 188.
Suzuki, Y., W. Horiuchi, and K. Arai, 2009, Nucl. Phys. **A823**, 1.
Suzuki, Y., W. Horiuchi, and D. Baye, 2010, Prog. Theor. Phys. **123**, 547.
Suzuki, Y., W. Horiuchi, M. Orabi, and K. Arai, 2008, Few-Body Syst. **42**, 33.
Suzuki, Y., R. Lovas, K. Yabana, and K. Varga, 2003, *Structure and Reactions of Light Exotic Nuclei* (Taylor & Francis, London).
Suzuki, Y., H. Matsumura, M. Orabi, Y. Fujiwara, P. Descouvemont, M. Theeten, and D. Baye, 2008, Phys. Lett. B **659**, 160.
Suzuki, Y., and K. Varga, 1998, *Stochastic Variational Approach to Quantum-Mechanical Few-Body Problems* (Springer, New York), Vol. 172.
Szalewicz, K., 2012, Wiley Interdisciplinary Reviews: Computational Molecular Science **2**, 254.
Szalewicz, K., and B. Jeziorski, 1979, Mol. Phys. **38**, 191.
Szalewicz, K., and B. Jeziorski, 2010, Mol. Phys. **108**, 3091.
Szalewicz, K., B. Jeziorski, H. J. Monkhorst, and J. G. Zabolitzky, 1982, Chem. Phys. Lett. **91**, 169.
Szalewicz, K., B. Jeziorski, H. J. Monkhorst, and J. G. Zabolitzky, 1983a, J. Chem. Phys. **78**, 1420.
Szalewicz, K., B. Jeziorski, H. J. Monkhorst, and J. G. Zabolitzky, 1983b, J. Chem. Phys. **79**, 5543.
Szalewicz, K., B. Jeziorski, H. J. Monkhorst, and J. G. Zabolitzky, 1984, J. Chem. Phys. **81**, 2723.
Szalewicz, K., K. Patkowski, and B. Jeziorski, 2005, Struct. Bond. **116**, 43.
Taut, M., 1993, Phys. Rev. A **48**, 3561.
Thakkar, A. J., and V. H. Smith, Jr., 1977, Phys. Rev. A **15**, 1.
Theeten, M., H. Matsumura, M. Orabi, D. Baye, P. Descouvemont, Y. Fujiwara, and Y. Suzuki, 2007, Phys. Rev. C **76**, 054003.
Thompson, D., M. Lemere, and Y. Tang, 1977, Nucl. Phys. **A286**, 53.
Thompson, D. C., and A. Alavi, 2002, Phys. Rev. B **66**, 235118.
Tornow, W., 2011, Few-Body Syst. **50**, 443.
Truemper, J., W. Pietsch, C. Reppin, W. Voges, R. Staubert, and E. Kendziorra, 1978, Astrophys. J. Lett. **219**, L105.
Tung, W. C., M. Pavanello, and L. Adamowicz, 2010, J. Chem. Phys. **133**, 124106.
Tung, W. C., M. Pavanello, and L. Adamowicz, 2011, J. Chem. Phys. **134**, 064117.
Usukura, J., Y. Suzuki, and K. Varga, 1999, Phys. Rev. B **59**, 5652.
Usukura, J., K. Varga, and Y. Suzuki, 1998, Phys. Rev. A **58**, 1918.
Varga, K., 1999, Phys. Rev. Lett. **83**, 5471.
Varga, K., 2011, Few-Body Syst. **50**, 175.
Varga, K., S. Fleck, and J. M. Richard, 1997, Europhys. Lett. **37**, 183.
Varga, K., P. Navratil, J. Usukura, and Y. Suzuki, 2001, Phys. Rev. B **63**, 205308.
Varga, K., and Y. Suzuki, 1995, Phys. Rev. C **52**, 2885.
Varga, K., Y. Suzuki, and R. G. Lovas, 1994, Nucl. Phys. **A571**, 447.
Varga, K., Y. Suzuki, and I. Tanihata, 1995, Phys. Rev. C **52**, 3013.
Varga, K., Y. Suzuki, and J. Usukura, 1998, Few-Body Syst. **24**, 81.
Varga, K., J. Usukura, and Y. Suzuki, 1998, Phys. Rev. Lett. **80**, 1876.
Vincke, M., and D. Baye, 1989, J. Phys. B **22**, 2089.
Viviani, M., A. Deltuva, R. Lazauskas, J. Carbonell, A. C. Fonseca, A. Kievsky, L. E. Marcucci, and S. Rosati, 2011, Phys. Rev. C **84**, 054010.
Viviani, M., A. Kievsky, and S. Rosati, 1995, Few-Body Syst. **18**, 25.
Volosniev, A. G., D. V. Fedorov, A. S. Jensen, and N. T. Zinner, 2011, Phys. Rev. Lett. **106**, 250401.
von Stecher, J., 2010, J. Phys. B **43**, 101002.
von Stecher, J., 2011, Phys. Rev. Lett. **107**, 200402.
von Stecher, J., J. P. D'Incao, and C. H. Greene, 2009, Nat. Phys. **5**, 417.
von Stecher, J., and C. H. Greene, 2007, Phys. Rev. Lett. **99**, 090402.
von Stecher, J., and C. H. Greene, 2009, Phys. Rev. A **80**, 022504.
von Stecher, J., C. H. Greene, and D. Blume, 2007, Phys. Rev. A **76**, 053613.
von Stecher, J., C. H. Greene, and D. Blume, 2008, Phys. Rev. A **77**, 043619.
Wang, L. M., Z.-C. Yan, H. X. Qiao, and G. W. F. Drake, 2011, Phys. Rev. A **83**, 034503.
Wang, L. M., Z.-C. Yan, H. X. Qiao, and G. W. F. Drake, 2012, Phys. Rev. A **85**, 052513.
Wang, X., and H. Qiao, 2008, Phys. Rev. A **77**, 043414.
Wang, Y., J. P. D'Incao, and C. H. Greene, 2011, Phys. Rev. Lett. **106**, 233201.
Wenzel, K. B., J. G. Zabolitzky, K. Szalewicz, B. Jeziorski, and H. J. Monkhorst, 1986, J. Chem. Phys. **85**, 3964.
Werner, F., and Y. Castin, 2006a, Phys. Rev. A **74**, 053604.
Werner, F., and Y. Castin, 2006b, Phys. Rev. Lett. **97**, 150401.
Wheeler, J. A., 1946, Ann. N.Y. Acad. Sci. **48**, 219.
Williams, H. L., T. Korona, R. Bukowski, B. Jeziorski, and K. Szalewicz, 1996, Chem. Phys. Lett. **262**, 431.
Wiringa, R. B., S. C. Pieper, J. Carlson, and V. R. Pandharipande, 2000, Phys. Rev. C **62**, 014001.
Wiringa, R. B., V. G. J. Stoks, and R. Schiavilla, 1995, Phys. Rev. C **51**, 38.
Witała, H., and W. Glöckle, 1999, Phys. Rev. C **60**, 024002.
Wojs, A., and P. Hawrylak, 1996, Phys. Rev. B **53**, 10841.

Wolniewicz, L., 1995, J. Chem. Phys. **103**, 1792.
Wright, G. L., M. Charlton, G. Clark, T. C. Griffith, and G. R. Heyland, 1983, J. Phys. B **16**, 4065.
Yahiro, M., M. Nakano, Y. Iseri, and M. Kamimura, 1982, Prog. Theor. Phys. **67**, 1467.
Yan, Z.-C., J. F. Babb, A. Dalgarno, and G. W. F. Drake, 1996, Phys. Rev. A **54**, 2824.
Yan, Z.-C., and G. W. F. Drake, 2003, Phys. Rev. Lett. **91**, 113004.
Yan, Z.-C., and Y. K. Ho, 1999, Phys. Rev. A **59**, 2697.
Yan, Z.-C., W. Nörtershäuser, and G. W. F. Drake, 2008, Phys. Rev. Lett. **100**, 243002.
Yan, Z.-C., J.-Y. Zhang, and Y. Li, 2003, Phys. Rev. A **67**, 062504.
Yannouleas, C., and U. Landman, 1999, Phys. Rev. Lett. **82**, 5325.
Yuan, J., B. D. Esry, T. Morishita, and C. D. Lin, 1998, Phys. Rev. A **58**, R4.
Zaccanti, M., B. Deissler, C. D'Errico, M. Fattori, M. Jona-Lasinio, S. Müller, G. Roati, M. Inguscio, and G. Modugno, 2009, Nat. Phys. **5**, 586.
Zenezini, A., B. Huang, M. Berninger, S. Besler, H.-C. Nägerl, F. Ferlaino, R. Grimm, C. H. Greene, and J. von Stecher, 2012, arXiv:1205.1921.
Zhang, J. Y., and J. Mitroy, 2011, Phys. Rev. A **83**, 022711.
Zhang, J.-Y., and J. Mitroy, 2007, Phys. Rev. A **76**, 014501.
Zhang, J.-Y., and J. Mitroy, 2008, Phys. Rev. A **78**, 012703.
Zhang, J.-Y., J. Mitroy, and K. Varga, 2008, Phys. Rev. A **78**, 042705.
Zhang, J.-Y., J. Mitroy, and K. Varga, 2009, Phys. Rev. Lett. **103**, 223202.
Zhang, S., and H. Krakauer, 2003, Phys. Rev. Lett. **90**, 136401.
Zhukov, M. V., B. V. Danilin, D. V. Fedorov, J. M. Bang, I. S. Thompson, and J. S. Vaagen, 1993, Phys. Rep. **231**, 151.
Zumbühl, D. M., C. M. Marcus, M. P. Hanson, and A. C. Gossard, 2004, Phys. Rev. Lett. **93**, 256801.